UCLouvain

École polytechnique de Louvain

Master thesis – Impact of floating debris on flood barriers

Authors: **Tommy Chavet, Jonah Krings**
Supervisor: **Sandra Soares Frazao**
Readers: **Charles Ryckmans, Didier Bousmar, Igor Bouckaert**
Academic year 2023–2024
Master [120] in Civil Engineering

Acknowledgments

We would like to sincerely thank the following people, without whom our thesis would not have been possible.

First and foremost, we would like to thank our supervisor, Professor Sandra Soares-Frazão, for her constant supervision and support throughout the year. Her guidance and valuable advice were essential for this work.

We also express our sincere appreciation to Mr Charles Ryckmans, for his willingness to answer all our questions, his close supervision of our work, invaluable help and encouragement throughout the year.

Furthermore, we would like to thank Professor Didier Bousmar and Mr Igor Bouckaert, who agreed to read this work.

Our special thanks go to Mr Christophe Galloy for facilitating our collaboration with Buildwise and for his constant availability to address our questions. We are also grateful to Mr Nicolas Lambion for managing the analysis of the 3D camera images and providing them to us. Additionally, we extend our gratitude to all the other Buildwise employees who assisted us in conducting the tests.

Moreover, we would like to thank Mr Nathan Buss for reviewing and correcting our work and giving us advice on writing the thesis.

Finally, we would like to express our heartfelt thanks to our families and friends, who have stood by us and supported us not only throughout this thesis but also throughout our entire academic journey.

Abstract

Flooding has been an increasing concern since records began, affecting many countries worldwide. Belgium, in particular, experienced severe impacts during the floods of July 2021, which caused significant material damage, especially to buildings. Catastrophic events like this one show that qualitative protective measures are necessary to reduce or even prevent damage.

One effective way to mitigate such damage is by installing flood barriers on doors and windows. Although various barriers are available on the Belgian market, there are currently no established standards for them. The FLOOD project, initiated by Buildwise in collaboration with UCLouvain, aims to develop these standards. The project is heavily influenced by the American FM Approvals standard, which includes a series of tests: a hydrostatic test, a 600 Joule impact test, and a second hydrostatic test following the impact.

This master's thesis contributes to the development of these standards and is divided into two main sections. The first section addresses what the barriers must withstand, including the types of debris that could occur during floods and the impact they might have on the barriers. It also examines the potential velocities of floodwaters. This information also draws from numerical simulations of the 2021 floods in Pepinster, Belgium. Based on this information, the energy that flood barriers must be able to withstand is calculated. The results are then compared to the suggestions of the American test standard.

The second, experimental part of the study describes the development of a test setup and procedure for the impact test. Initially, a method was devised using a miniature model, which was later applied to two full-scale barriers in the complete test series. The results are thoroughly analysed, leading to a final section where suggestions for improvement and an enhanced test procedure is provided. These recommendations are intended to support future testing or research in this area.

Contents

1 Introduction **1**

1.1 The severity of floods in the world and in Belgium 1

1.2 Project FLOOD 11

2 Research **15**

2.1 FM Approvals: Approval standard for flood mitigation equipment . . . 15

2.1.1 Performance testing 18

2.1.1.1 Pre-deployment installation configurations 19

2.1.1.2 Deployment 19

2.1.1.3 Hydrostatic load test 20

2.1.1.4 Redeployment 20

2.1.1.5 Dynamic impact test 21

2.1.1.6 Post hydrostatic load test 22

2.2 British standard 23

2.2.1 Static leakage test 24

2.2.2 Wave leakage test 24

2.2.3 Current leakage test 25

2.2.4 Dynamic impact test 25

2.3 German guideline 28

2.4 Impact test 30

2.4.1 Contextualising 600 Joule 30

2.4.1.1 Flow velocity 30

2.4.1.2 Floating debris 33

2.5 Velocity analysis of the July 2021 flood in Pepinster 42

2.5.1 Visualisation of the traces left behind by the flood 43

2.5.2 Velocity analysis 45

3 Experimental Part **52**
3.1 Test modelling . . . 53
3.1.1 Inspiration of the test setup . . . 53
3.1.2 Get to know the program and materials . . . 55
3.1.3 First tests at Buildwise . . . 57
3.1.4 Small scale model . . . 64
3.1.4.1 First test series . . . 66
3.1.4.2 Second test series . . . 69
3.1.4.3 Third test series . . . 78
3.2 Final test setup and procedure . . . 82
3.2.1 Test setup . . . 82
3.2.2 Test procedure . . . 87
3.2.2.1 Hydrostatic test before impact . . . 87
3.2.2.2 Impact test . . . 88
3.2.2.3 Hydrostatic test after impact . . . 90
3.3 Analysis of the tests . . . 91
3.3.1 Barrier X . . . 91
3.3.1.1 Description . . . 91
3.3.1.2 Hydrostatic test before impact . . . 93
3.3.1.3 Impact Test . . . 94
3.3.1.4 Hydrostatic test after impact . . . 99
3.3.2 Barrier Y . . . 101
3.3.2.1 Description . . . 101
3.3.2.2 Hydrostatic test before impact . . . 102
3.3.2.3 Impact test . . . 103
3.3.2.4 Hydrostatic test after impact . . . 108
3.4 Analysis of the results and improvements . . . 109
3.4.1 Result comparison . . . 109
3.4.1.1 Height measurement . . . 111
3.4.1.2 Camera calibration . . . 112
3.4.2 Improvements . . . 114
3.4.2.1 Height measurement solution . . . 114
3.4.2.2 Camera calibration solution . . . 114
3.5 Final methodology . . . 116

3.5.1 Preparation 116
3.5.2 Preliminary impact test series 116
3.5.3 Hydrostatic load test 117
3.5.4 Impact test 117
3.5.5 Post hydrostatic load test 118

4 Conclusion **119**

Appendix **124**

A Flow velocity **124**

B Energy variation for different wood densities **125**

C Test results **128**
C.1 Barrier X - Test results 128
C.1.1 First test 128
C.1.2 Second test 131
C.2 Barrier Y - Test results 133
C.2.1 First test 133
C.2.2 Second test 136

Chapter 1

Introduction

1.1 The severity of floods in the world and in Belgium

When water submerges an area that is usually dry, it is called a flood. Floods are one of the most common and destructive natural disasters worldwide. In recent years, flood disasters have increased in both frequency and severity. It is not unusual to read, hear or see in the media about flood disasters and their economic and social consequences around the world.

The graphics and most of the information presented in this section are taken from OurWorldInData [19]. Figure 1.1 shows the total number of reported floods compared to the total number of natural disasters over the last century. As can be seen, floods make up the majority of natural disasters. The extreme differences between the first and second half of the curve is mainly due to increased data reporting and not only due to an increase in the number of natural disasters.

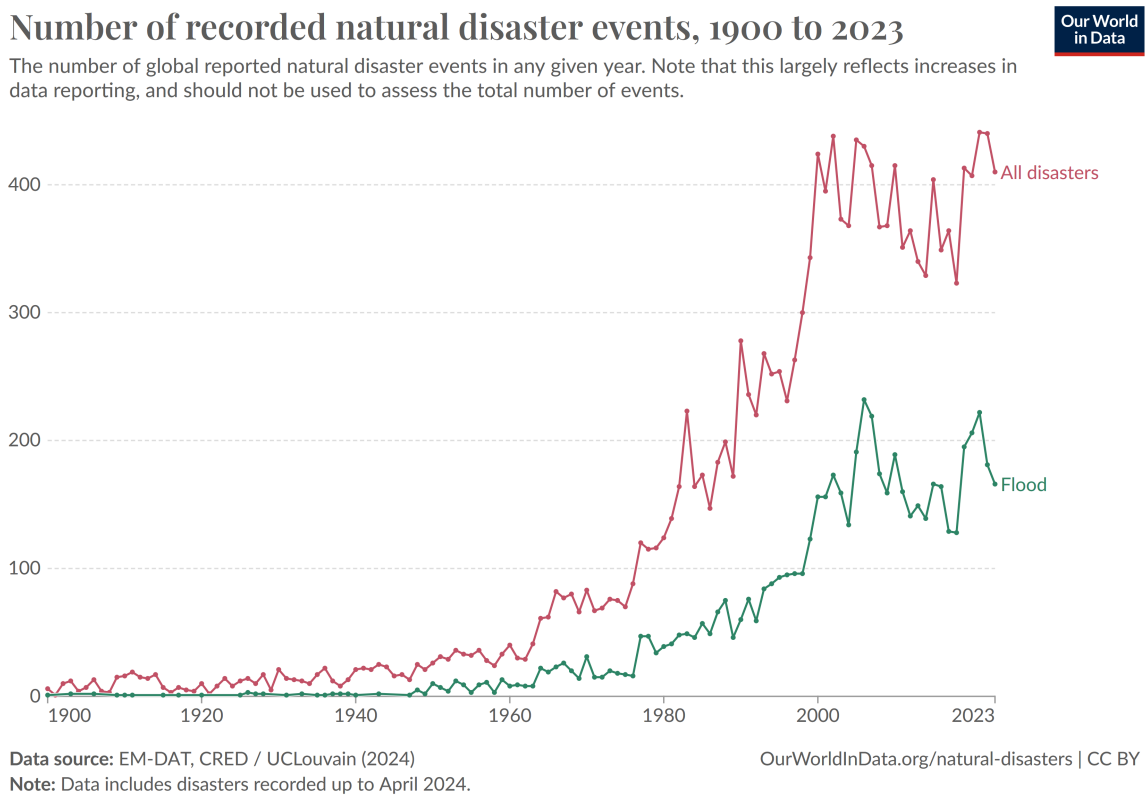


Figure 1.1: Number of natural disasters worldwide. [19]

Figure 1.2 represents the annual death numbers from flooding events over the last 50 years. As can be seen, there is a high variation in the 70s and 80s. On average, flood events caused around 7000 deaths per year during these decades. In the 90s there is an increase in the death rate leading to an average of around 9500 deaths per year. In the 21^{st} century flooding claims in average 5000 to 5500 lives worldwide every year as can be seen on the graph.

Even if the trend of flooding is increasing, this is not the case for the number of deaths. On the contrary, these numbers are rather decreasing. This decline is partly due to coordinated actions, advances in technology, better infrastructure and early warning systems.

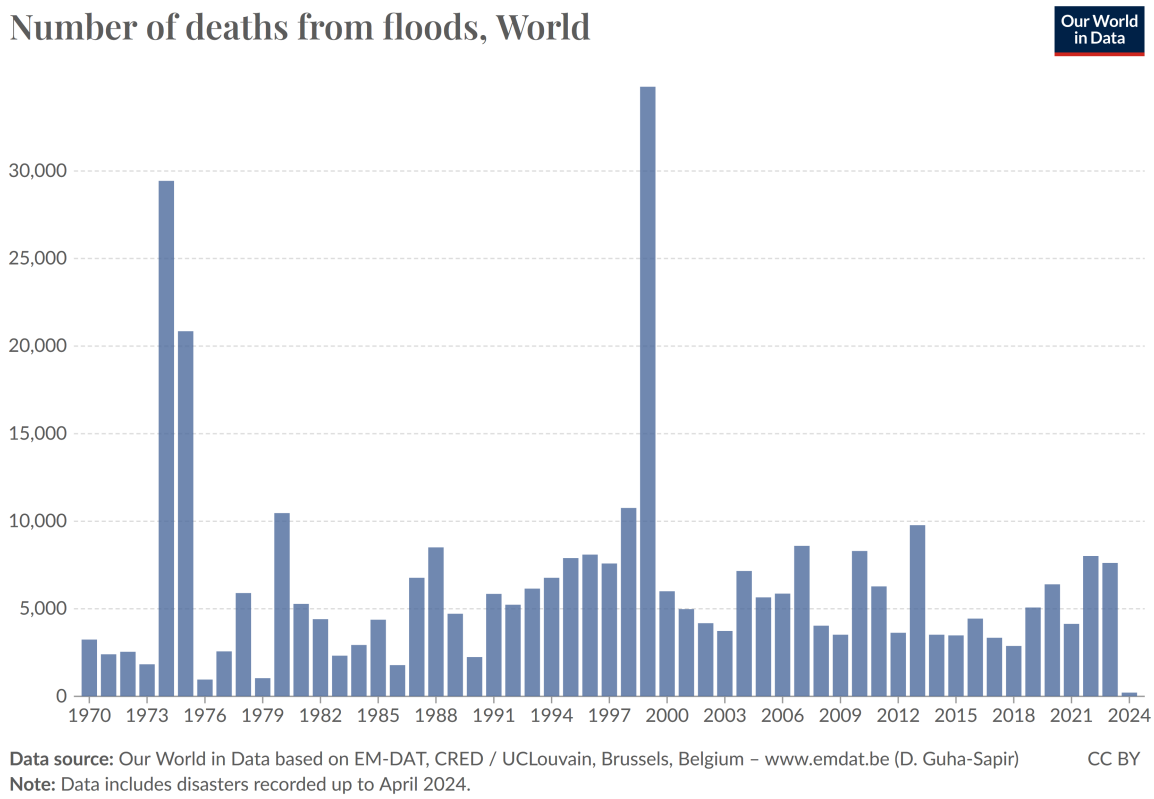


Figure 1.2: Deaths from floods. [19]

Compared to other natural disasters, such as earthquakes or extreme temperatures, the death rate due to floods is relatively low. However, the number of people affected by flooding is very high. The total number of people affected by flooding includes those injured, in need of assistance and those made homeless. Figure 1.3 depicts the total number of people affected by floods over the last 50 years. It can be seen that in the number of affected people increased in the 20^{th} century from an average of around 22 million in the 70s to 144 million in the 90s. However a decrease in the 21^{st} century can be observed. From an average of 95 million in the beginning of the century the value dropped to a value of 31 million in the current decade. It should be noted that the average value is calculated as the average value over a subsequent ten-year period. This means the average value for the 2000s is obtained by taking the values from 2000-2009. Therefore the average value of the current decade still keeps changing.
The decreasing trend after the peak in the 90s shows that the measures taken against flooding have been effective.

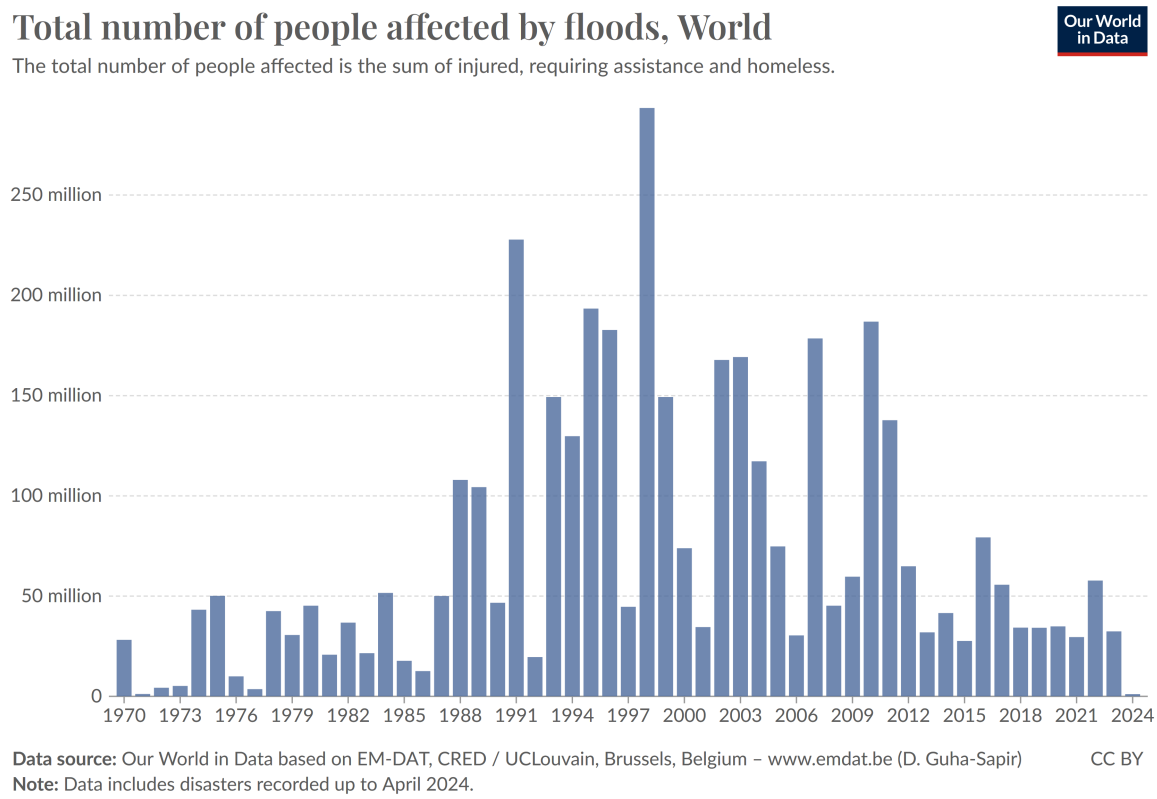


Figure 1.3: Number of people affected by floods worldwide. [19]

Besides the high number of people affected, floods cause billions in economic damage. Figure 1.4 illustrates the global economic damages from floods expressed in current US-Dollar per year. As can be seen, the costs caused by the damage were relatively low in the 1970s, averaging less than 1 billion USD per year. In the 80s there was an increase in the costs caused by damage, which were in the single-digit billion range. Furthermore, it can be seen that in the 90s the numbers are much larger and in the range of 20 billion USD per year. This value remains about the same at the beginning of this century. It can be observed that this value has almost doubled since the 2010s and averages around 40 billion USD per year across the last decade.

In contrast to the last two categories, the number of deaths and the number of people affected, where there is a downward trend in the last years, the value for the economic damages continues to rise. This can be explained by the fact that raw materials, products, living standards, etc. are becoming more and more expensive. Another factor leading to the increased economic damage is the rapid expansion of urban areas near

rivers.

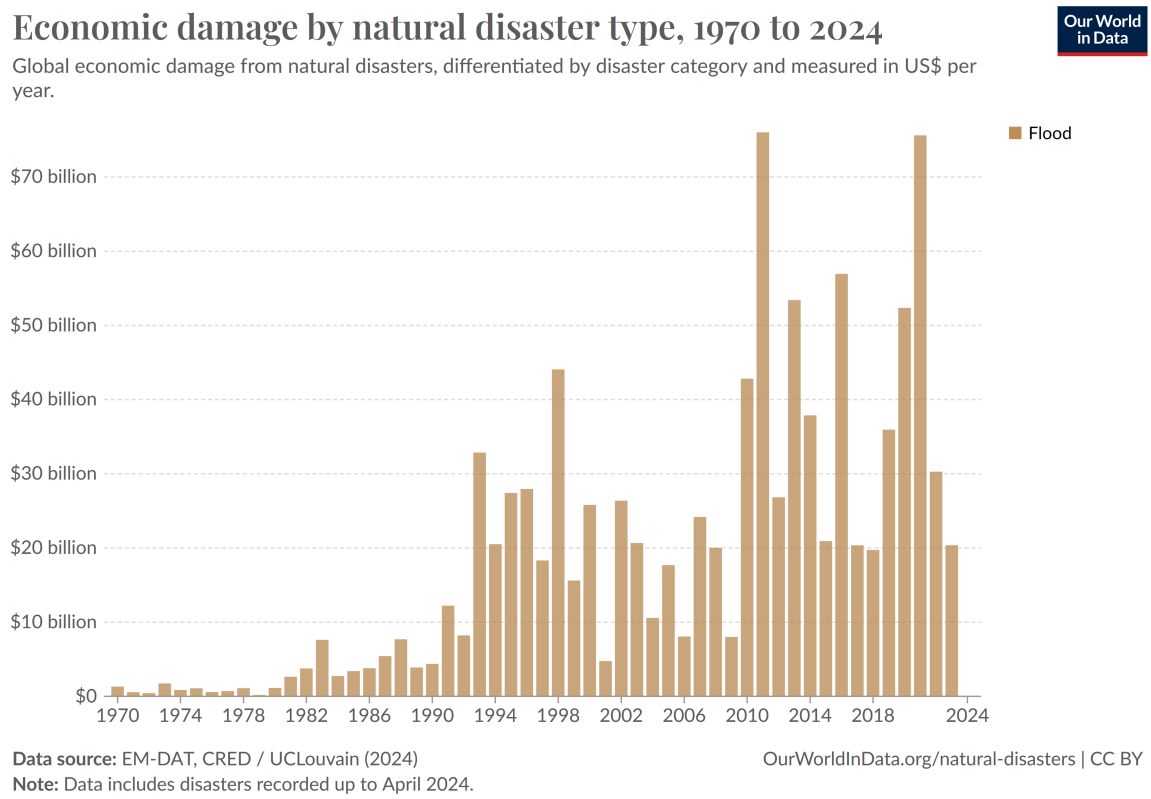


Figure 1.4: Economic damages due to floods. [19]

Let's take a closer look at the situation in Europe and especially in Belgium. Europe is very advanced when it comes to measures against floods. Therefore, the number of deaths and people affected is very small compared to the global numbers. Figure 1.5 shows the number of deaths per year due to floods over the last 50 years. In the 1970s, an average of almost 130 people died each year in Europe as a result of flooding. Since then, the rate has been reduced to below 100 people.

Figure 1.6 depicts the number of people affected by floods every year in Europe. As can be seen, an average of 260,000 people were affected by floods in the 70s. In the 80s, the average fell below 100,000 before reaching a peak of 450,000 in the 90s. In the first 2 decades of the 21^{st} century, the annual average was 340,000 people. In the 2020s, the value rises again and reaches a current value of around 420,000 people affected by floods per year in Europe.

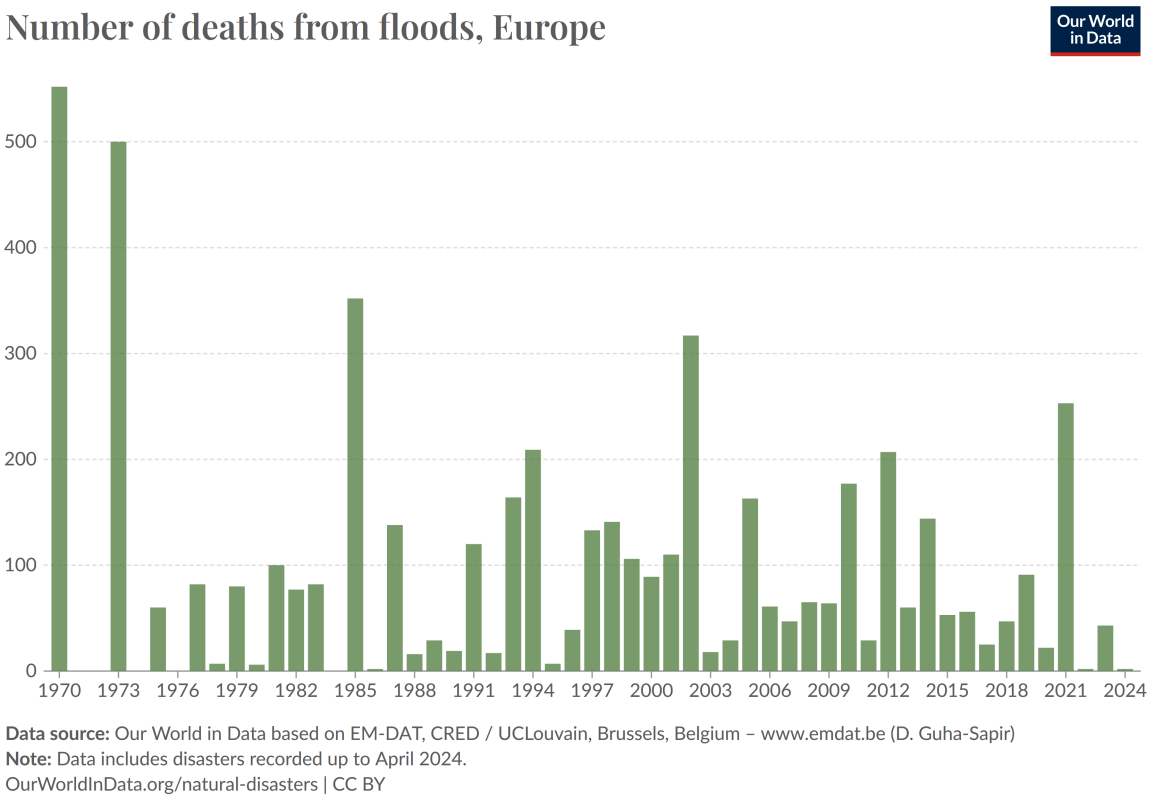


Figure 1.5: Deaths from floods in Europe. [19]

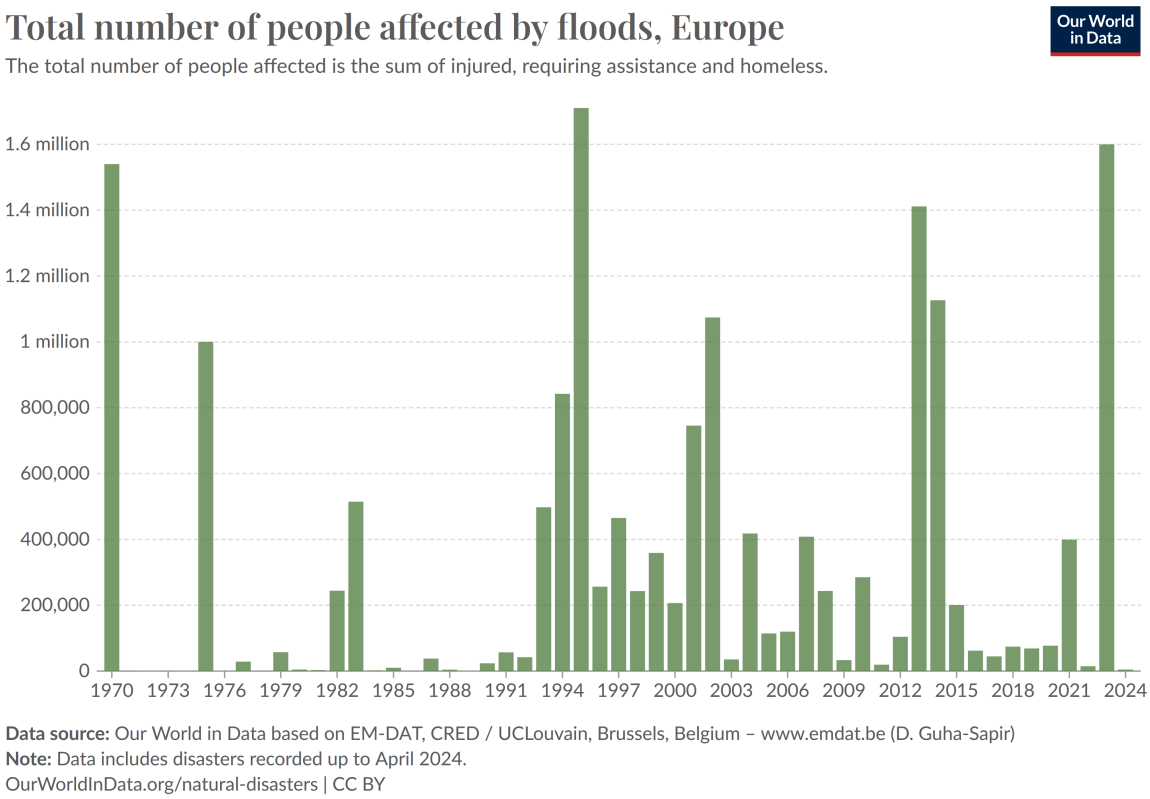


Figure 1.6: People affected by floods in Europe. [19]

In Belgium, deaths from flooding are rare and the average is less than one person per year. The exception is 2021, when 39 people died as a result of flooding. The average number of people affected is less than 100 per year. Except in the 2000s, when the number climbed to around 260. A huge change can be observed in the last years. The 2021 floods disasters affected more than 100,000 people and around 3000 people were affected by floods in 2023. The map in Figure 1.7 shows the distribution of the decadal average of people affected by floods by country. As it can be seen, Belgium is among the most affected countries. In addition to the high number of people affected, the 2021 floods caused economic damage totalling 200 million USD.

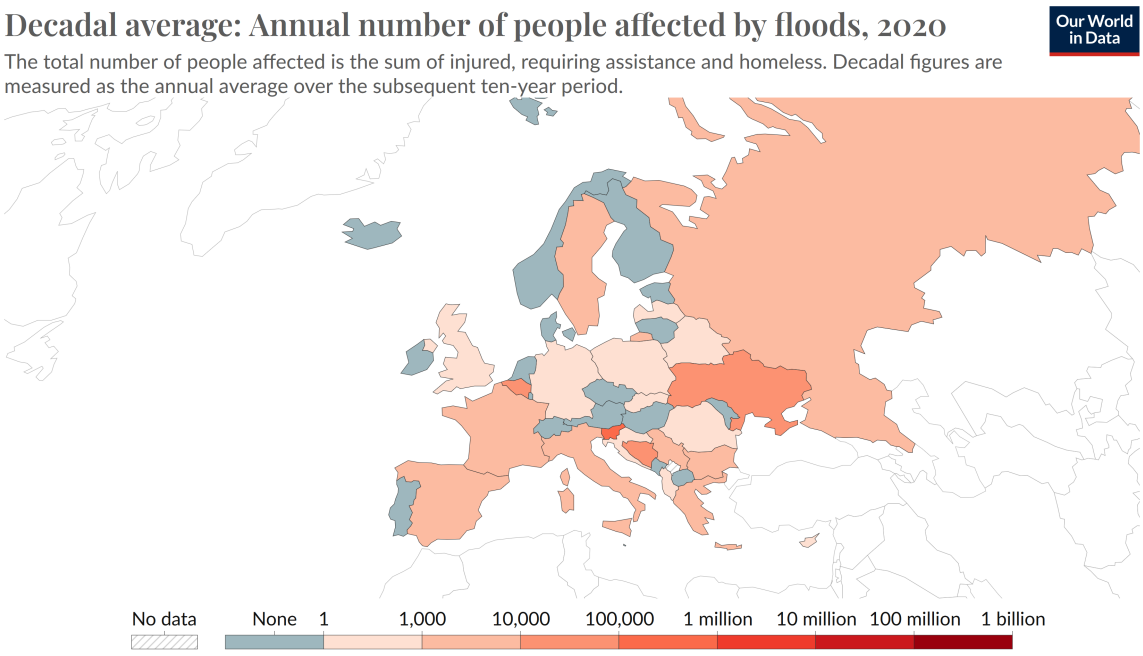


Figure 1.7: Average number of people affected by floods in Europe. [19]

Some regions in Belgium, such as Pepinster, were hit very hard by the 2021 floods. The water reached a level of over 2 metres in some places. Entire sections of road were washed away. Bridges were impassable due to instability. Houses were damaged, became uninhabitable or even collapsed completely. Figure 1.8 gives an insight into the devastating extent of this natural disaster. It shows the remains of a house of which the flood only left ruins.

Water infiltration into buildings can cause significant damage and make them uninhabitable for long periods of time. The damage and the duration of uninhabitability depend on many factors. The height of the water and the length of time it remains standing in the house have a major influence. Higher water levels and longer duration cause more damage. Electrical and plumbing systems may need to be repaired, which can take a considerable time depending on their condition. Water contamination also plays a role, as it can increase the extent of the damage. Problems with structural integrity, as well as inspections and delay of approvals from local authorities, can have



Figure 1.8: Pepinster 2021. [22]

further impact on the duration until moving back in. Mould growth caused by moisture is a health hazard and can delay the time to move back in. Therefore, it is important to dry out and clean the house. The time it takes to make a house habitable again can vary widely, ranging from one to two weeks to several months or even a year, depending on the severity of the flood damage and the efficiency of the restoration process. [12][18] The water from rivers is usually muddy and often carries a lot of debris during heavy floods, which is left behind after the water recedes. In the Figure 1.9, the entrance of a house is shown, with the ground covered in several centimetres of thick mud left behind by the flood, causing significant damage.



Figure 1.9: Remaining mud in a house after the 2021 floods in Pepinster. [22]

Although there have been some floods in Belgium's history, they have never been this devastating. But why has there been such a change in the recent years? Not only in Belgium and Europe, but all over the world, flood disasters that cause considerable damage are on the rise, as described above.

There are several reasons for an increased risk of flooding. One reason is the climate change which causes variation in the global weather. More severe precipitation is leading to higher discharges and higher water levels and therefore to an increasing frequency of flooding. Another reason for the increased risk is a change in land use. More and more areas are deforested, drained for agriculture or lose their function as wetland. These human-inducted changes lead to a reduction in the water storage capacity of catchment areas. This results in higher discharges, higher river levels and flood peaks. The aim to control the water flow by river regulation, such as rectification of the river bed, contributes to a higher discharge peak, as well. Another major cause for floods is urbanisation. On the one hand, the creation of impermeable concrete surfaces leads to a higher flow rate because the soil's ability to absorb water is restricted. On the other hand, due to population growth, urbanised areas are being expanded and as people have always lived close to water, more and more people, buildings and other infrastructure are exposed to the risk of flooding. In particular, building in floodplains, which are high-risk areas and are naturally under water when the river is overflowing, increases the risk of exposure to flooding. [21]
The combination of the aforementioned factors leads to such devastating flood disasters as the one in July 2021.

1.2 Project FLOOD

As explained above, the risk of the occurrence of floods is rising significantly. That is why building in flood-prone areas is more and more dangerous and hence not advisable. There is awareness of this but it is still permitted. Not only new buildings are a concern but also existing buildings, which have to be adapted to resist the more frequent and more devastating floods.

This raises a number of questions:

How can protection be provided taking into account the type or the current state of a building?

Does the placement and the specific source of flooding in the region have an impact on the selection of measures?

Which measures have to be combined to achieve an ideal protection?

The Project FLOOD aims to provide guidelines and strategies for water-resistant renovation and construction, providing answers to the above questions and to many more, as well. [7]

The project is divided into three main tasks, which are depicted in Figure 1.10 [7]:

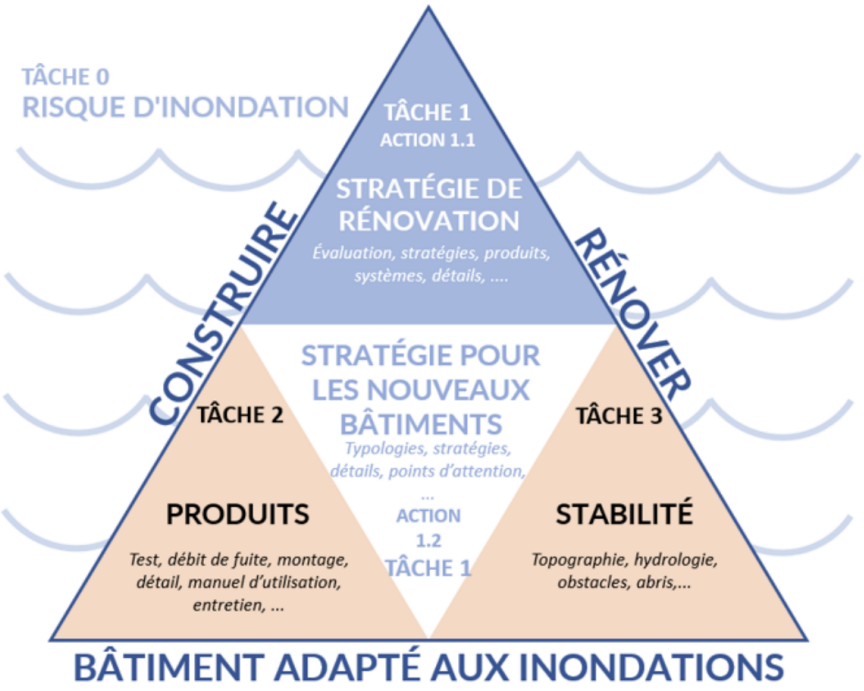


Figure 1.10: 3-task scheme. [7]

- Task 1:
  The first objective is to develop comprehensive guidelines and strategies for constructing and renovating buildings to be water-resistant in flood-prone areas.
  This involves conducting thorough studies to understand the entire process, considering various options and strategies based on specific flood scenarios and the condition of existing buildings. The focus is on providing advice, methodologies, and overarching water resistance strategies specifically designed for the Belgian construction sector. This will include assessment frameworks and checklists for both existing and new buildings, facilitating the identification and prioritisation of vulnerabilities, as well as selecting appropriate protection materials, systems, and methodologies that consider the unique characteristics of the environment and the building.

- Task 2:
  The second task aims to establish the scientific framework necessary for testing and assessing flood prevention products, with a focus on various components such as flood barriers for facade solutions, building envelopes, windows, doors, gates, crack sealing products, and facade surface treatments. Emphasis will be placed on testing under different conditions including static, dynamic, and impact loads, evaluating operational effectiveness, leakage rates, ease of installation, sensitivity to conditions, installation time, detailed connections, adherence to substrates, and maintenance requirements.

- Task 3:
  Task 3 involves establishing the foundation for evaluating building stability during flood conditions, prompted by recent devastating floods in our country. Developing design and calculation guidelines for assessing stability, especially for existing buildings, is crucial. This section will focus on creating practical guidelines to swiftly but accurately evaluate hydrodynamic forces on buildings during floods in Belgium. Factors such as location, building boundary conditions, and immediate surroundings will be considered. The goal is to devise assessment protocols considering overall topological conditions, soil characteristics, building construction type, and surrounding obstacles.

This thesis is part of the second task and more precisely focuses on flood barriers. Flood barriers are available on the Belgian and European markets. There are various standards such as the American FM Approvals, the British standard or the German guideline for the classification of flood protection products. The problem is that there is no standard for the Belgian and European market that guarantees standardised tests for uniform use. Standardised tests would make it possible to test, classify and certify flood barriers.

In collaboration with Buildwise, the founder of the FLOOD project, the aim of this work is to develop a part of a standard for the Belgian market and test existing flood barriers for facade solutions available on the Belgian market. The American standard, FM Approvals, is to be adapted for the Belgian context. More specifically, this work will address the impact test, which is part of a whole series of tests. The impact test simulates the collision of debris with a flood barrier. In short, the American standard requires that the barrier withstand an impact energy of 600 Joule. But what exactly are 600 J? What does 600 J represent physically?

One goal of this work is to further clarify what kind of debris collision an impact test with an impact energy of 600 J could represent. The other goal is to determine a suitable experimental setup for this test, which will allow flood barriers to be tested uniformly.

In the first part of this paper, the American standard, FM Approvals, is examined in more detail and compared with the British standard and a German guideline. Furthermore, the objects that can occur as floating debris during floods are discussed, as well as the flow velocities that can occur during such events. These results are expressed in terms of energy to make the connection to the 600 J impact test. Finally, some velocity analyses from a simulation of the July 2021 floods in Pepinster are discussed, to further specify and demonstrate the inpact of floods on a current, concrete example.

The second part describes the laboratory tests that were carried out in order to develop a uniform impact test for Belgian flood barriers. Firstly, the development of a test setup that serves to analyse the impact test is described. This includes getting to know the available equipment as well as the program used. This is followed by the

analysis of an initial test at Buildwise in the laboratory, which served to further develop the test setup. Furthermore, a small-scale model was designed to make it quicker and easier to resolve any problems that occurred in the test setup and in the test itself. Then, both, the final test setup and the test procedure are described. This is followed by the presentation of the tests on two different flood barriers and the analysis of their results. In addition to the impact test, these tests also include two hydrostatic tests. Finally, the results of the impact tests are compared and the causes of inaccuracies as well as improvements to the test procedure and setup are discussed.

The work concludes with a summary of findings, results and some comments.

Chapter 2

Research

In this section, the American FM Approvals, the British standards, and the German guidelines are presented and compared. Then, in order to adapt the FM Approvals to the Belgian context, a connection between the impact test and real floods is made, taking into account a simulation of the 2021 flood in Pepinster.

2.1 FM Approvals: Approval standard for flood mitigation equipment

FM Approvals is a product certification and testing program of the industrial insurance company FM Global. They provide third-party approval and certification services for products and systems related to property risk management. They ensure that property loss prevention products and services meet the highest standards of quality, technical integrity and performance. Initially founded in the USA, FM Approvals standards are available worldwide and recognised by many companies. The certification covers a wide range of areas, including fire protection, flood protection, electrical equipment, building materials, and cybersecurity, among others. [3]

All the information about this standard is extracted from document [4]. The standard defines FM Approvals criteria, such as design and performance requirements, to be met by flood protection equipment for the following three situations: Flooding caused by rivers, tides or rainfall.
Flood mitigation equipment must be FM Approved for specific flood protection appli-

cations, which are defined and categorised by the following criteria:

- Function (permanent or temporary)
- Operation (active or passive)
- For flood barriers: intended protection area (openings or perimeter)

Furthermore, this standard contains the requirements for the following product categories:

- Flood barriers for Opening Barrier Applications
- Flood Barriers for Perimeter Barrier Applications
- Flood Mitigation Valves
- Flood Mitigation Pumps
- Penetration Sealing Devices

In this thesis the focus will be exclusively on flood barriers for opening barrier applications.
But what is a flood barrier for open barrier application, exactly? The terms 'flood barrier' and 'open barrier application' are described in the standard. By combining the two, flood barriers for opening barrier applications can be defined as follows:

> A flood barrier for opening barrier applications is a structure designed to prevent or mitigate water leakage into a protected area when exposed to floodwaters. These barriers can be either permanent or temporary and may operate actively or passively. They are specifically used to protect against water entering through openings in a structure between two linear points, such as doorways, windows, or receiving bays, and are supported by the permanent structure on both sides or along the full perimeter of the barrier opening.
> Common products for opening barrier applications include flood doors, flood panels, and flood planks, as well as flexible membrane barriers, sluice gates, and flood glazing. These flood barriers are evaluated and tested to withstand quasi-static flood conditions to ensure their effectiveness in protecting the designated openings.

An active flood barrier is a barrier whose manual deployment requires human intervention. The installation can be either permanent or temporary. A passive flood barrier is a barrier that no longer requires human intervention after its initial installation. Such barriers are always permanent. Examples of passive barriers include flood glazing, seals around pipes/cables and automatic flood barriers.

It should be noted that this standard only approves the flood barriers for quasi-static flood conditions. Therefore, the standard does not cover flood barriers for applications near the coast. Only protection from tidal-related floods away from the coast, where quasi-static conditions are present, is included.

2.1.1 Performance testing

The performance testing is used to simulate quasi-static flood conditions. To evaluate the performance a series of tests must be conducted on a same flood barrier. The Table 2.1 shows the procedure and the sequence for testing.

Test description	**Condition**	**Duration [h]**
Deployment	N/A	Manufacturer's specification
Hydrostatic load	$10\% \cdot h \pm 0.6$ cm	2
Hydrostatic load	$100\% \cdot h \pm 0.6$ cm	20
Redeploy	Disassemble and redeploy	Manufacturer's specification
Dynamic impact load	Water drained, min 2x 600 J impacts	N/A
Post hydrostatic load	$10\% \cdot h \pm 0.6$ cm	1
Post hydrostatic load	$100\% \cdot h \pm 0.6$ cm	1

Table 2.1: Performance Test Series - Flood barriers for opening barrier applications.

Note Table 2.1:
*"h" is the maximum design water depth specified by the manufacturer.
**Hydrostatic load testing may be required at additional water depths, at the discretion of FM Approvals, if the design of the barrier is such that increased leakage may occur at other depths besides those prescribed above. Additional water depths shall be tested for a minimum duration of 1 h. Hydrostatic Load testing at 10% h may be waived if the design of the barrier is such that compression forces applied by the water column do not influence the barrier's sealing capabilities.

To conduct the tests, a suitable test enclosure is required, which must be large enough to fulfil all the specified test procedures. Additionally, the test enclosure must be able to withstand the maximum design water depth without significant leakage. Limited leakage of the test enclosure is allowed, but the tested water level must remain constant. Therefore, a system must be installed to maintain the water level at the required depths with the specified accuracy during the designated time periods.

2.1.1.1 Pre-deployment installation configurations

This part includes the installation of barrier components such as frames and rails that are intended to be permanently installed in the protected opening before the barrier is deployed. Both, the barrier manual, which contains all possible installation options, and the post-installation checklist, must be checked for accuracy and completeness. These documents must be submitted before the start of the test series. If there are several installation configurations, such as external installation on a structure, internal installation on a structure, installation on a door jamb, then the performance test series must be carried out on all configurations required to be certificated.

2.1.1.2 Deployment

The barrier should be deployed within the test enclosure in the same manner as it would be during a flood event. Furthermore, the completeness of the barrier's Manual should be verified. It should include at least the following information:

- A list of the materials, tools, and equipment needed for the installation of the barrier.
- The number of people needed to install the barrier.
- The time to install the barrier.
- A detailed step by step guide for how to install the barrier.
- Additional installation requirements, which were performed during the installation test process, should be detailed. This includes foundation requirements, special construction considerations, application limitations, and notes on what to do if damage should occur during installation.
- If the barrier is to be reused, a description of the correct disassembly and storage of the barrier parts should be available.

2.1.1.3 Hydrostatic load test

Criteria to fulfil:

Flood barriers should resist hydrostatic loads caused by quasi-static floodwater. Over any 15 minutes period the leakage rate has to be limited to one Liter per hour per linear metre of seal (1 L/h/m). The linear length of the seal is the opening width (measured from barrier seal-to-seal) plus two times the water height. In case the maximum design water height is greater than the flood barrier height, such as for fully submerged windows, the linear seal length is defined as the opening width plus twice the water height, or plus the barrier perimeter, whichever is smaller. If the barrier is parallel to the ground surface, such as subway stair or grate barriers, the linear seal length is defined as the perimeter of the barrier.

Test procedure:

In the first step, the wet-side of the test apparatus must be filled to 10% of the maximum water design height $h \pm 0.6$ cm. Measure the leakage rate at 15-minute intervals until it either stops or stabilises. Maintain the desired water level for at least 2 hours. Record the leakage rate during the final 15 minutes. If the leakage rate continues to increase, extend the test duration until stabilisation is achieved. In a second step, raise the water height to 100% of the maximum design water depth $h \pm 0.6$ cm. Keep the water level constant for a minimum of 20 hours. Measure the leakage rate at 15-minute intervals until it either stops or stabilises. Record the leakage rate during the last 15 minutes. If the leakage rate does not stabilise, measure it at the following intervals, at a minimum: 15 min, 30 min, 45 min, 1 h, 20 h. If the leakage rate continues to increase, extend the test duration until stabilisation is achieved.

2.1.1.4 Redeployment

This step simply involves disassembling or opening the barrier after the hydrostatic test, depending on what is applicable. The barrier should be inspected for wear or possible damage. The barrier then needs to be reinstalled for further testing.

2.1.1.5 Dynamic impact test

Criteria to fulfil:

Flood barriers have to resist a minimum of two impacts of 600 J. The impact is produced by a rigid falling object, which is intended to simulate floating debris. The functionality cannot be impacted by the damage caused by the impacts.

Test procedure:

First, the wet-side of the test apparatus must be emptied before starting the test. The impact object should be a piece of saw-cut wood with a diameter of 30.5 cm and a density similar to that of wet southern pine (480 kg/m^3). One end of the log should have a straight, vertical cut, while the other end should be cut at a 15-degree angle from the centre, with no rounded edges. The straight-cut end of the wood should be attached to a steel block so that the total weight of the object is 50 kg. A similar impact object may be used at the discretion of FM Approvals, provided that the impact trajectory and impact energy criteria are met.
The impact on the barrier should be directed such that the front edge of the impacting object strikes the predetermined point on the barrier. A suggested layout for this test is shown in Figure 2.1.
To reach the required impact force of $E = 600$ Joule, the test will be performed as follows: Lift the impact object to a height of 1.22 m above the impact point. Then, drop the object such that it falls under gravitational acceleration, along a circular trajectory, and impacts the barrier in the horizontal position.
The first impact location should be at a predetermined weak point of the barrier structure or at the horizontal center of the barrier at 80% of the maximum water depth (h) specified by the manufacturer.
The second impact location should be as close to the edge of the barrier as possible, at roughly the same height as the first impact. This location is used to assess the barrier's connection to the supporting structure. Additional impact locations on the barrier may be required at the discretion of FM Approvals (e.g., hinges, plastic parts, etc.).

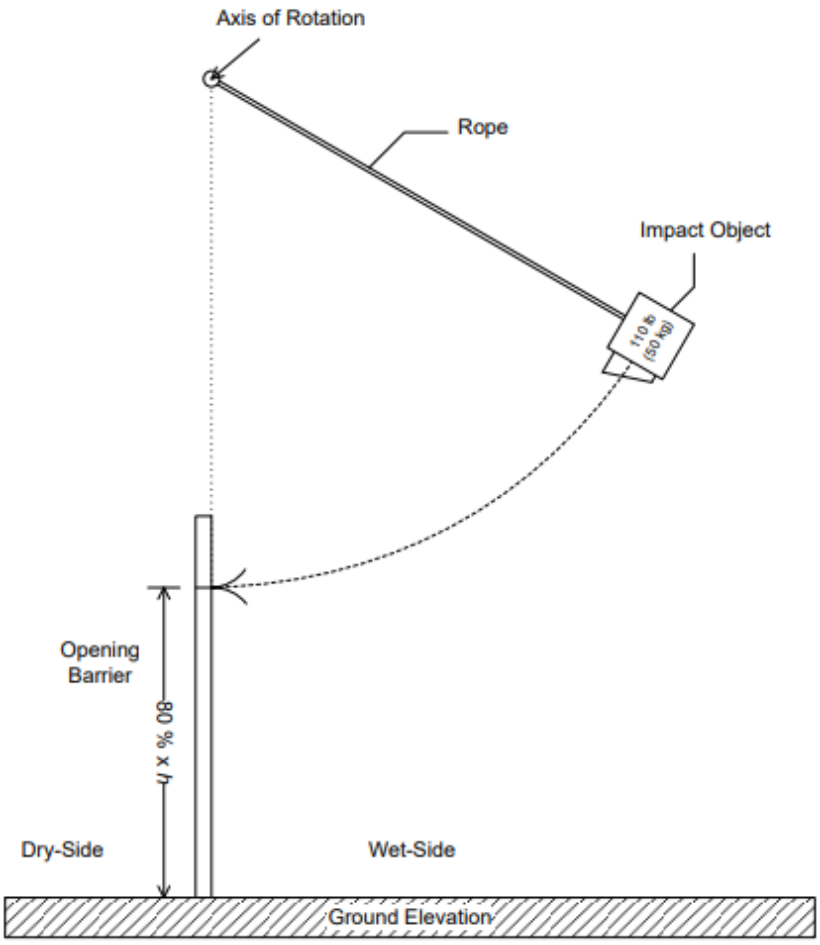


Figure 2.1: Impact test scheme. [4]

The energy of 600 J is derived using the formula for potential energy:

$$E = m \cdot g \cdot h \quad [Joule] \tag{2.1}$$

where $m = 50$ kg is the mass of the impact object, $g = 9.81$ m^2/s is the gravitational acceleration, and $h = 1.22$ m is the height from which the impacting object falls.

2.1.1.6 Post hydrostatic load test

Do the Hydrostatic Load Test again. Each post-impact test phase should last at least 1 hour at each water level. If the leakage rate increases, FM Approvals may extend the test duration.

2.2 British standard

All information about the British standard is taken from document [11].
The British Standard, like the FM Approvals, specifies the criteria to be met for the performance, the test method, the production, and the manual for different types and configurations of flood resistance products. The British standard covers flood resistance products designed for the temporary sealing of building openings and property entrances exposed to static floods that rise at least 54 cm above the threshold level of the opening. The standard includes boards, skirt and wall sealant systems, and flood doors, all of which are designed to be operational for water depths from ground level to the maximum design height. It applies to wall aperture closure systems and foam products. The standard is applicable to building openings with a nominal width of up to 6 metres.

A major difference between the British standard and the FM Approvals can already be seen in the requirements for watertightness. The British standard is much stricter and only allows a leakage rate of 0.5 litres per hour per metre of product seal width or opening width, whichever is greater.
There is also a difference in terms of the test procedure. The British standard requires more test sequences which are divided into three cycles:

- First, the barrier to be tested must be installed.
- Execution of the first cycle
  - a static head leakage test, including dynamic impact test,
  - a wave leakage test,
  - a current leakage test.
- Disassembly and redeployment of the test specimen,
- Execution of the second cycle:
  - a static head leakage test,
  - a wave leakage test,
  - a current leakage test.
- Disassembly and redeployment of the test specimen,

- Execution of the third cycle:
  - a static head leakage test (different from the previous).

Before and after each test, some pictures and relevant information, such as deployment time, deformations, and movements of the tested barrier, should be taken and noted.

2.2.1 Static leakage test

In a first step, the test system must be filled up to 1/3 (±0.5 cm) of the maximum design depth. Then, after 1 hour, the total leakage has to be measured. During this time span, the water depth has to be kept constant with a maximum variation of ±1 cm. Now, only for the first cycle, the two impact tests are executed. In a second step, exactly the same is done except that the system is filled up to 2/3 of the water design depth. Then, in a third step, the system is filled up to the full height (±0.5 cm) of the maximum water design depth. This time, the water level has to be maintained (±1 cm) for a period of 18 hours. The total leakage over the first and the last hour has to be measured, respectively.
The static leakage test for the third cycle is a bit different and somewhat the reverse of the others. First, the system is filled for 24 hours up to the total height of the maximum water design depth. The total leakage is measured over the first and the last hour of the test. Second, the water level is reduced to 2/3 of the maximum design depth and maintained for 1 hour and the total leakage is measured. Finally, the water level is reduced to 1/3 of the maximum design depth and again maintained for 1 hour and again the total leakage is measured.

2.2.2 Wave leakage test

For the wave leakage test, the water level in the test apparatus is set according to the middle column of Figure 2.2. DMWD is the designated maximum water depth. Then, random waves with a JONSWAP spectrum should be applied. The waves should have a significant wave height of 10 cm (±1 cm) and a mean wave period of 1.03 seconds. These waves should be directed perpendicular to the face of the building opening. A temporary barrier or similar should be added on top of the tested barrier to prevent water from overtopping. Measure the total leakage over a period of 30 minutes. The

static water depth in the test apparatus has to stay constant (±1 cm) before and after the wave test.

DMWD	Wave testing depth	Current testing depth
Apertures		
540 mm to 840 mm	$\text{DMWD} - \left(\frac{((\text{DMWD} - 540) \times 50)}{100} + 150 \right)$	DMWD – 100
>840 mm	DMWD – 300	DMWD – 100

Figure 2.2: Wave and current testing depths. [11]

2.2.3 Current leakage test

Similar to the wave test, for the current leakage test the test apparatus must be filled to the water level mentioned in the right column of Figure 2.2. Then, a water flow parallel to the opening should be applied to reach an average velocity of 1 (±0.1) m/s on the vertical centreline of the opening, at mid-depth above the invert level, 15 cm from the external face of the test barrier. As for the other tests, the water level should stay constant.

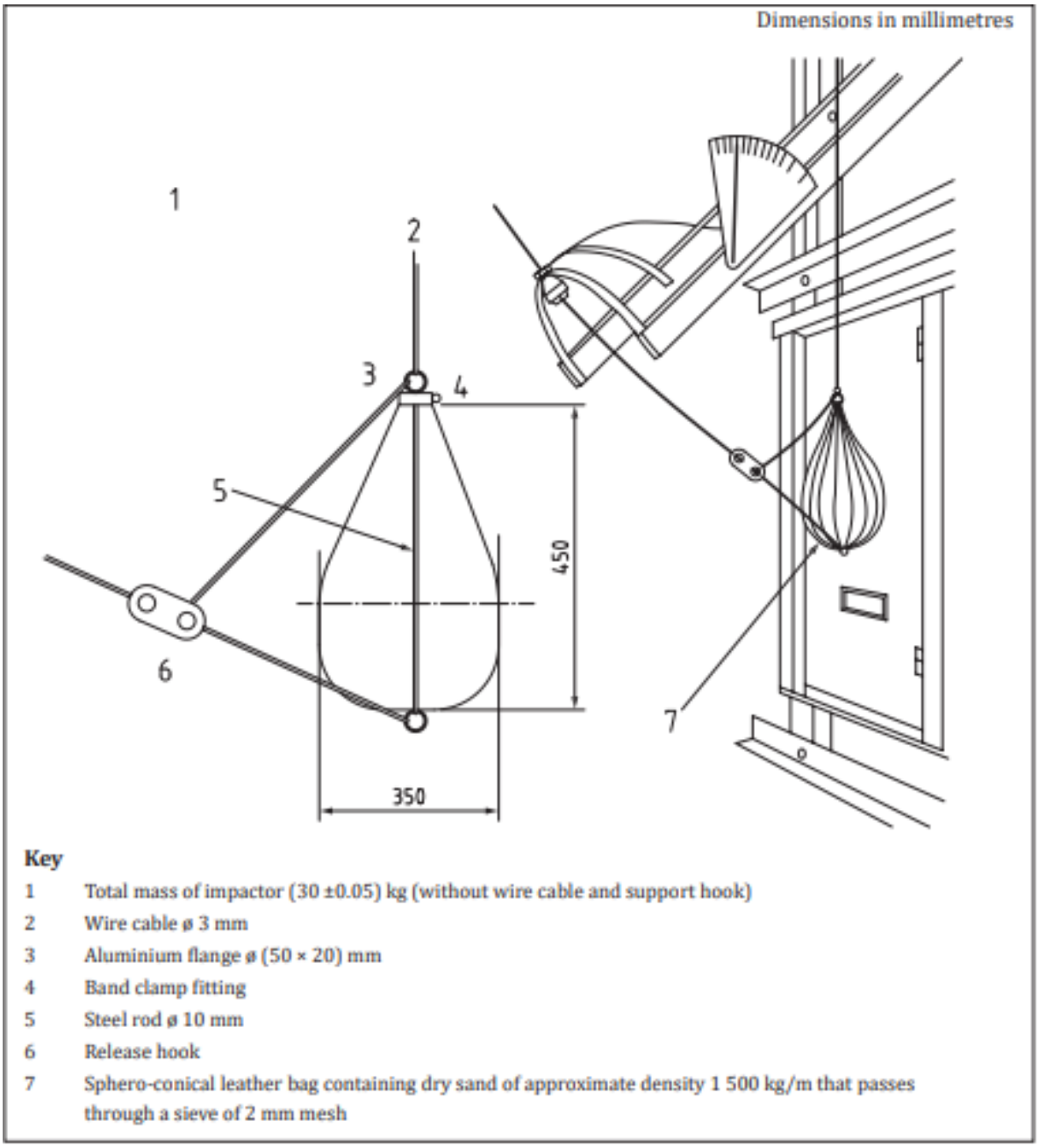
2.2.4 Dynamic impact test

As for the FM Approvals, the dynamic impact test in the British standard is used to simulate floating debris. The barrier should be able to resist two impacts. Another common feature is that a pendulum is also used here to carry out the test.

In terms of the performance criteria to be met, there is already a major difference in the British standard compared to the FM Approvals. The FM Approvals only require that the watertightness (with a limited leakage) of the barrier must remain intact after the impact test. In order to be certified by the British standard, the barrier may only have a limited deformation in addition to a limited leakage. The maximum plastic deformation resulting from the impact must be less than L/120 or 2.5 cm, whichever is smaller. L is the width of the opening.
Another difference to the FM Approvals is that the test apparatus is not emptied. The impact test is carried out after the first leakage test, when the water depth is 1/3 of the maximum design water depth. Both, the first and the second impact, should hit the barrier in a predetermined weak point. If no such point exists, then the first impact

should be located at the horizontal centre of the barrier at a height of 20 cm above the static water level. The second impact should also be located at the horizontal centre but at a height of 80% of the maximum designed water depth. Here, the second impact test is not carried out at the edge of the barrier to test the stability of the connection, as is the case with FM Approvals.
There is also a difference between the standards in the impact object itself. The FM Approvals use a wooden block, i.e. a hard body object. The British standard, on the other hand, only requires that the barrier must be able to withstand a soft body object. The object consists of a leather spherical-conical bag filled with fine, dry sand. The bag should have a diameter of about 35 cm, resulting in a total weight of 30 kg when filled with sand (grain size < 2 mm and density $= 1500$ kg/m^3). The British standard also precisely describes the resting position of the object: The impact surface of the object should not be more than 1 cm from the flood barrier surface and no more than 2.5 cm away from the determined impact point in any direction. The impact object should be attached to a cable of at least 1.5 m and aligned in such a way that the pendulum movement is in a plane perpendicular (with a permitted deviation of 5°) to the impact surface. A scheme of the impact object and the impact apparatus is shown on Figure 2.3.
To execute the test, the impact object must be lifted such that the vertical distance between the gravitational center of the impact object and the impact point on the barrier is 80 cm (± 1 cm). Then, drop the object and let it fall under gravitational acceleration. Due to the circular trajectory of a pendulum, the object will hit the barrier at its horizontal position. After each impact test, the final deformation must be measured and recorded and the barrier must be checked for proper functioning. Finally, the total leakage should be measured over one hour at a constant water level.

By using the formula for the potential energy as described in equation 2.1 and the corresponding values as described above, a initial potential energy of $E = 235.44$ J is found. This corresponds to just over a third of the energy used in FM Approvals to certify flood barriers. The FM Approvals provide flood barriers that are much more resistant to impact in comparison to the British standard.



Key

1	Total mass of impactor (30 ±0.05) kg (without wire cable and support hook)
2	Wire cable ø 3 mm
3	Aluminium flange ø (50 × 20) mm
4	Band clamp fitting
5	Steel rod ø 10 mm
6	Release hook
7	Sphero-conical leather bag containing dry sand of approximate density 1 500 kg/m that passes through a sieve of 2 mm mesh

Figure 2.3: Dynamic impact test of the British standard. [11]

2.3 German guideline

Unlike the FM Approvals and the British standard, which also apply in several applications, the German guideline is limited to windows and doors and their connection to the building. Even though this guideline primarily applies to windows and doors, it can also be considered applicable to flood barriers, as their aim is similarly to prevent water infiltration.
The directive defines a closure as watertight up to a certain water level if no water is detected at the inside of the closure over a 24 hour period. Even if a certain leakage exists the closure is still classified as flood resistant if the leakage is limited to 240 Liters within 24 hours (10 L/h). In addition to the limited leakage rate, the German directive requires that a closure must be able to withstand a water level of at least 0.5 metres. Furthermore, as the directive primarily applies to windows and doors, the glazing and load-bearing components that are important for stability, such as window mullions, must not break due to water pressure. [9]

For the test execution, the test specimen must be installed in a suitable four-sided surrounding concrete frame in accordance with the installation instructions. Alternatively, a steel frame can be used if the installation is carried out in an existing wall opening and sealing to the masonry is ensured.
As for the FM Approvals and the British standard, a suitable test apparatus, which allows to fill the required water levels on the water-exposed side, is needed.
In a first step, the water depth will be raised to a level of 0.5 m. Then, the water level is increased in 0.5 m increments until the first water entry. Next, the test apparatus is emptied and the test specimen is dried at open state before re-closure. In a second step, the test apparatus is filled to the last water depth without leakage. Then, the water level is increased in 0.1 m increments until failure or until the highest water level desired by the user. The water level has to stay constant (± 2 cm) for a period of 24 hours and the total leakage has to be measured. During the test, when increasing the water level, the rise must not exceed 0.1 m/min. [9]

There is a second German guideline that is almost identical to the one described above. The difference lies in two small impact tests that are carried out before the watertightness test. The first is a 'soft' impact, performed according to DIN EN 12600 (impact test of glass in construction) with a drop height of 75 cm. The second is a

'hard' impact, involving an object suspended from a double pendulum with a diameter of 10 cm and a weight of 10 kg. The impact surface is made of beech veneer wood with bevelled edges of 2-4 mm. The 'hard' impact is made with a drop height of 60 cm, 1x at all corners (20 cm from the edge) and 3x in the centre. The aim of both tests is to simulate the impact of flowing water. However, as there is no test of the dynamic pressure and as there is no real flowing water, this test is not really meaningful. [15]

As already mentioned, the German guideline is designed for doors and windows rather than flood barriers. As far as watertightness is concerned, the guideline is not as strict as the FM Approvals or the British standard. There is also no dynamic impact test to simulate the impact of floating debris. Windows and doors certified with this directive can be used in new buildings or renovations, such as basement windows, as they still offer a certain degree of protection. Additional flood barriers would no longer be necessary if floating debris can be avoided. Such certified windows and doors also provide protection against fully submerged openings, at least to a certain extent. Flood barriers do not necessarily fill the opening completely and as soon as the water level rises higher than the barrier, water will still enter. The guideline could be further improved, for example, by applying certain criteria from FM Approvals so that doors and windows are designed to automatically function as flood protection barriers. However, as this is not the aim of the work, this approach will not be described in further detail.

2.4 Impact test

As previously described in the section on FM Approvals, the object of 50 kg is raised to a height of 1.22 m above the impact point on the barrier to generate an impact energy of 600 J. This would mean that it is assumed that 100% of the potential energy is converted into kinetic energy, since a weight of 50 kg at a height of 1.22 m would correspond to close to 600 J of potential energy.

In reality, however, a small part of the initial potential energy is lost through air friction and the kinetic energy is smaller. The question now is whether the portion lost due to friction is small enough to be negligible.

Another observation is that the vertical distance of 1.22 m is measured at the tip of the impact object. The relevant height to calculate the potential energy is actually the height of the centre of gravity. Measuring the height at the tip of the object instead of the centre of gravity could result in false potential energies.

The resulting questions are dealt with and analysed more in detail in Chapter 3.

2.4.1 Contextualising 600 Joule

For the impact test, FM Approvals requires the flood barrier to withstand an impact energy of 600 Joule. But are 600 J reasonable? And what do 600 J physically represent? In order to know what 600 J represents in terms of floating debris, it is necessary to know on the one hand what floating debris is common and on the other hand the velocity of this floating debris.

2.4.1.1 Flow velocity

It can be assumed that flood debris flows at the same velocity as the water [17]. To determine the impact energy, it is therefore central to know the velocity of flood water.

Among other things, the paper "Constructions sur pilotis : Étude de prédimensionnement pour des bâtiments résidentiels situés en zone d'aléa" [10] deals with data on water velocities during floods with return periods of 25, 50, 100 and 1000 years. More

specifically, it is about data on the catchment area of the Vesdre river, which includes communities like Pepinster or Theux, as can be seen in Figure 2.4. The values of the four return periods also take into account the 2021 floods. In total, 18 sites have been analysed.



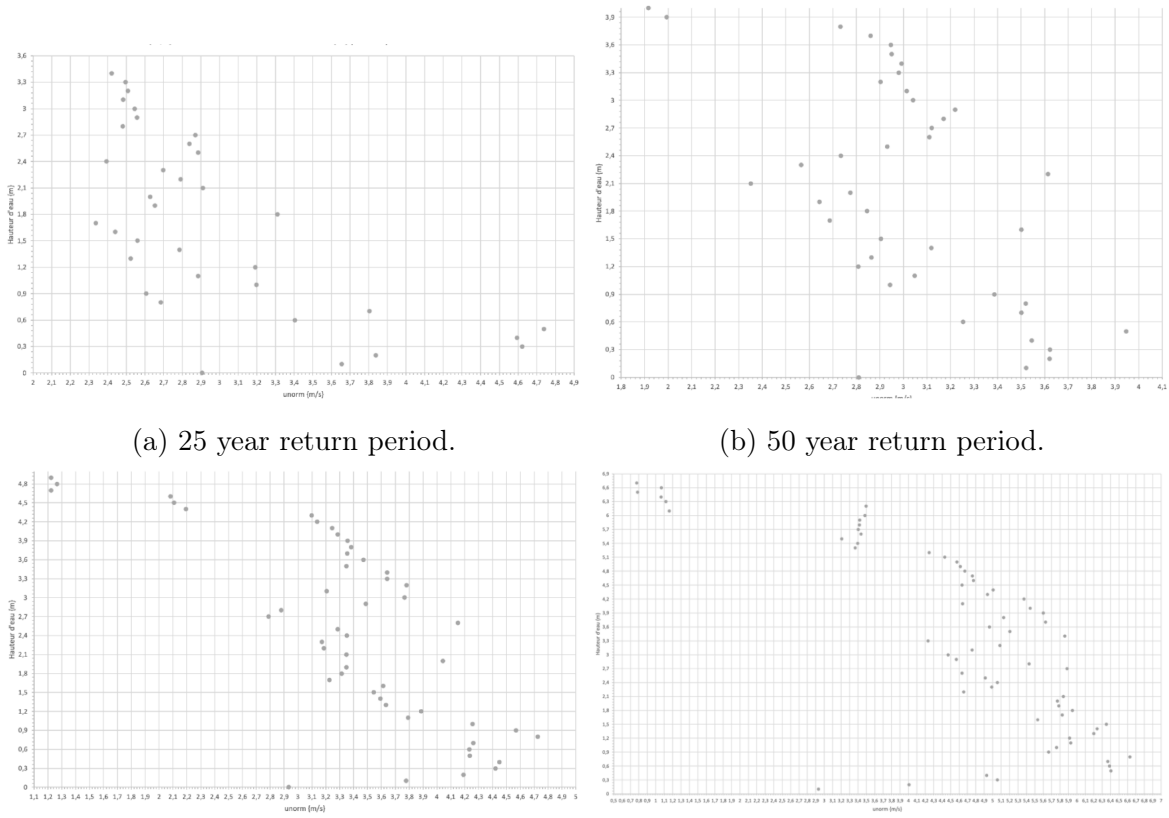
Figure 2.4: Catchment area of the Vesdre river. [10]

The data was sorted to find the maximum velocity per 10 cm of water height at each site. This made it possible to determine the value of the highest water velocity per 10 cm of water height for all 18 locations. This was done for all four return periods. Figures 2.5a, 2.5b, 2.5c, and 2.5d show the maximum water velocity as a function of different water depths (every 10 cm) for the 25, 50, 100, and 1000 year return period, respectively.
Locking only at water heights up to one metre, the following velocity variations can be observed for the different return periods:

- 25 year return period: 2.6 to 4.74 m/s.
- 50 year return period: 2.8 to 3.9 m/s.
- 100 year return period: 2.9 to 4.73 m/s.
- 1000 year return period: 2.93 to 6.64 m/s.

Furthermore, for water depths up to one metre and taking not only the maximum velocities, the biggest part of the flow velocities fall into an interval of 0 to 4.5 m/s

except for the 1000 year return period where the maximum values lay mostly above 5 m/s. The values shown in Figure 2.5a can also be found in the form of a list in Appendix A.



(a) 25 year return period.

(b) 50 year return period.

(c) 100 year return period.

(d) 1000 year return period.

Figure 2.5: Water velocity as a function of the water depth for different return periods. [10]

The velocities obtained correspond to velocities along the river. It is therefore quite possible that the flow velocities in streets are more likely to be in the lower range of the interval.

This can be confirmed by values found in the work done by Adyns L. and Adriaens D. in 2022-2023 [1]. This work was carried out in association with Buildwise as part of the project FLOOD and presents an experimental study of the resistance of buildings to flooding.
A water velocity lower than 3 m/s was assumed to simplify calculations by allowing the

neglect of the hydrodynamic impact. In an experimental part, a small scale dam break and the effects on a building were simulated. Among other things, the water velocity was measured. The measurements showed a velocity variation from 0 to around 2.2 m/s over time. Furthermore, a numerical model has been done to reproduce the experiment, which confirms the velocities.
A numerical model has also been applied to the July 2021 floods in Pepinster. The aim was to determine the pressure and the forces acting on the buildings. This also includes the water velocities when they meet a building facade. The velocities perpendicular to the facades varied from very small values up to 3.05 m/s.
The simulations and on-site investigations revealed considerable damage to some buildings, which of course also depends on the position and condition of the building, even if only slow velocities were detected on the facades. [1]

In conclusion, it can be said that the impact velocity and thus the velocity of the impact objects vary from 0 to about 7 m/s. Here the velocity is limited to a maximum of 4.5 m/s, as higher velocities only occur in extreme floods and only along the river.

2.4.1.2 Floating debris

Flood debris consists of loose, unattached objects floating on the surface of rivers, lakes or oceans. This can include natural elements like branches, logs, and other plant matter, as well as human-made objects such as plastic products, cans, and other forms of litter. During floods, cars, building materials of any kind, even entire houses or anything else that becomes detached can become floating debris.
Accumulations of floating debris along rivers or in cities, mostly on bridges, lead to blockages that further worsen flooding and damage the bridge. In addition to such accumulations, floating debris can also be swept into the streets by the water and cause damage to buildings when hitting them.

According to Daan Poppema, a postdoc researcher at the TU Delft who works on floating debris during the 2021 floods, trees are the most common type of flood debris. During the 2021 flood, they made up to 50% of the total debris volume in Belgium and Germany. Sometimes they were trees with branches on them, but mostly the branches were broken off, resulting in several logs. Even though the longest trees observed were slightly longer than 10 metres, they only make up a very small proportion of the total

volume. Smaller logs are much more common. The other type of debris, which takes up a larger part of the total volume, is construction wood and building rubble. This ranges from wooden beams and insulation parts to the roofs of buildings. But larger objects such as cars, caravans and tanks or containers of various sizes are also included, even if they only make up a small proportion. The largest object observed was a ship container. Figures 2.6, 2.7, 2.8, and 2.9 show an accumulations of debris from the 2021 flood. As can be seen, some of the aforementioned floating debris is present. Usually, such accumulations are smaller than the one shown in Figure 2.6 and contain more tree pieces.



Figure 2.6: Debris accumulation, Germany 2021 (photo by D. Poppema).



Figure 2.7: Debris accumulation, Belgium 2021 (photo by D. Poppema).



Figure 2.8: Debris accumulation, Belgium 2021 (photo by D. Poppema).



Figure 2.9: Debris accumulation, Belgium 2021 (photo by D. Poppema).

The above-mentioned flood debris occurs in rivers. Some roads along rivers can turn into rivers during floods. Then, a greater water depth and higher water velocity allows large objects to float along. On many roads, however, the flow velocity and water height are reduced and large objects such as cars are dragged across the road surface or do not move at all. Since the flood barriers are only about one metre high, it is very unlikely that they are exposed to an impact by a large and heavy object. Nevertheless, for completeness, the flood debris is divided into classes to see which impact energy results:

- Class 0: Logs (100 kg).
- Class 1: Trees (565 kg).
- Class 2 (reduced): Cars (700 kg).
- Class 2: Cars (1400 kg).
- Class 3: Containers (2300 kg).

The impact energy corresponds to the kinetic energy and is calculated using the following formula:

$$E_{kin} = \frac{1}{2} \cdot m \cdot v^2 \quad [Joule] \tag{2.2}$$

where m is the mass, and v is the velocity. The following two hypothesis are made:
- The velocity of the object equals the velocity of the water.
- The objects are floating entirely.

The second hypothesis does not apply to class 2 (reduced). A friction coefficient of 0.5 was applied here, which is intended to simulate dragging across the floor.
By using aforementioned masses and the flow velocities of the previous subsection and inserting them into Equation 2.2, the graph shown in Figure 2.10 was obtained. As can be seen from the graph, the impact energy for a speed of 2 m/s for class 0 is 200 J. Even at a higher speed of up to 3.4 m/s, a barrier certified with FM Approval would be able to withstand a Class 0 floating debris. For all other classes, the impact energy at 2 m/s is already over 1000 J. At 4600 J, class 3 has more than seven times the minimum impact energy.

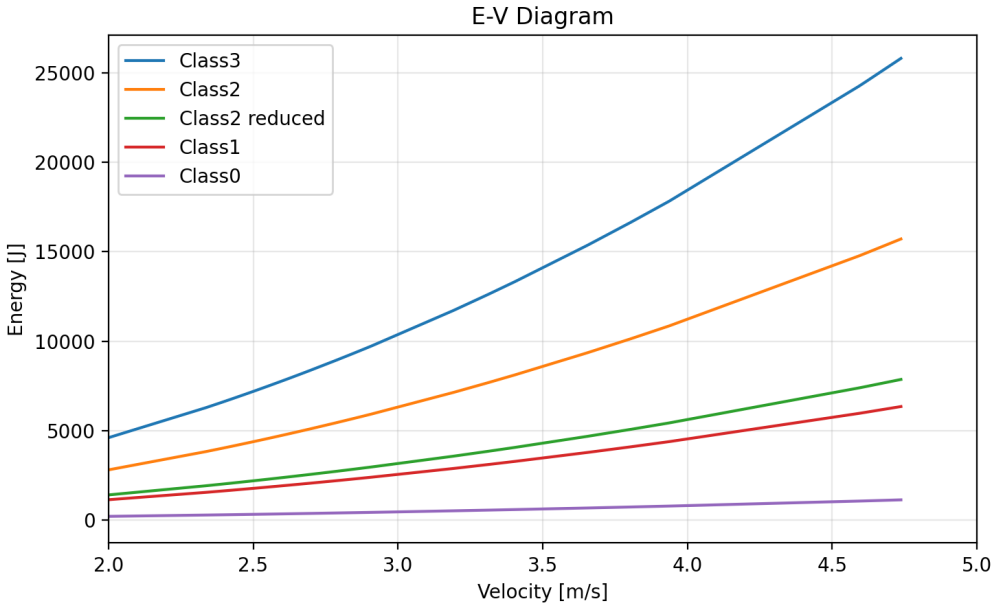


Figure 2.10: Impact energy in function of the velocity.

Figure 2.11 depicts a larger variation of masses that could represent bigger flood debris, such as containers and vehicles. Even for a low velocity of 1.5 m/s, almost all cases would lead to an impact energy much bigger than 600 J. A flood barrier would probably not withstand such impacts.

The higher velocities and heavy objects, along with the resulting high impact energy shown at the top right of the graphic on Figure 2.11, illustrate the destructive power of floods.

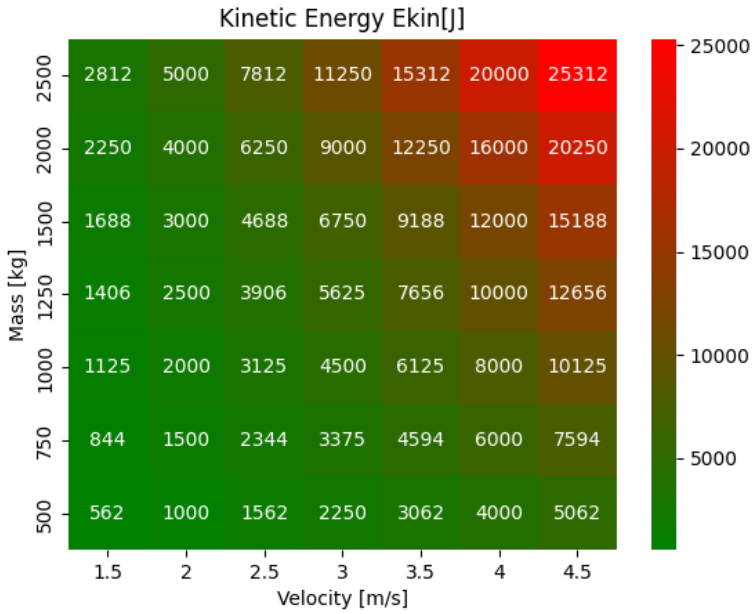


Figure 2.11: Impact energy for large objects.

Even if 100 kg of wood gives a better idea of what 600 J represents, this is not satisfactory yet. As previously stated, wood is the most common type of flood debris. A big part of wooden flood debris is due to dead wood.

Forests have many positive effects against natural hazards. The roots of the trees mechanically reinforce the upper soil layers and reduce erosion and superficial landslides. In addition, the forest has positive effects on soil properties such as a higher infiltration capacity and faster drainage of the water storage capacity. All of these factors help to protect against flooding. The effect depends on the condition of the forest and the soil properties. However, riparian vegetation leads to driftwood. Various processes such as landslides, bank erosion and windthrow ensure that wood ends up in streams. Even though deadwood naturally provides important ecological functions - such as altering the hydrodynamic behavior of water, providing food, and creating habitats - it also plays a significant role in the risk of flooding. [8]

To analyse the driftwood present in riverbeds, 10 different 1 km long stream sections in the Swiss Alps and Pre-Alps were studied. All pieces of wood with a length of at least one metre and a diameter of 10 cm were included. In total, 6,728 pieces were counted. About one-third of the pieces consist of whole trees or trunk sections with root plates. These pieces are particularly dangerous when transported. The majority of the wood pieces, approximately 80%, have a length of less than 5 m and a diameter smaller than 23 cm as can be concluded from Figure 2.12 and Figure 2.13. The y-axis shows the number of logs, while the x-axis displays the length and diameter, respectively. [8]

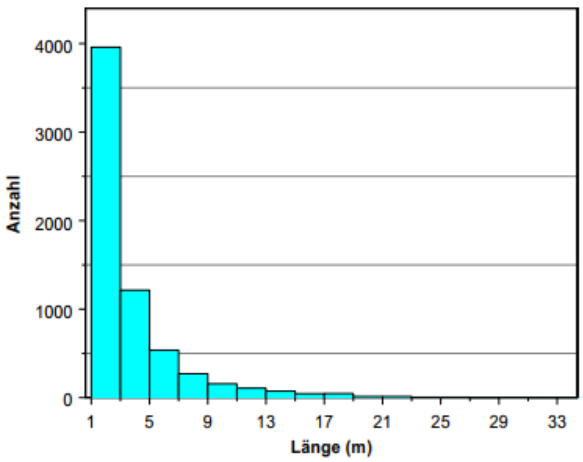


Figure 2.12: Distribution according to length. [8]

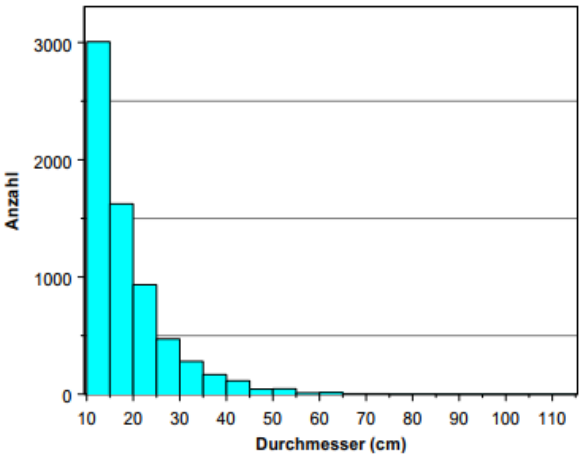


Figure 2.13: Distribution according to diameter. [8]

Since only a limited number of observed sections are available and each studied section has its own individual characteristics, the results are not necessarily transferable to other regions. [8]
Since around 50% of the floating debris in the 2021 floods was attributable to wood and, as described above, it was mainly smaller logs, it can be assumed that the results of the research carried out in Switzerland can also be applied to Belgium and Germany.

Since several parameters can be varied to calculate the impact energy, both the object length and the volumetric weight are assumed to be constant. Only the diameter and the flow velocity will be varied.
Referring to Figure 2.12, and considering 80% of the total number, an average length of 2 metres can be determined for driftwood. The volumetric weight is set at 700 kg/m^3

as this is an average value. The following diameters are used for different sizes: 10 cm, 15 cm, 20 cm, 25 cm, and 30 cm, as can be seen in Figure 2.13 For the flow velocity, the values described in the previous subsection are used. Calculating the different energies, the diagram in Figure 2.14 was obtained.
As can be seen in the lower and left parts of the graph, the impact energy for small diameters and varying velocity or small velocity and varying diameters is relatively small. However, it can also be seen that the values in the upper right area of the graph are in or slightly above the required order of magnitude.

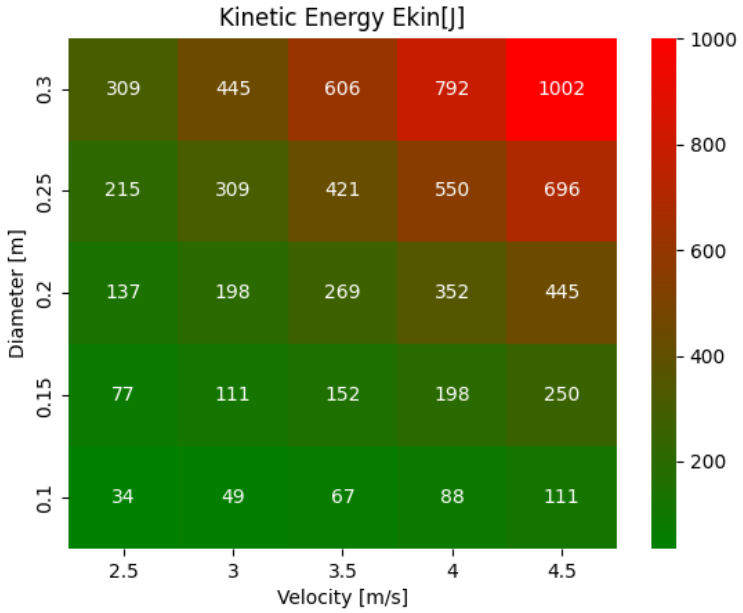


Figure 2.14: Impact energy for common driftwood with a density of 700 kg/m^3.

One parameter that is assumed to be constant in the Figure above is the density of the wood. However, Belgium has many different tree species such as oak, beech, ash, maple, larch, pine, birch, spruce and poplar. In reality, the wood density therefore is subject to great variation. Additionally, the moisture content also plays a role in the variation of density.

Figure 2.15 shows the variations in impact energy when the density varies in addition to the velocity and diameter. For the density, the values were varied in steps of a hundred from 500-900 kg/m^3 to cover as large a range as possible. [14]. For wood

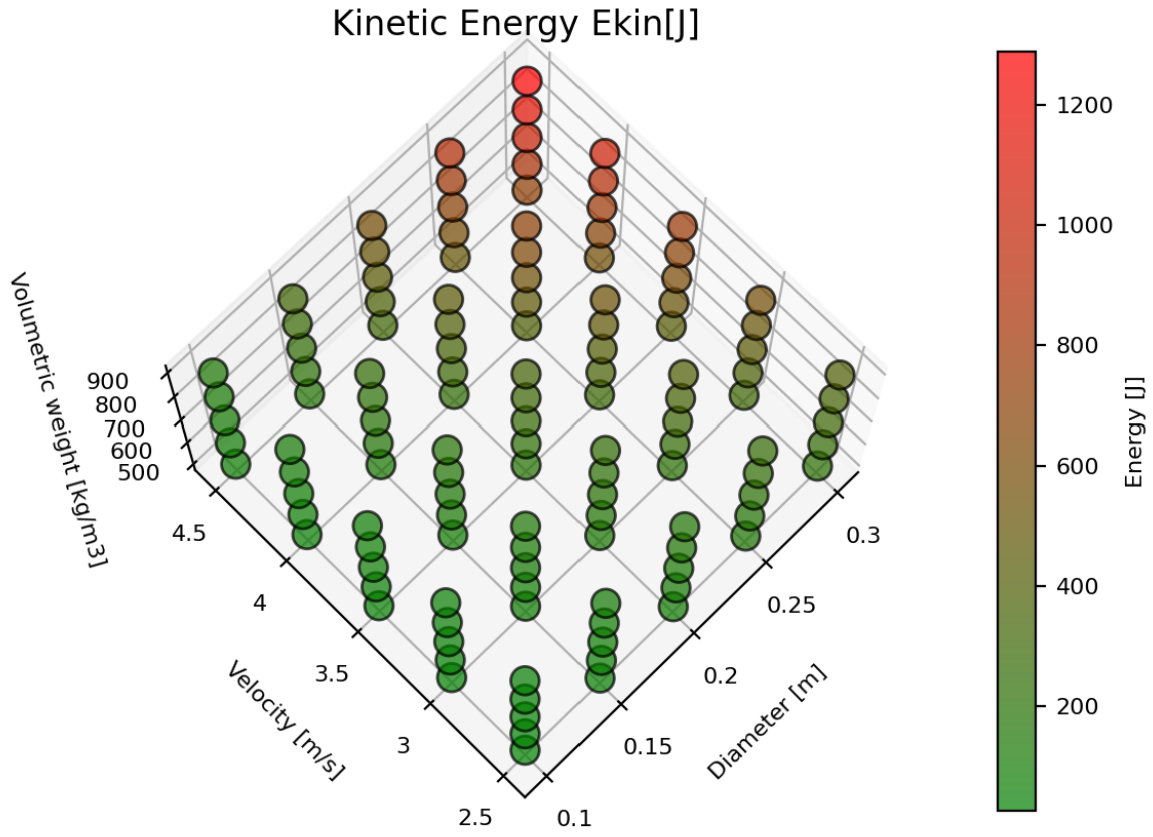


Figure 2.15: Impact energy for common driftwood with varying density.

with a density of 400 kg/m^3, all values in the range of the considered velocities and diameters are below 600 J and therefore not explicitly represented in the graphic. The lower the density, the lower the energy. As can be seen, for a density of 500 kg/m^3, all but the most extreme values, i.e. a speed of 4.5 m/s and a diameter of 30 cm, are below 600J. The greater the density, the more values fall into the range above 600 J. In all cases, the values for low velocities and diameters remain far below 600 J. The logs with intermediate velocities and diameters approach the value of 600 J quite well. Appendix B contains 2D Graphics for the different densities.

A precise specification of the dimensions of an object would be as follows: A log with a density of 700 kg/m^3, a length of 2m and a diameter of 30 cm at a flow velocity of just under 3.5 m/s would impact with an energy of 600 J.

2.5 Velocity analysis of the July 2021 flood in Pepinster

Pepinster, a town in the Belgian province of Liège, was hit very hard by the 2021 floods. The town is situated at the confluence of the Vesdre river and its tributary, the Hoëgne river, which worsened the situation. Figure 2.16 shows a satellite image of the city and the course of both rivers. The flooding of both rivers caused immense economic damage and even claimed lives. The whole centre of the city was submerged, as shown by two different views on Figure 2.17 and Figure 2.18.



Figure 2.16: Course of the Vesdre and Hoëgne river. [1]



Figure 2.17: Pepinster flood. [2]



Figure 2.18: Pepinster flood. [13]

2.5.1 Visualisation of the traces left behind by the flood

Figure 2.19 shows a house which stands directly alongside the river. The rising water levels and their velocity caused high hydrostatic and hydrodynamic forces and a huge hole was torn into the wall due to scouring, which led to instability in certain areas as can be seen. Other buildings were even completely washed away. Not everywhere there was such extensive external damage.

In a lot of buildings, doors and windows have been destroyed by the water masses as illustrated in Figure 2.20. Figure 2.21 shows a facade from which a piece was torn out due to an impact. As can be seen in the example in the picture, the height of the impact is approximately in the area of the lower half of a door. This illustrates how important it is that the flood barriers are tested for impact. In Figure 2.22 it is possible to see how high the water was in the street from the traces on the facade (approximately the mid-height of the door). At other locations, the ground floor has been completely submerged.



Figure 2.19: Damage due to scour. [6]



Figure 2.20: Broken windows. [20]



Figure 2.21: Damage due to impact. [20]



Figure 2.22: Water traces up to the middle of the door opening. [20]

2.5.2 Velocity analysis

Based on the analysed data from L.Adyns and D.Adriaens from 2022-2023 [1], an analysis on the velocities present during the 2021 flood has been done.
For the analyses and simulations, the hydrodynamic numerical simulation code "Watlab" has been used. The blue area in Figure 2.23 represents the flooded area. The outline drawn in red represents the calculation domain, where a mesh for the simulation will be created. As can be seen, it does not exactly match the blue area, but is slightly larger. This serves to provide some security against inaccuracies in the blue area. The boundaries intersect at the outlets, where the inflow boundary conditions are established. The downstream boundary was selected because there is a significant decrease in housing density beyond this point. [1]

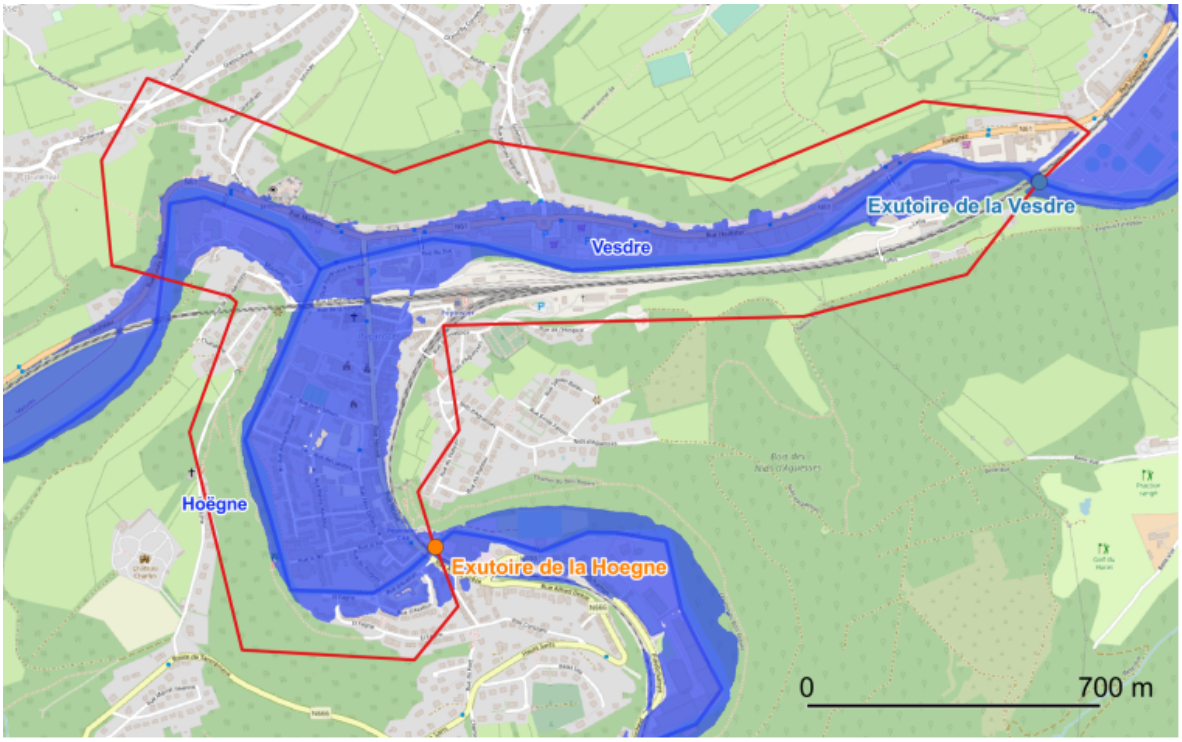


Figure 2.23: Flooded area and domain outline. [1]

Chloé Noiset, who has followed up on the work of L.Adyns and D.Adriaens and is working on simulations of the 2021 floods in Pepinster, has kindly provided some graphics and files on simulated flow velocities. For the simulation the following parameters have been used:

- Upstream boundary condition: The Vesdre hydrograph (in the top right of Figure 2.23) and the Hoëgne hydrograph (at the bottom of Figure 2.23).
- Downstream boundary condition: transmissive condition (in the top left of Figure 2.23).
- Manning coefficient: 0.06 [/]
- Mesh refinement: uniform mesh with a characteristic size of 10 m (121,925 cells in total).

The hydrographs have been constructed with the tool ATHYS and are shown in Figure 2.24.

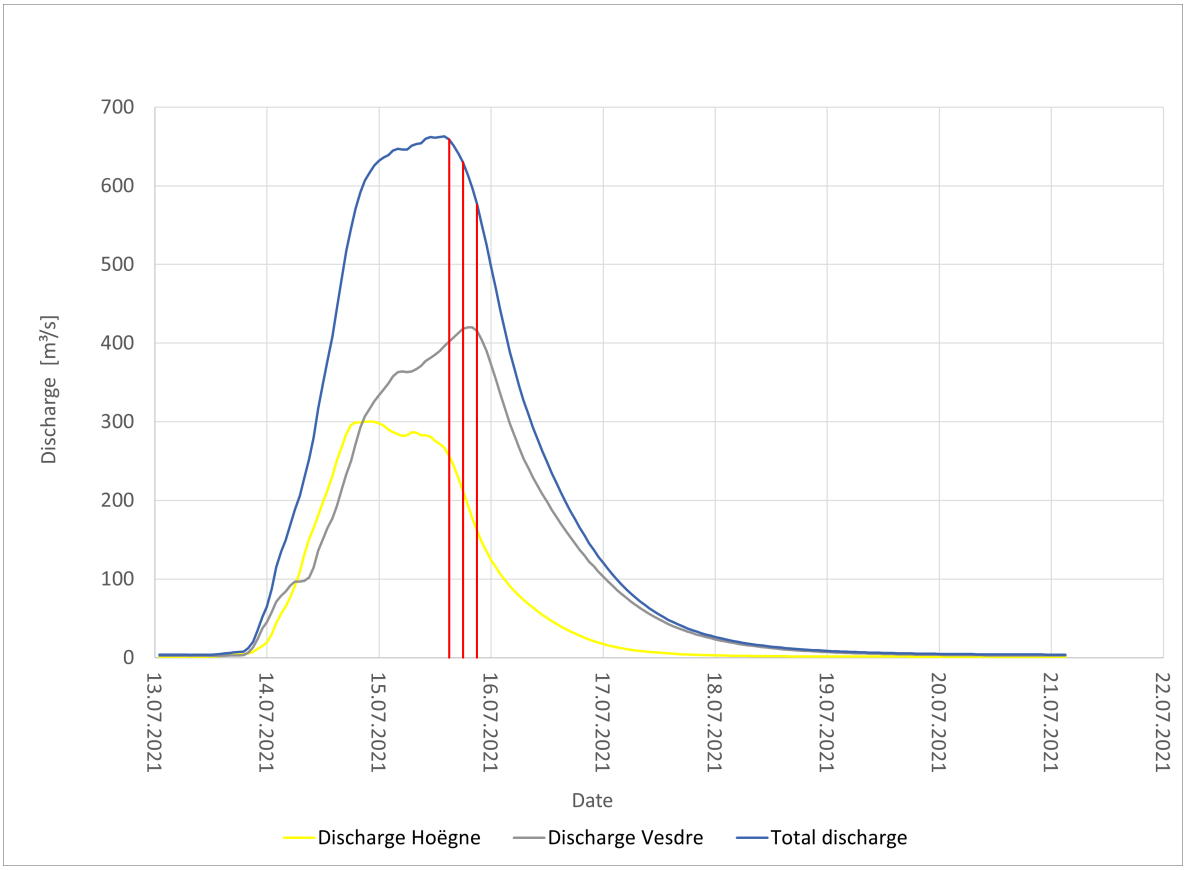


Figure 2.24: Discharge of the Vesdre river after confluence. [1]

The velocity analyses were carried out for three different time steps. The three instances are indicated in Figure 2.24 by the red lines and correspond to the following

times during the flood: 15:00, 18:00, and 21:00 on 15 July 2021. The corresponding velocities for each of the three cases are represented in the Figures 2.25, 2.26, and 2.27, respectively.

As can be seen, the velocity at 18:00 is slightly higher than for the time steps before (15:00) and after (18:00). It can also be seen that there are some areas with no velocity. This corresponds mostly to areas which remained dry. Furthermore there is a large area where the velocity is around 2-4 m/s, which matches the values described in section 2.4.1.1, although higher velocities, reaching values above 4.5 m/s, can be seen along the course of the two rivers. Regarding the very high velocities of 10-11 m/s, these are clearly inconsistencies related to boundary conditions. Therefore, they can be neglected.

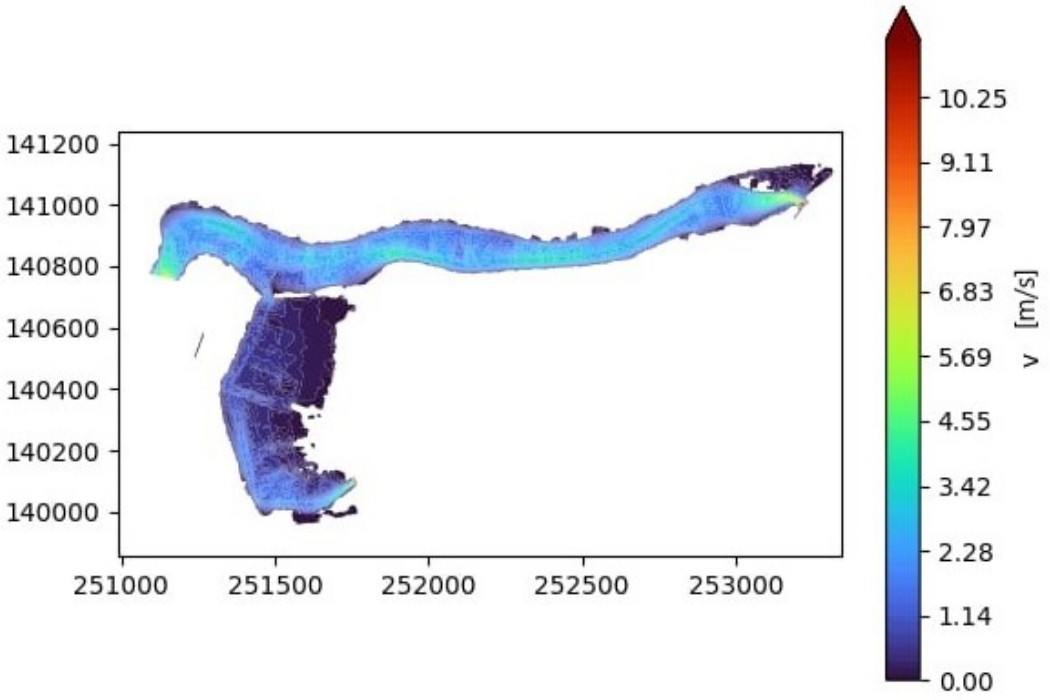


Figure 2.25: Velocity at 18:00 on 15 July 2021 (graphic by C.Noiset).

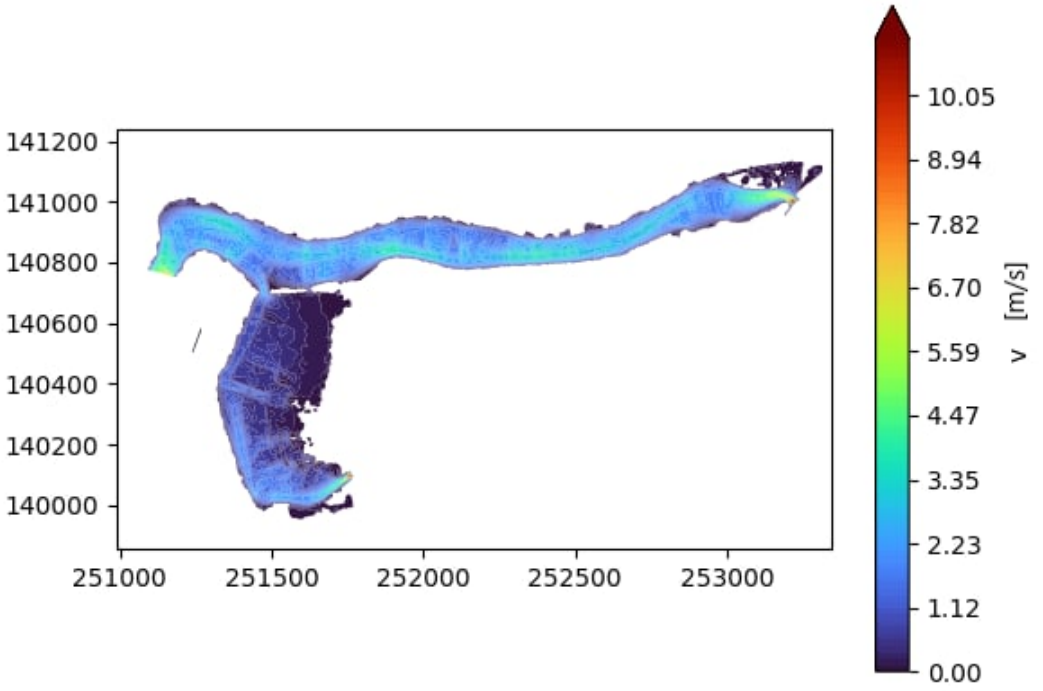


Figure 2.26: Velocity at 15:00 on 15 July 2021 (graphic by C.Noiset).

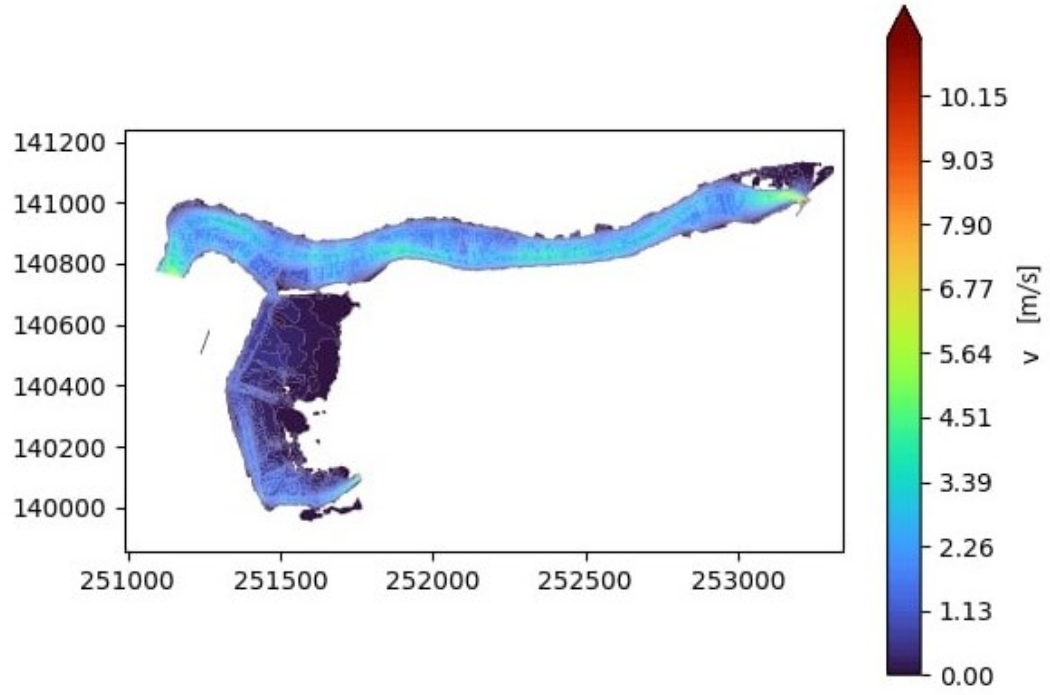


Figure 2.27: Velocity at 21:00 on 15 July 2021 (graphic by C.Noiset).

In order to have a more precise overview of the frequency of the velocities, some data from the simulation was extracted and processed manually. The output files contained, among other parameters, the water depth for each cell (i.e. 121,925 in each file) as well as the linear flow per unit length for the x and y directions. Knowing these two parameters, it is possible to calculate the velocities in the x and y directions by using equation 2.3 and than the total velocity by using the formula 2.4.

$$V_{x/y} = q_{x/y} \cdot h \tag{2.3}$$

where $V_{x/y}$ is the velocity in the x or y direction in m/s, $q_{x/y}$ is the linear flow per unit length in the x or y direction in m^2/s, and h is the water depth in m.

$$V = \sqrt{V_x^2 + V_y^2} \tag{2.4}$$

The data had to be filtered before and after calculations. First, all lines with a water depth $h < 0.01$ m were removed. To remove all lines with a value equal to 0 is obvious as in these cells no water is present. The reason to also remove all values up to 10cm is that objects will not flow for small water heights or are very small and will not have a high impact energy. All other water depths have been maintained even if the flood barriers have only a height of 1m. The reason to keeping higher values is that when the flood barrier is placed in a window opening, it will still be operational when the total water depth in the street is greater than 1m. Furthermore, this enables a more variable applicability for larger barriers. Secondly, once the velocities were calculated, all velocities $V < 0.1$ m/s were removed to avoid falsifications. Due to this filtering, the total number of remaining cells for each of the three cases varies slightly and is between 38,800 and 43,300.
The remaining values were divided into different velocity intervals, and then the percentage share of each interval in the total number was calculated. The results for all three cases are summarised in the Tables 2.2, 2.3, and 2.4, respectively. It should be noted that each class contains the value of the upper limit but not the lower limit, except for the first, where 0.1 m/s is included.

All three cases have very similar percentage distributions. Furthermore, very high values do not occur often and make up only a very small part. Over 90% of the velocities are below 3 m/s. As the hydrodynamic effect can be neglected for those values, the simplified calculations can be applied to determine the water pressure most of the time.

Velocity [m/s]	**# values**	**%**
0.1 - 1	16,551	35.04
1 - 2	11,068	23.43
2 - 3	12,379	26.21
3 - 4.5	2,523	5.34
>4.5	362	0.77

Table 2.2: Percentage distribution of velocities at 18:00 on 15 July 2021.

Velocity [m/s]	**# values**	**%**
0.1 - 1	16,511	38.18
1 - 2	11,675	27.00
2 - 3	12,282	28.40
3 - 4.5	2,415	5.58
>4.5	364	0.84

Table 2.3: Percentage distribution of velocities at 15:00 on 15 July 2021.

Velocity [m/s]	**# values**	**%**
0.1 - 1	13,500	34.71
1 - 2	11,013	28.31
2 - 3	11,770	30.26
3 - 4.5	2,322	5.97
>4.5	293	0.75

Table 2.4: Percentage distribution of velocities at 21:00 on 15 July 2021.

Around 60% of the velocities are below 2 m/s. Considering mainly smaller logs as floating debris as described in section 2.4.1.2, it can be concluded that in more than half of the cases, the impact energy on flood barriers is relatively small. In just over 30% of cases, the impact energy approaches 600 J. The higher flow velocities, which would cause a large impact energy, occur in the course of the river and not in the streets. Therefore, the probability of objects hitting barriers at such velocities is very low.

Barriers that are certified with the standard currently under development would be resistant enough in terms of impact to be used in floods such as the one in 2021.

Chapter 3

Experimental Part

This section presents the experimental part of this paper. It is divided into five subsections:

- As a first step, the materials are introduced. The first real tests on already tested barriers are described to get a feeling of how they work, as well as tests in a smaller model to determine the final setup and configurations.
- The second part contains an explanation of the final setup for the actual test series and the test procedure.
- In the third part, the results of the actual test series on new flood barriers are presented and analysed.
- In Part 4, the results of the tested barriers are compared to each other. Additionally, it is explained why different results occur and how they can be avoided.
- Part 5 proposes a recommendation for a final test procedure, incorporating the previous analyses.

For the sake of simplicity, the cameras are often described as camera 1, camera 2 and camera 3. They correspond to the following cameras:

- Camera 1: Photron Fastcam Mini type 800K-M-32G
- Camera 2: Photron Fastcam SA3 Model 120K-M1
- Camera 3: 25 Hz Aramis 3D DIC Camera

3.1 Test modelling

The small-scale model should serve to find a good working method and experimental setup to carry out the impact tests under the best possible conditions. However, as there were a number of ideas before the final test setup was developed, this section explains the reasons why and how the final test setup was chosen.
So starting with where the inspiration for this experimental set-up comes from, each individual stage of its development is then explained, from learning how to handle the material and the programs required to the final experimental set-up.

3.1.1 Inspiration of the test setup

The test setup was inspired by the tests described in the paper "Low-velocity out-of-plane impact tests on double-wythe unreinforced brick masonry walls instrumented with optical measurements" [16]. In this test series a pendulum with a certain weight and height is released onto brick walls, similar to the impact tests on the flood protection barriers. The test setup is shown in Figure 3.1.

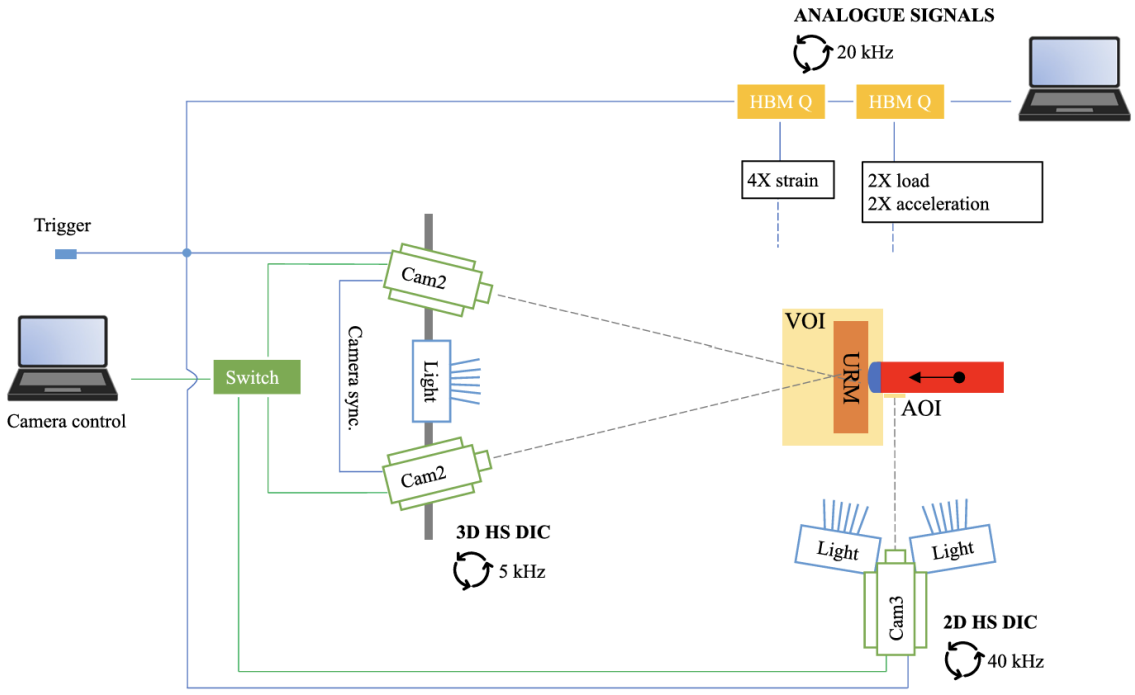


Figure 3.1: Setup low-velocity out-of-plane impact tests on double wythe unreinforced brick masonry walls instrumented with optical fibre measurements. [16]

In this setup, two different data acquisition systems were used. One collected the analogue signal data, including the measurements of the post-tensioned rods and the accelerations of the drop weight by accelerometers. The other was used to collect data from the three HS DIC (Digital Image Correlation) cameras. The 2D HS DIC camera was used to monitor the movement of the drop weight, i.e. the displacement, velocity and acceleration. It was equipped with a 200 mm focal lens and was positioned about 1.9 metres away from the drop weight, perpendicular to it. The 3D HS DIC cameras, which were synchronised with each other, were intended to measure the deformation of the wall.

We had no accelerometers available for our setup. However, in the orignal setup the accelerometers and the 2D HS DIC cameras both measurered the accelerration of the drop weight and when comparing the results from the accelerometers for the impact speed with those from the 2D HS DIC camera, very good agreement was found with a few oscillations around the average value, but with little or no influence on the main impact measurements. Therefore, removing the accelerometers from the setup should not lead to a significant reduction in the accuracy of our final results.

The idea is therefore to use a 2D camera to measure the velocity before and after the impact in order to derive the kinetic energy right before the impact and after it and thereby how much energy was absorbed.
We also use 3D DIC cameras to measure the deformation. The difference is that in our setup they have to be positioned on the side of the impact, due to spatial constraints.

3.1.2 Get to know the program and materials

The aim of the first test was to understand how to use the camera, an 800 kHz Photron Mini UX100, and the PFV4 (Photron Fastcam Viewer 4) program, with which all image analyses were carried out. For this purpose, the barrel of a dart was used as the impact object, which was released against cardboard. The camera was put in a perpendicular position to the dart barrel. The setup is shown in Figure 3.2.

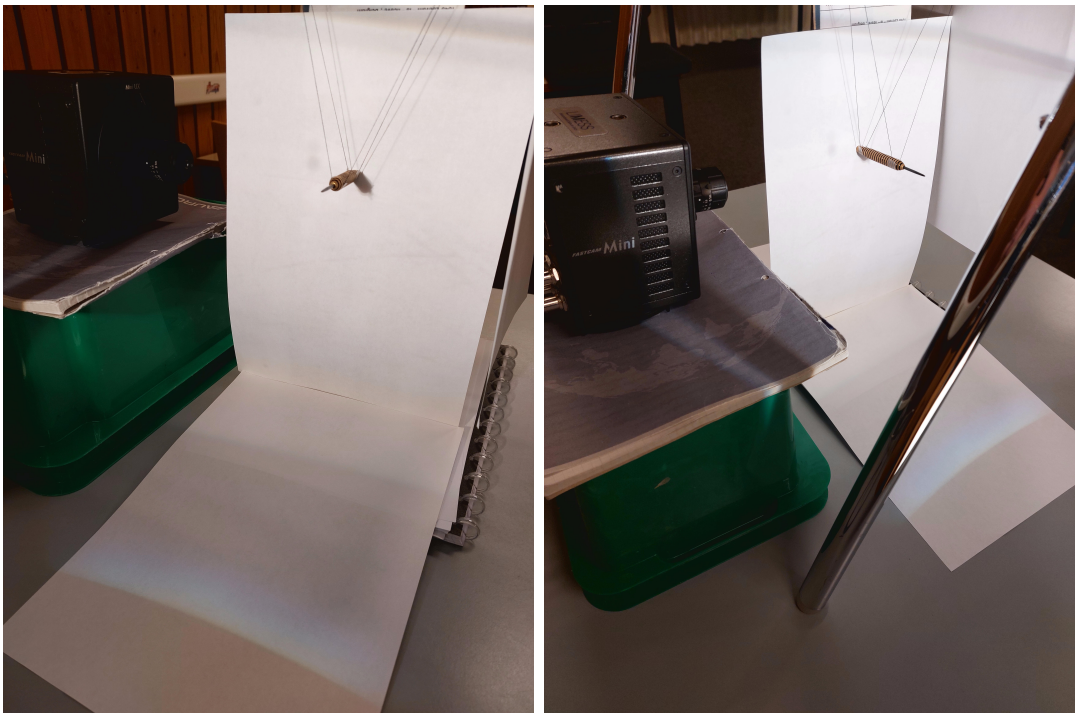
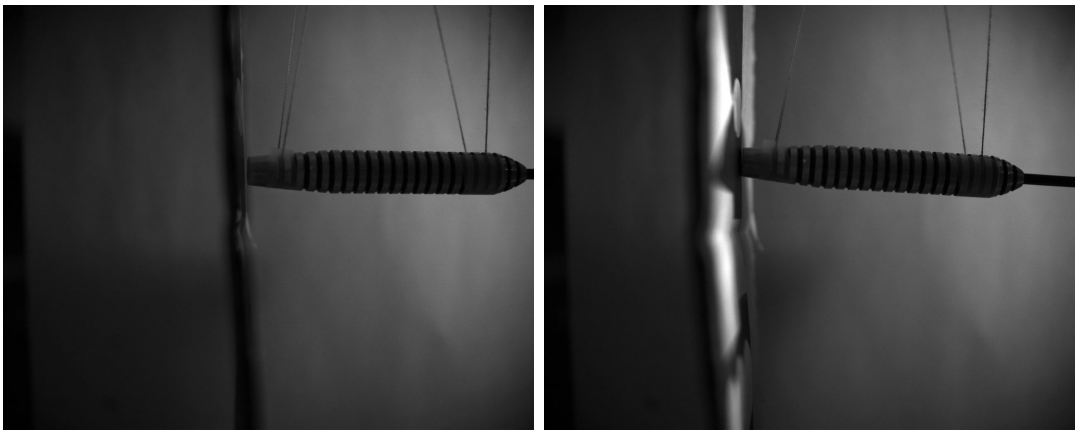


Figure 3.2: First setup with dart barrel as impact object.

The focus of the test was to measure the impact and the return speed. The length of the barrel was used to calibrate the camera to be more accurate, to know how many µm a pixel represents. In this case a value of 87.63 µm/px was found. Figure 3.3a shows the dart barrel shortly before impact and Figure 3.3b the maximum deformation of the carton.



(a) Dart barrel just before impact. (b) Dart barrel at maximum deformation.

Figure 3.3: Camera images dart setup.

The given values as well as the results are displayed in Table 3.1.

Barrel weight [g]	24
Barrel length [mm]	58.9
Camera calibration [µm/px]	87.63
$E_{kin,impact}$ [mJ]	33.17
$E_{kin,return}$ [mJ]	14.74
$\Delta_{E_{kin}}$ [mJ]	18.43

Table 3.1: Given values and results.

As the table shows, it was possible to measure the kinetic impact energy $E_{kin,impact}$ as well as the kinetic return energy of the impact object $E_{kin,return}$. $E_{kin,return}$ being around 55% of $E_{kin,impact}$, it can be stated that those are possible and reasonable values which were found, given that cardboard is a non-elastic material, which therefore would be expected to absorb a big part of the initial impact energy.

3.1.3 First tests at Buildwise

To get a feel for how the tests are carried out correctly, some initial tests were performed on barriers that had already been tested.
The aim was also to find out whether the kinetic energy measured right before the impact corresponds to the potential energy of the impact object when it is released. The setup for the test is shown in Figure 3.4.

Each camera has a specific responsibility or task. Camera 1 is used to determine the impact velocity, the return velocity and the contact time of the impact object with the barrier. In combination with Camera 2 it is also intended to determine the deformation of the barrier at any time during the impact. Camera 3 measures the 3D deformation of the barrier. The reason why cameras 1 and 2 are also used to measure the 3D deformation is that camera 3 can take very precise measurements of the 3D deformation, but with a recording frequency of 25 Hz (25 frames per second, i.e. one image every 40 ms) it cannot capture every moment of the deformation.
In similar tests, contact times of around 30 ms were found, which means that camera 3 can most likely only measure the final deformation and not the maximum deformation during the impact. [16][17]

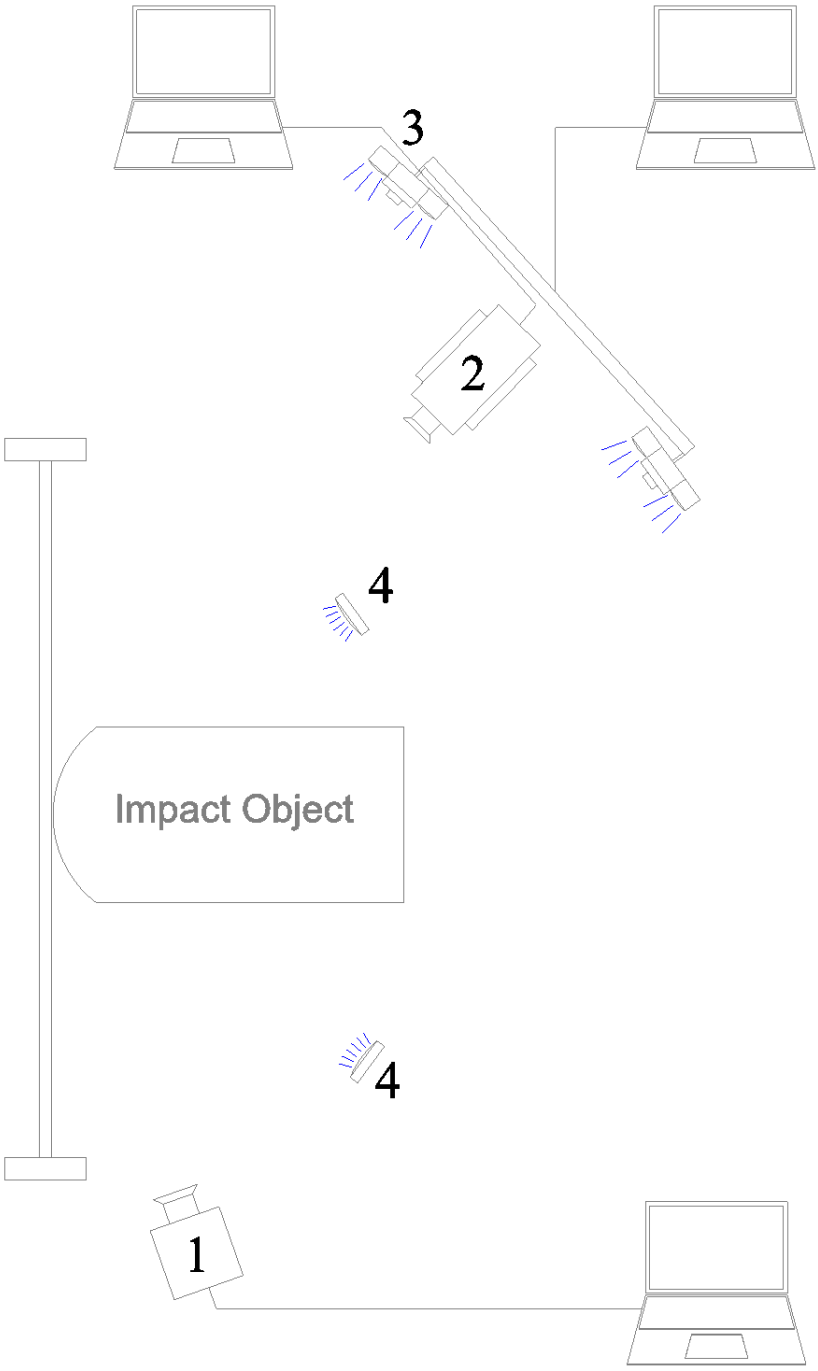
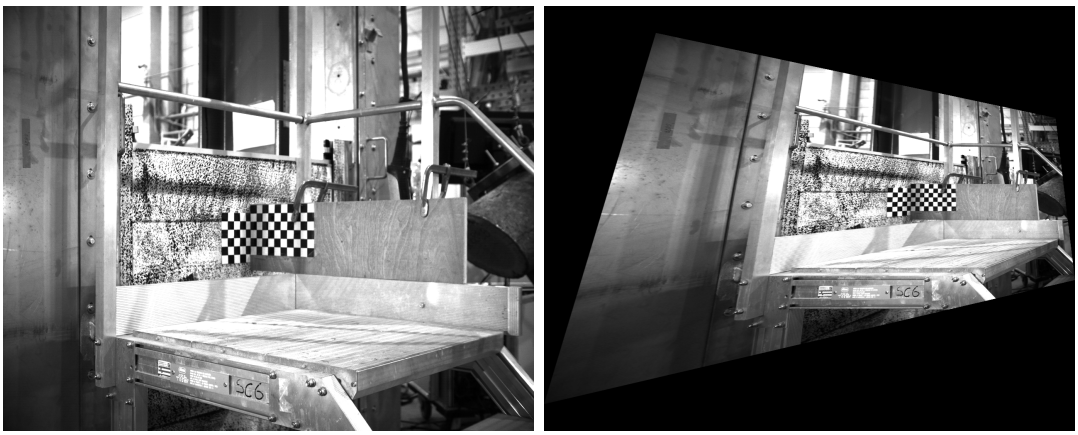


Figure 3.4: Setup first tests at Buildwise.
1: Photron Fastcam Mini type 800K-M-32G
2: Photron Fastcam SA3 Model 120K-M1
3: 25 Hz Aramis 3D DIC Camera
4: Black light spots

For the test, the complete test procedure was fixed as follows:

- Step 1: Calibrate Camera
- Step 2: Start Test
- Step 3: Measure Impact Moment
- Step 4: Apply Keystone correction
- Step 5: Measure Impact and Return Speed
- Step 6: Analyse the 3D Deformation measured with camera 3 (see Fig. 3.4)
- Step 7: Verify 3D Deformation with cameras 1 and 2 (see Fig. 3.4)

Unlike the test with the dart barrel, the calibration cannot take place on the impact object itself, as the object is significantly thicker and the length could be distorted by the angle of the camera. For this reason, chess patterns were attached to the barrier and to a board, which was then held perpendicular to the barrier at the height of the impact point to calibrate the camera, as can be seen in Figure 3.5a .



(a) Initial calibration picture. (b) Applied Keystone correction.

Figure 3.5: Calibration pictures with chess pattern on barrier and impact object.

The calibration picture is also used to apply the Keystone correction. Keystone correction digitally adjusts the image to counteract distortion from the camera's angle. This process involves compressing the wider side of the image and stretching the narrower side, producing a rectangular image when projected on the screen.

In this case, the keystone correction was applied to the chess pattern perpendicular to the barrier, as the speed is measured in this plane. Figure 3.5b shows the Keystone Correction applied to the image in Figure 3.5a.

The given values and results for the measured values are listed in Table 3.2.

m [kg]	49.2
h [m]	1.2
fps	500
#frames	5
Δt [ms]	2
v_{impact} [m/s]	6.24
v_{return} [m/s]	/
E_{pot} [J]	579
$E_{kin,impact}$ [J]	956

Table 3.2: Values and results.

where,

- m: the weight of the impact object
- h: the height of the impact object measured from the tip of it, 1.2 m above the impact point on the barrier. (see Fig. 3.6)
- fps (frames per second): the frequence of the camera recording
- #frames: the amount of frames taken for the measurement
- Δt: the time step taken for the measurement
- v_{impact}: the speed of the impact object right before the impact
- v_{return}: the return speed of the impact object measured as soon as there is no more contact between barrier and impact object
- E_{pot}: the potential energy of the impact object at height h calculated as:

$$E_{pot} = m \cdot g \cdot h \tag{3.1}$$

where g=9.81 $\frac{m}{s^2}$, the gravitational acceleration

- $E_{kin,impact}$: the kinetic energy of the impact object right before the impact, calculated as:

$$E_{kin,impact} = \frac{1}{2} \cdot m \cdot v_{impact}^2 \tag{3.2}$$

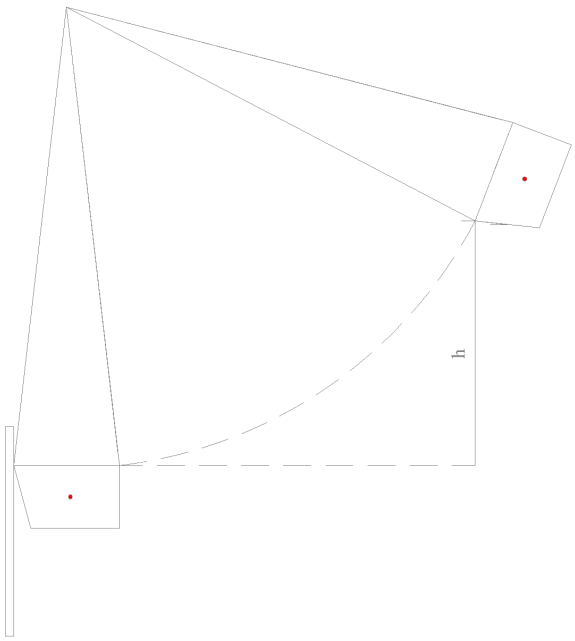


Figure 3.6: Method to measure height h.

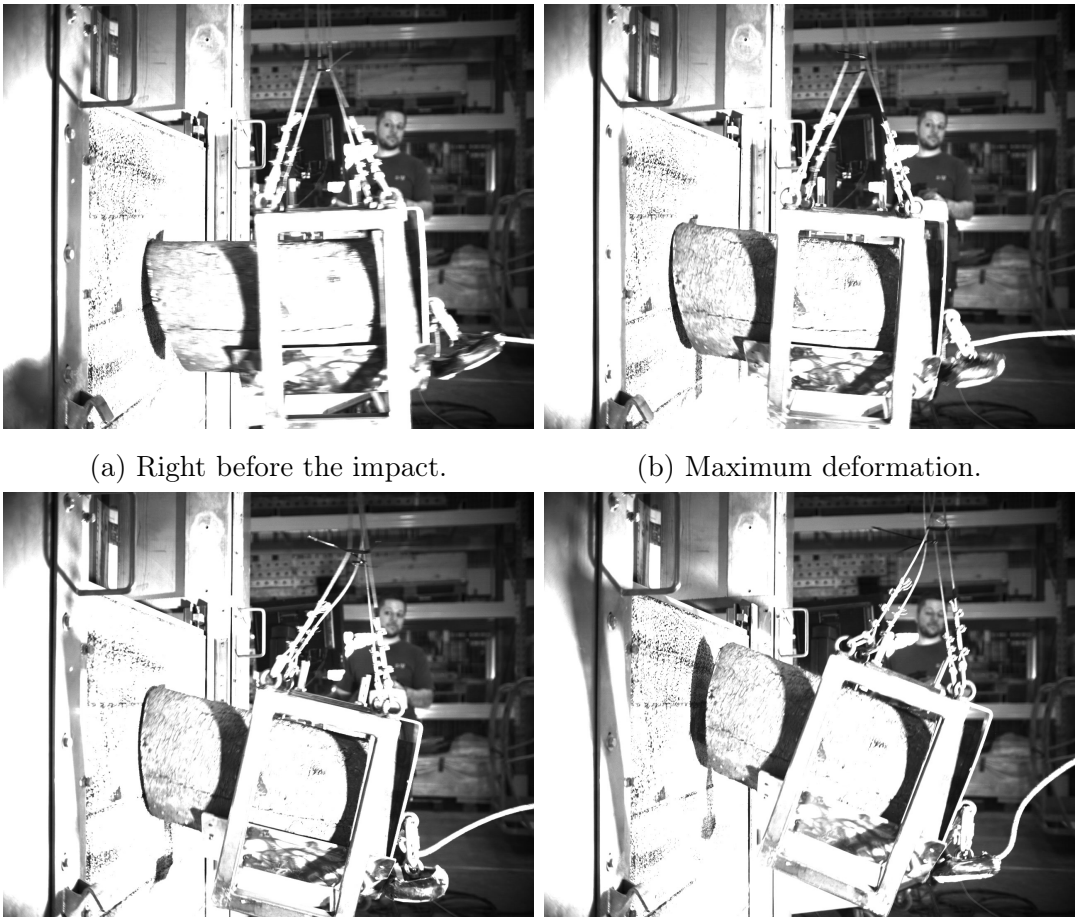
When looking at the results in Table 3.2 it is noticeable that the kinetic energy $E_{kin,impact}$ is greater than the potential energy, which is not possible with a classical pendulum according to the law of conservation of energy. The kinetic energy should therefore be at most as great as the potential energy, if friction is not taken into account, which of course subtracts part of the potential energy.

There may be several reasons for this:

- The recording area for the camera is too large, which can lead to inaccurate measurements.
- There was no real reference point to guide the measurements.
- The reference plan, i.e. the chess pattern which the camera was calibrated on, does not correspond to the plan of the actual impact.
- The perspective, i.e. the camera angle, causes inaccuracies. In other words, the Keystone correction results in a loss of image quality.

- The point for measuring the height h is incorrectly selected.

Another point that stands out is that the return velocity could not be measured, as the movement of the impact object did not simply drift backwards as hoped and as seen in older recordings, but upwards. The main reason for this were the cable ties that were attached to the steel cables to adjust the height of the impact object correctly. These caused a kind of a ball joint to form at the point where the cable ties were attached, as can be seen in the images in Figure 3.7.
Another reason could be that the barrier had already been tested and the impact object therefore slid upwards in the existing hollow created through a previous test.



(a) Right before the impact. (b) Maximum deformation.

(c) Slipping of the impact object. (d) Upwards motion of the impact object.

Figure 3.7: Pictures of the first test at Buildwise.

One final point to note is that there were problems with the connection of a laptop to camera 2 as the laptop was not powerful enough and so the recording signal to a

camera took a very long time to be transmitted. This meant that it arrived too late for some trials and we therefore had no recordings from this camera for certain trials. It is therefore advisable to connect both cameras to a single laptop with enough computing power, which can also simplify the subsequent analysis.

3.1.4 Small scale model

The idea of the first small scale model was to solve the problems that occurred during the first tests, i.e. the reason for the excessive kinetic energy, an improvement of the calibration system, the optimisation of the camera position and the incidence of light. In the small scale model, tests can only be carried out with the two Photron cameras, as the 3D DIC camera is owned by Buildwise and hence stayed in their laboratory.

To make the experiment as realistic as possible, a piece of wood with a diameter of around 5.8 cm was cut at an angle of 15°. With the help of thread, it was then possible to create a pendulum that resembled the real impact object.
A table surface was initially used as a barrier, but this surface was too hard for such a small impact, especially compared to the real tests, which is why cardboard was used for later experiments.
The setup for the small scale model test is shown in Figure 3.8. As no black light spots are required without camera 3 (Aramis 3D DIC camera) and none were available for the small scale model, these were replaced by simple spotlights.

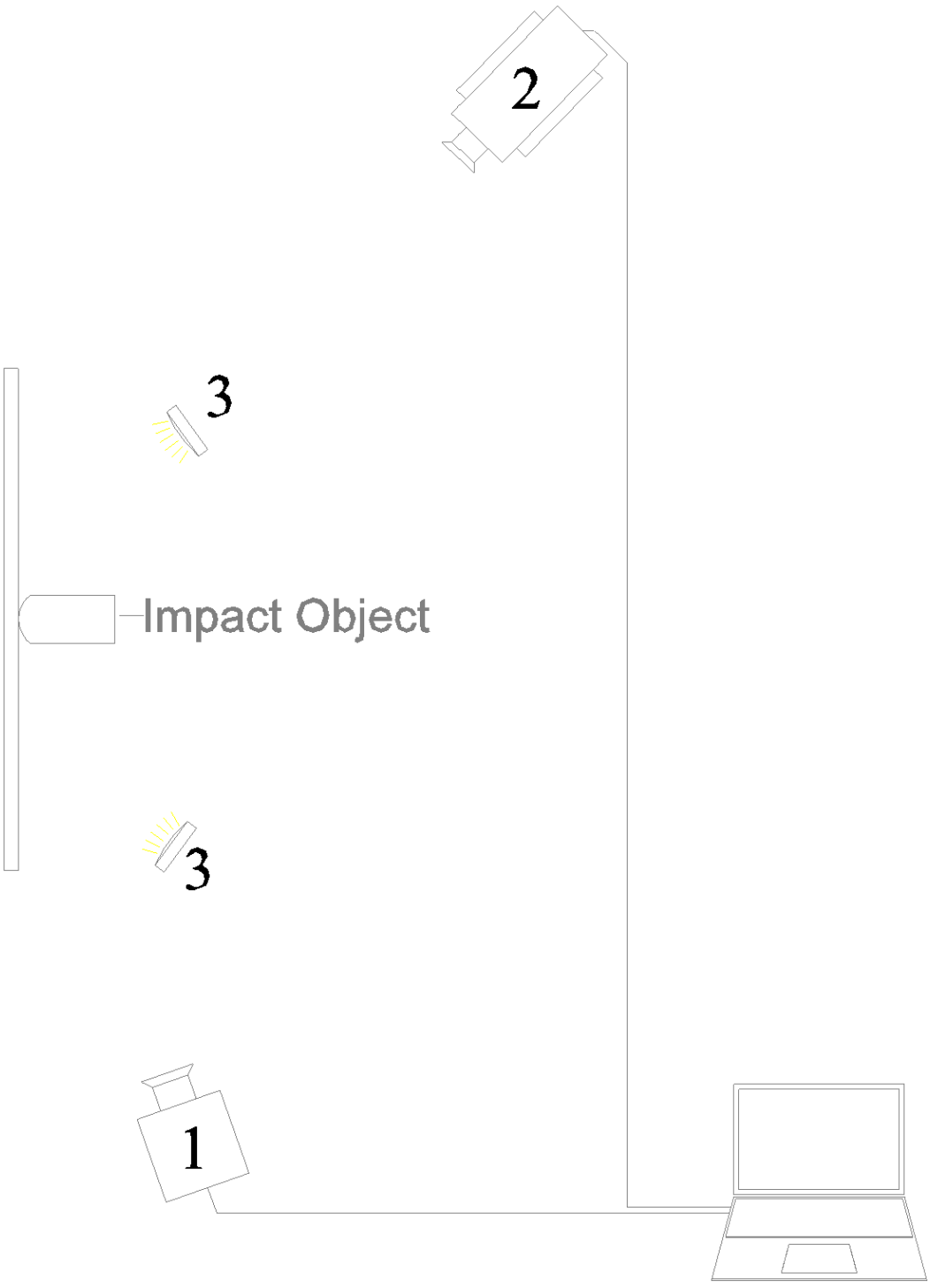


Figure 3.8: Setup small scale model.
1: Photron Fastcam Mini type 800K-M-32G
2: Photron Fastcam SA3 Model 120K-M1
3: Spotlights

3.1.4.1 First test series

The main goal of the first series of tests was to find a good calibration method and the optimum camera lenses for both cameras.
During the first test series in the small model, the position of camera 1 and 2 were swapped, but this had no effect on the results of the tests. The setup for this test can be seen in Figure 3.9.

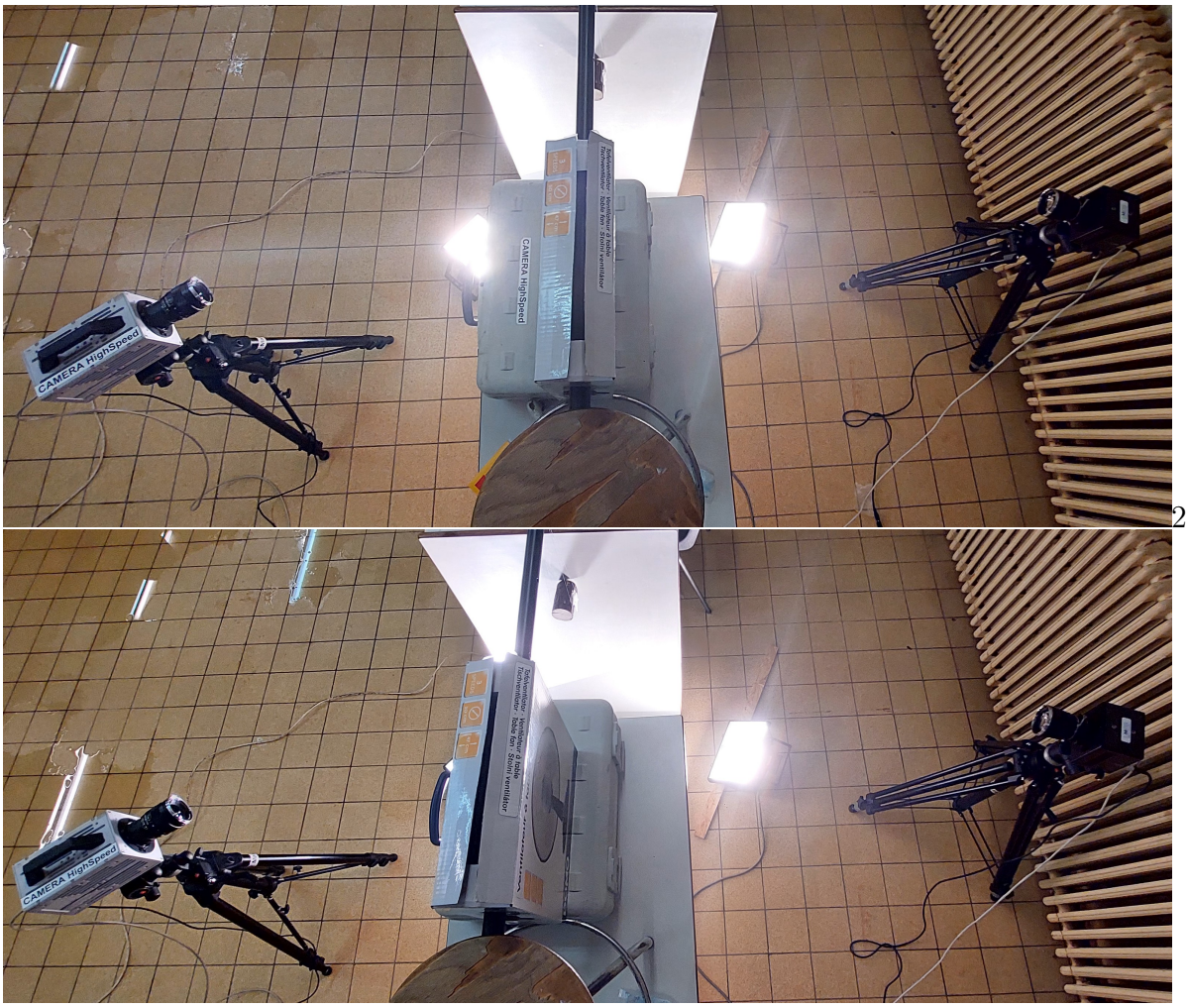
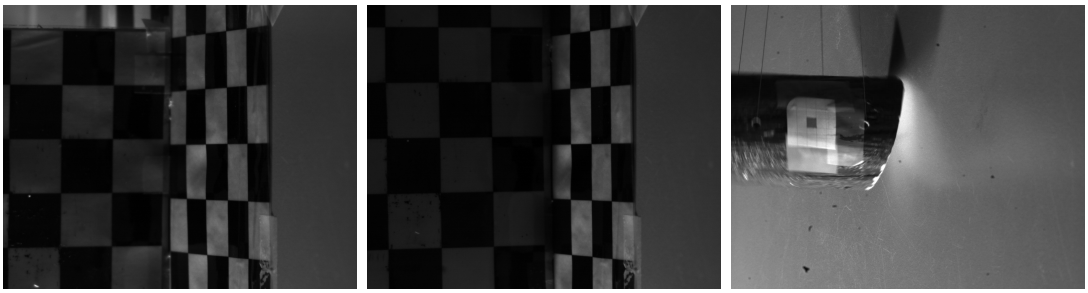


Figure 3.9: Setup first test small scale model.

Before real tests were carried out, various camera lenses were tested. This is important as the images from camera 1, which are used to measure the speed, must be as accurate as possible in order to minimise measurement errors. This means that the camera has to zoom in as far as possible while maintaining a sharp image. For this, the

focal length of the camera lens must be as high as possible.
The camera lens with the maximum focal length available was one of 85 mm.
Camera 2 is equipped with a lens with a focal length of 25 mm.
Now, with the camera lenses selected, three different reference plans were tested, which are used to calibrate the camera.

- The first reference plan is positioned at the impact point. Similar to the tests at Buildwise, a chess pattern is held at that position so that an image can be taken with which the camera can be calibrated (see Fig. 3.10a).
- The second reference plan is located on the front side of the impact object, facing the camera. Here too, the chess pattern is used for calibration (see Fig. 3.10b).
- For the third reference plan, a paper with a black square is provisionally attached to the object itself, which the camera is calibrated on (see Fig. 3.10c).



(a) Calibration on middle reference plane.

(b) Calibration on front reference plane.

(c) Calibration on impact object.

Figure 3.10: Calibration methods.

In order to compare these three calibration methods, one test was carried out. This test was then analysed using each calibration method. The given values are listed in Table 3.3.

fps	500
#frames	5
Δt [ms]	2
m [kg]	0.103
h [m]	0.095
E_{pot} [mJ]	95.99

Table 3.3: Given values.

Table 3.4 compares the results based on the three calibration methods

	Middle Reference Plane	Front Reference Plane	Calibration on Object
v_{impact} [m/s]	2.02396	2.21457	1.33615
$E_{kin,impact}$ [mJ]	210.96	232.96	91.94
$\frac{E_{kin,impact}}{E_{pot}}$ [%]	219.78	242.68	95.78

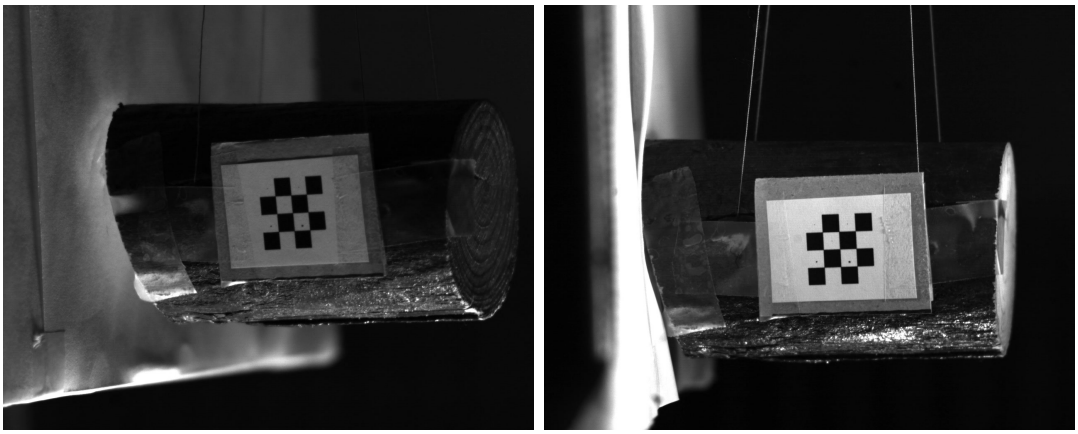
Table 3.4: First test results.

As the comparison shows, the measurements calibrated using the chess patterns in the front and middle reference plane give kinetic energies that are clearly too high, over 200% of the potential energy, which is not possible.
Only the measurement where the camera was calibrated on the object itself resulted in possible values with a kinetic energy of around 96% of the potential energy.
From now on, the camera is therefore always calibrated on the object for further tests. This also prevents the reference plane from having to be different from the one used for calibration due to changes when the impact object is released. More precisely, if the image taken shortly before the impact itself is used to calibrate the camera, there can be no inaccuracies with the reference plane.

3.1.4.2 Second test series

The aim of the second series of tests was to find out the right reference point for measuring the height, the optimum camera positioning, as well as the ideal incidence of light and the right frequency for the camera.
It is important to note that the higher the recording frequency, the shorter the recording time or the poorer the image quality.
As camera 1 has 32 GB of internal memory, there is considerably more flexibility than with camera 2, which only has 2 GB of memory.
For this test series, Camera 2 could not be used as it was under repair. This wasn't a problem as the general objectives for this test series could be achieved with camera 1.

Knowing that calibration on the impact object is the best solution, in this test series a printed chess pattern was attached to the impact object with different reference points for the measurements.
For optimal recording several angles and light levels were tried out (see Fig. 3.11).



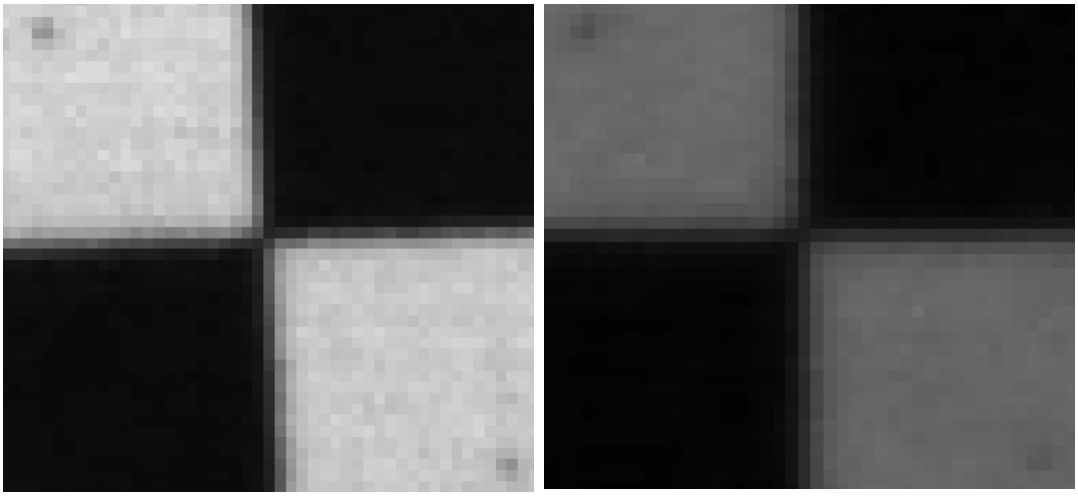
(a) Camera positioned with a small angle to the the barrier.

(b) Camera positioned perpendicular to the impact object.

Figure 3.11: Camera positionings.

It turned out that the measurements are most precise when the camera is perpendicular to the impact object (see Fig. 3.11).
In this case, no Keystone correction needs to be made. Keystone correction mostly leads to a loss of image quality. This is a problem in that the contrast of black and white in the chess pattern disappears, meaning that it is no longer possible to recognise

exact boundaries in the pixels of the image. This can be seen in Figure 3.12. While the corners of the black squares are clearly recognisable in Figure 3.12a, in Figure 3.12b, in which the keystone correction was applied, no clear boundary can be seen. The greater the angle of the camera to the barrier, the blurrier the image after Keystone correction.



(a) Picture without Keystone correction. (b) Picture with Keystone correction.

Figure 3.12: Picture quality differences.

Even if this may not be a big difference, we are in ideal conditions here. In the real tests, the spots cannot necessarily be positioned perfectly, which can lead to the difference being significantly greater. In addition, the image distortion caused by the Keystone correction can lead to errors in length calibration, which can also be prevented by positioning the camera perpendicularly.

With respect to the frame rate, it was attempted to keep the image quality at the maximum, while also retaining enough recording time to allow for manual recording. Based on these conditions, a frame rate of 4000 fps was set for camera 1 after several tests.

Once the cameras were correctly positioned and configured, the tests could take place. The test setup was as shown in Figure 3.13. This time the barrier was made of cardboard.

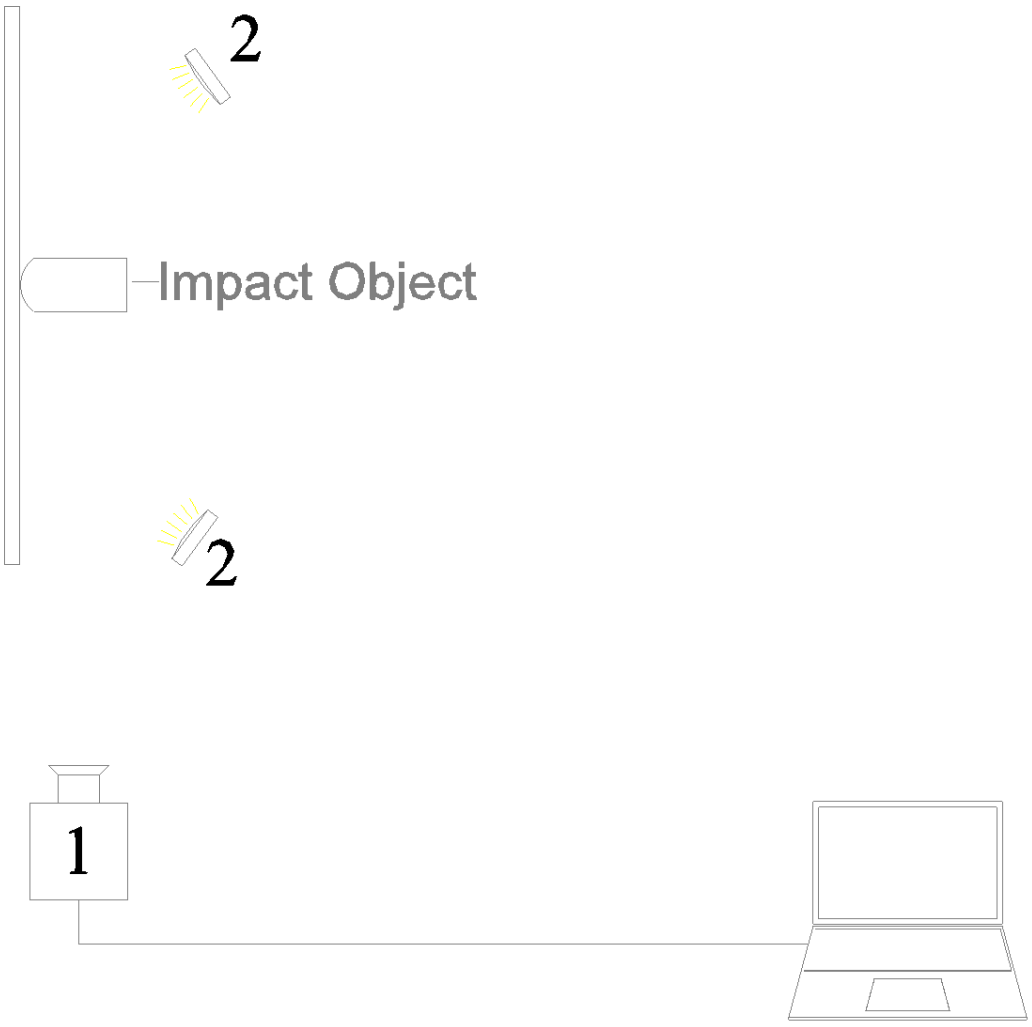


Figure 3.13: Setup small scale model - Second test series.
1: Photron Fastcam Mini type 800K-M-32G
2: Spotlights

The aim of the test series itself was to find out from which point the drop height should be measured.
Previously, this was measured from the tip of the impact object in order to follow the American standard.
However, a more logical approach is to start from the centre of gravity of the object and measure the potential energy from this point (see Fig. 3.14).
Since the impact object's shape was a trapezoid, the centre of gravity was calculated

accordingly.

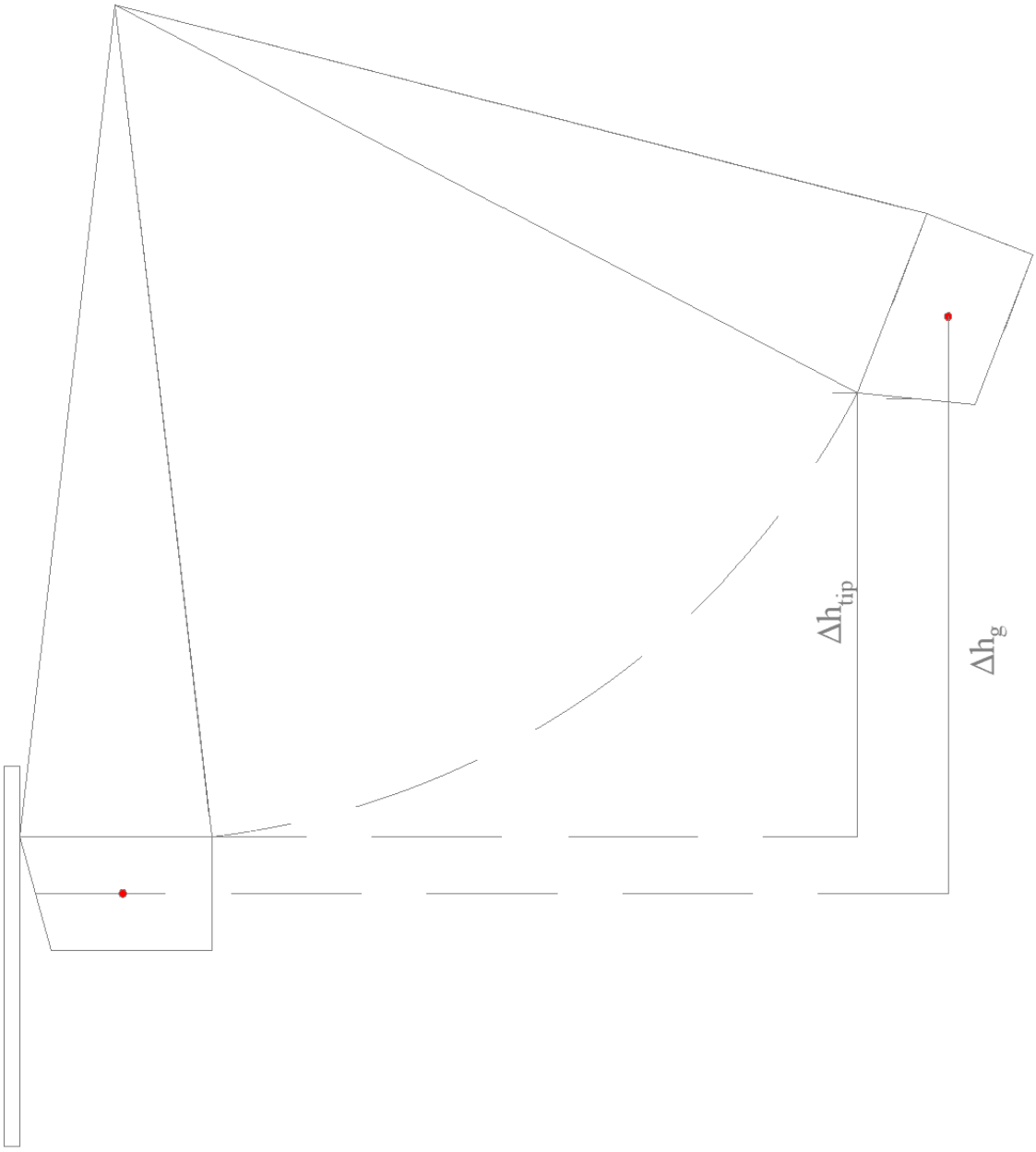


Figure 3.14: Drop height measurement (in red: centre of gravity).

As Figure 3.14 shows, the height measured from the centre of gravity is significantly higher than that measured from the tip of the object. This would mean that the real potential energy is greater than that measured from the tip of the impact object. This, in turn, would explain why a kinetic energy greater than the potential energy can be

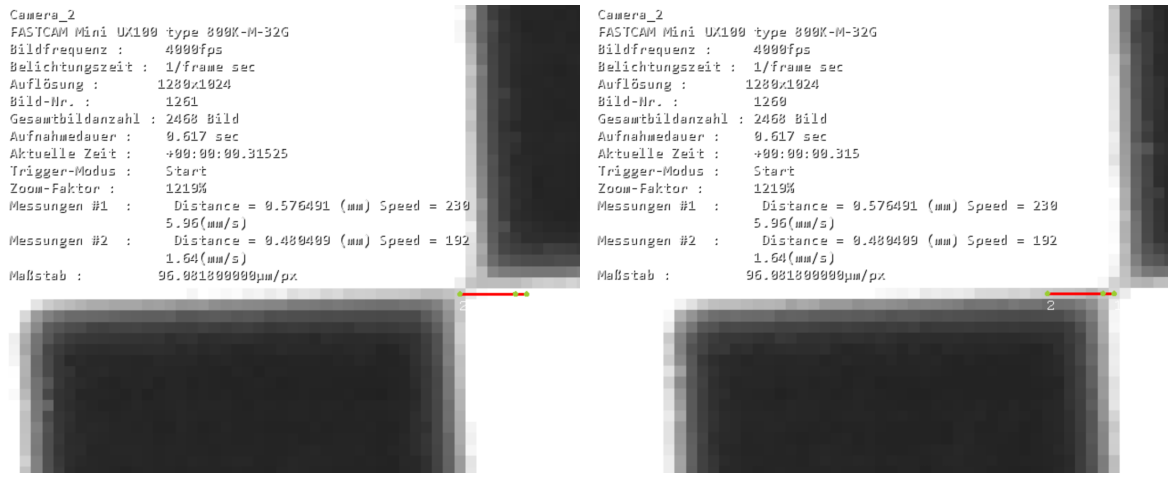
found, if the potential energy is measured from the tip of the object.

The given values for the analysed test with a height difference measured from two different points, from the tip of the impact object h_{tip} and from the centre of gravity h_g, are shown in Table 3.5.

fps	4000
m [kg]	0.103
Δh_{tip} [m]	0.179
Δh_g [m]	0.2625
$E_{pot,tip}$ [mJ]	180.87
$E_{pot,g}$ [mJ]	265.24

Table 3.5: Given values.

The following methodology was used for the analysis of the measurements of the tests: The speed was measured over different time steps, 0.25, 1, 2, 3 and 4 ms.
At each time step, 2 speed measurements were taken from the same starting point. This is necessary because it is not always clear exactly which pixel is the correct one for the measurement due to inaccuracies in the image sharpness.
An example can be seen in Figure 3.15, the measurements for a time step of 0.25 ms. For this measurement, the reference point was selected in the image of Figure 3.15a, the image directly before the impact. In the previous frame, however, it is not exactly visible which pixel matches in the selected frame, which is why 2 measurements are made with the two possible pixels (Fig. 3.15b). The average of the two measurements is then used for the analysis. The error is the difference between one value and the average.



(a) First measurement frame.

(b) Second measurement frame.

Figure 3.15: Measurements for a 0.25 ms time step.

In Table 3.6 and Table 3.7 the results of the analysis of one test are shown. Listed is:

- Time step Δt: the time step which was taken into account for this measurement.
- v: the measured speed right before the impact, two for each time step.
- Δv: the difference in speed between the two measured speeds for each time step.
- E_{kin}: the kinetic energy right before the impact, which can be calculated using the measured speed and the weight of the impact object given in Table 3.10.
- Ratio $\frac{E_{kin}}{E_{pot,tip}}$: the ratio of the kinetic energy over the potential energy, the height being measured from the tip of the impact object (see Fig.3.14).
- Mean of ratio $\frac{E_{kin}}{E_{pot,tip}}$: the mean of the two values for the ratio of the kinetic energy over the potential energy, the height being measured from the tip of the impact object.
- Ratio $\frac{E_{kin}}{E_{pot,g}}$: the ratio of the kinetic energy over the potential energy, the height being measured from the centre of gravity of the impact object.
- Mean of ratio $\frac{E_{kin}}{E_{pot,g}}$: the mean of the two values for the ratio of the kinetic energy over the potential energy, the height being measured from the centre of gravity of the impact object.

- $\Delta\frac{E_{kin}}{E_{pot,g}}$: the difference in percentage of the ratio of the kinetic energy over the potential energy between the two measured values, the height being measured from the centre of gravity of the impact object.

Time step Δt [ms]	**0.25**		**1**		**2**	
v [m/s]	1.922	2.306	2.018	2.114	2.066	2.114
Δv [m/s]	**0.384**		**0.096**		**0.048**	
$E_{kin}[mJ]$	0.19	0.274	0.210	0.230	0.220	0.230
Ratio $\frac{E_{kin}}{E_{pot,tip}}$ [%]	105.15	151.41	115.92	127.23	121.51	127.23
Mean of ratio $\frac{E_{kin}}{E_{pot,tip}}$ [%]	**128.28**		**121.57**		**124.37**	
Ratio $\frac{E_{kin}}{E_{pot,g}}$ [%]	71.7	103.25	79.05	86.76	82.86	86.76
Mean of ratio $\frac{E_{kin}}{E_{pot,g}}$ [%]	**87.47**		**82.9**		**84.81**	
$\Delta\frac{E_{kin}}{E_{pot,g}}$ [%]	**31.55**		**7.71**		**3.9**	

Table 3.6: Results: Second test series - Time steps 0.25, 1 and 2 ms.

Time step Δt [ms]	**3**		**4**	
v [m/s]	2.082	2.114	2.090	2.114
Δv [m/s]	**0.032**		**0.024**	
$E_{kin}[mJ]$	0.223	0.230	0.225	0.230
Ratio $\frac{E_{kin}}{E_{pot,tip}}$ [%]	123.4	127.23	124.35	127.23
Mean of ratio $\frac{E_{kin}}{E_{pot,tip}}$ [%]	**125.31**		**125.79**	
Ratio $\frac{E_{kin}}{E_{pot,g}}$ [%]	84.15	86.76	84.8	86.76
Mean of ratio $\frac{E_{kin}}{E_{pot,tip}}$ [%]	**85.45**		**85.78**	
$\Delta\frac{E_{kin}}{E_{pot,g}}$ [%]	**2.61**		**1.96**	

Table 3.7: Results: Second test series - Time steps 3 and 4 ms.

What is immediately noticeable based on the results in Tables 3.6 and 3.7 is that the values for the ratio of kinetic to potential energy $E_{pot,tip}$ are all higher than 100%, which, as already mentioned, is not possible in a pendulum according to the law of conservation of energy.
However, the values for the rate from kinetic to potential energy $E_{pot,g}$ are all lower on average and within a realistic range, between 82.9 and 87.47%.

On closer examination of the measurements themselves, it can be noticed that the differences in the measured speeds are enormous for a small time step. This is because even a difference of sometimes only one pixel is very large with a very small time step. Of course, this also has an effect on the kinetic energy. A speed difference of 0.4 m/s is so enormous that in terms of potential energy this is a difference of over 30%. In order to reduce this difference, larger time steps were taken and compared with each other. As the results show, the difference could be reduced to under 2% with a time step of 4 ms.
A graphical representation of this can be seen in Figure 3.16.
The green line represents the potential energy, which can be read off the y-axis, as well as all other energies. The two points of one colour are the two measurements of the kinetic energy for one time step. The time step can be read off the x-axis.

As it can be seen on the graph, the energy differences not only become smaller with larger time steps, but the curves also appear to converge. This means that there is only a small to no difference to the maximum kinetic energy whether you take the first measurement a few milliseconds before the impact or directly at impact. This also means that the results do not change if you do not find the perfect frame before the impact, so there is kind of a margin.

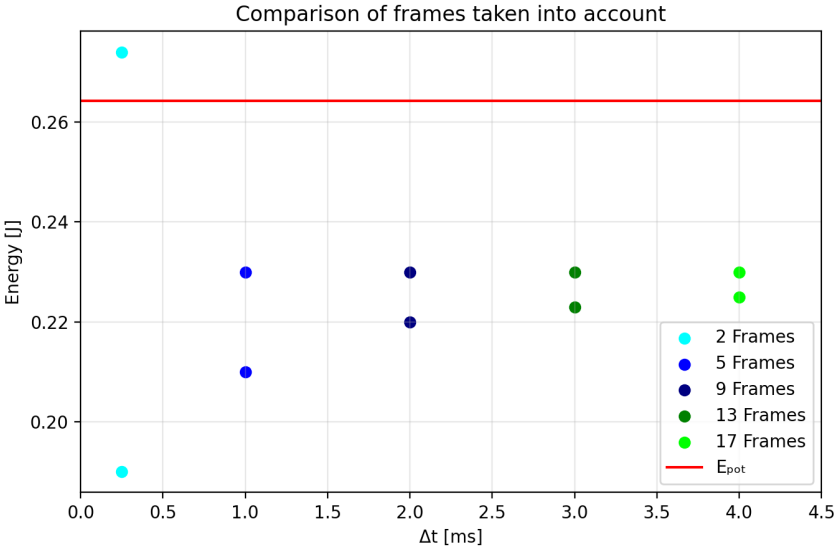


Figure 3.16: Graphical representation of the measurements with different time steps.

In addition to the impact energy, the return speed and contact time of the impact object with the barrier were also measured in this test. The values are listed in Table 3.8.

Contact time [ms]	15.5
v_{impact} [m/s]	2.1
$E_{kin,impact}$ [J]	0.227
v_{return} [m/s]	0.641
$E_{kin,return}$ [J]	0.021
$\frac{E_{kin,return}}{E_{kin,impact}}$ [%]	10.27

Table 3.8: Results: Contact time and absorbed energy.

In Table 3.8, both speed measurements are the mean value for a taken time step of 4 ms. Taking the ratio $\frac{E_{kin,return}}{E_{kin,impact}}$ [%], it can be seen that nearly 90% of the initial kinetic energy at the impact was absorbed. Looking at the camera footage and knowing that cardboard is hardly elastic, this seems like a realistic value.

In conclusion for the second series, it is incredibly important to use the centre of gravity as a reference point for height measurement. It is also important to use larger time steps for the measurements in order to minimise the differences as much as possible.

3.1.4.3 Third test series

The third test series served to find the optimal settings for camera 2, the Photron Fastcam SA3 Model 120K-M1, which could not be used in the second test series due to repair work.
Between the second and third test series, some provisional tests were carried out at Buildwise, purely to determine the positioning of the spots and cameras, i.e. not to take measurements. It was noticed that when camera 1 was aimed at the reference chess pattern, the tip of the impact object was no longer visible (see Fig. 3.17).
This is due to the fact that the chess pattern is attached to the steel frame, as this provides a straight surface and therefore no distortion of the image can occur during the analysis (see Fig. 3.18).

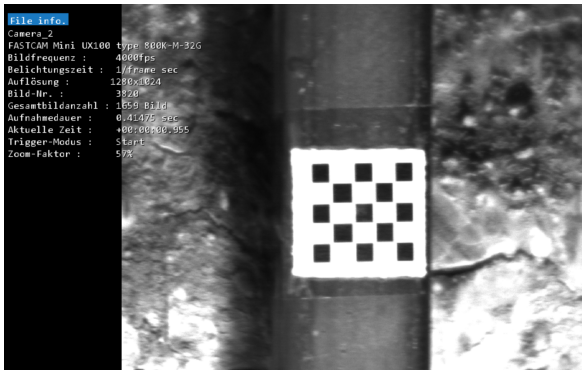


Figure 3.17: Camera calibrated on reference chess pattern.

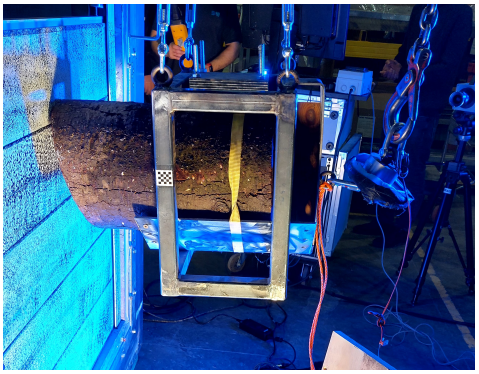


Figure 3.18: Chess pattern fixed on steel frame.

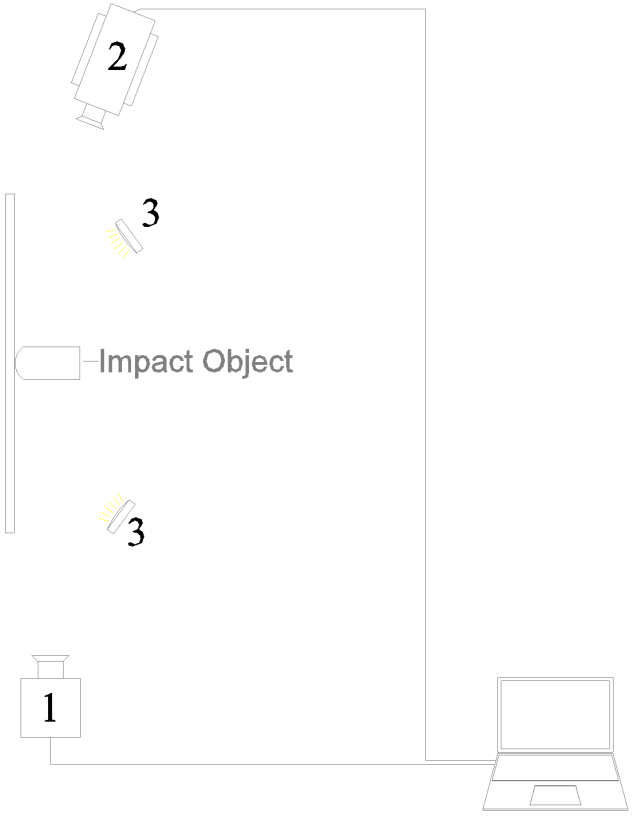
Because camera 1 no longer has the impact in its field of vision, it cannot determine the time of impact, nor can can it measure the 3D deformation of the barrier with the help of camera 2. Given that this was the only function of camera 2, it was in turn converted from measuring the 3D deformation to measuring the impact moment and contact time.
This in turn requires different camera settings and positioning. For this reason, camera 2 was positioned at a slight angle to the barrier, as can be seen in Figure 3.19c and 3.19d. This angle enables a better determination of impact moment.



(a) Third test series - Set up.



(b) Third test series - Set up.



(c) Setup small scale model.
1: Photron Fastcam Mini type 800K-M-32G
2: Photron Fastcam SA3 Model 120K-M1
3: Spotlights



(d) Close-up impact object.

Figure 3.19: Setup small scale model - Third test series.

The camera frequency should ideally be the same as that of camera 1 in order to be sure that the exact frame before the impact is used. However, as camera 2 only has a very small memory capacity of 2 GB, this means that the recording time falls below 1 second at full image resolution. As this is too short to start the recording manually, the image resolution must be reduced. However, as the impact can be recognised even at low resolution, this does not pose any problems.
Therefore, a resolution of 512x512 pixels was chosen, in order to sufficiently extend the recording time.

The only remaining problem is that, while the frequencies of the cameras match, they are not synchronised with each other. This is because, although both are connected to one single laptop, the signal for starting the recording does not arrive at both cameras at the same time. As no internal synchronisation method is available within the program, the videos need to be synchronised externally. This can be done using a manual trigger connected to camera 1 and a further connection between camera 1 and 2 that transmits the signal from the trigger at the same time. The final setup then looks as shown in Figure 3.20.

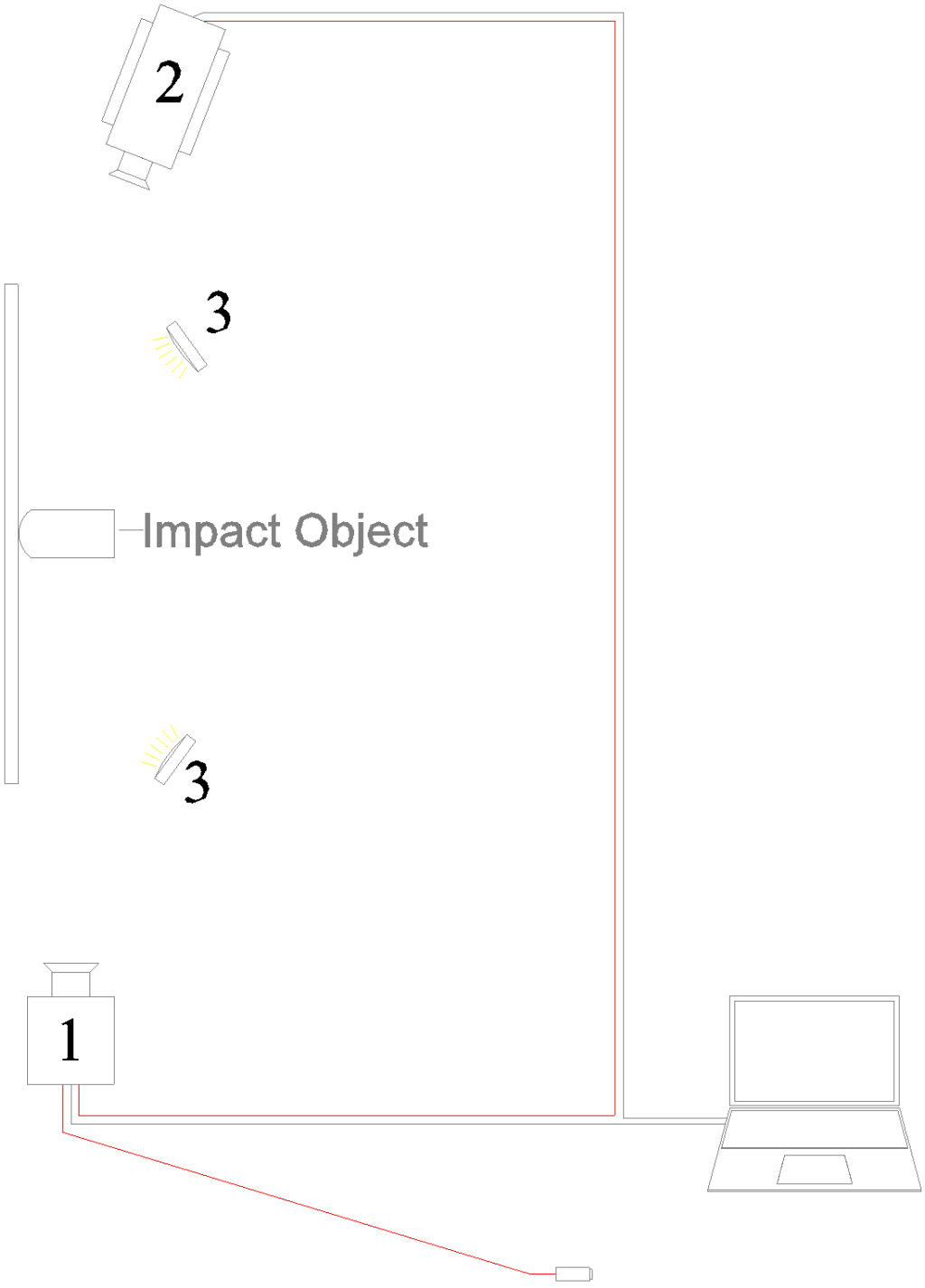


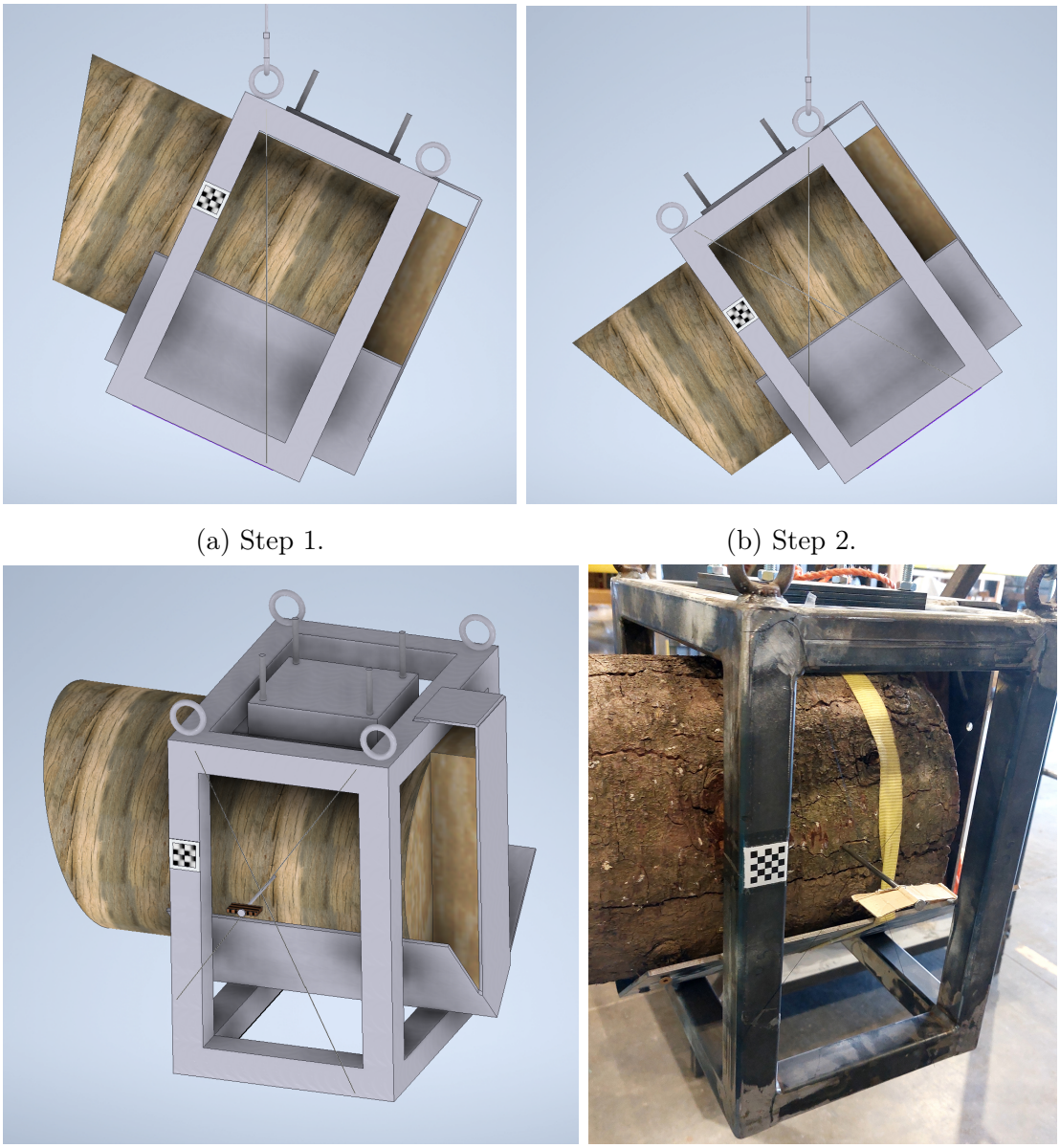
Figure 3.20: Setup small scale model.
1: Photron Fastcam Mini type 800K-M-32G
2: Photron Fastcam SA3 Model 120K-M1
3: Spotlights
In red: Manual Trigger

3.2 Final test setup and procedure

3.2.1 Test setup

There are some differences beetween the small scale model and the final setup.
The first difference concerns the method of finding the centre of gravity. As the impact object in the real test is not simply a block of wood, but also includes a steel frame, the centre of gravity cannot be determined in the same way. For this reason, the method described below is used. After measuring the weight and possibly increasing the weight by attaching steel plates to the impact object to reach the approximately 50 kg, the following method is used to determine the centre of gravity.

- Step 1: The impact object needs to only be attached to the two cables in front. The rear part hangs down. Now, a thread is used as a perpendicular to extend the line of the attached cables across the frame of the impact object. This thread will pass through the centre of gravity (see Fig. 3.21a).
- Step 2: The same procedure is repeated, only this time the rear cables are connected instead of the front two. The crossing of the two threads is the centre of gravity in this plane (see Fig. 3.21b).
- Step 3: Now a nail with a piece of cardboard is attached to the impact object at the height of the intersection point. The piece of cardboard now makes it possible to measure the height from the ground using a laser (see Fig. 3.21c and 3.21d).



(a) Step 1. (b) Step 2.

(c) Step 3. (d) Real impact object.

Figure 3.21: Determination centre of gravity.

Another difference to the small scale model is camera 3, which was not available for the tests in the small scale model. Since this camera requires black light to make the deformation on the barrier recognisable through contrasts, the positioning of the spots and therefore the incidence of light is also modified significantly. The setup can be seen in Figure 3.22.

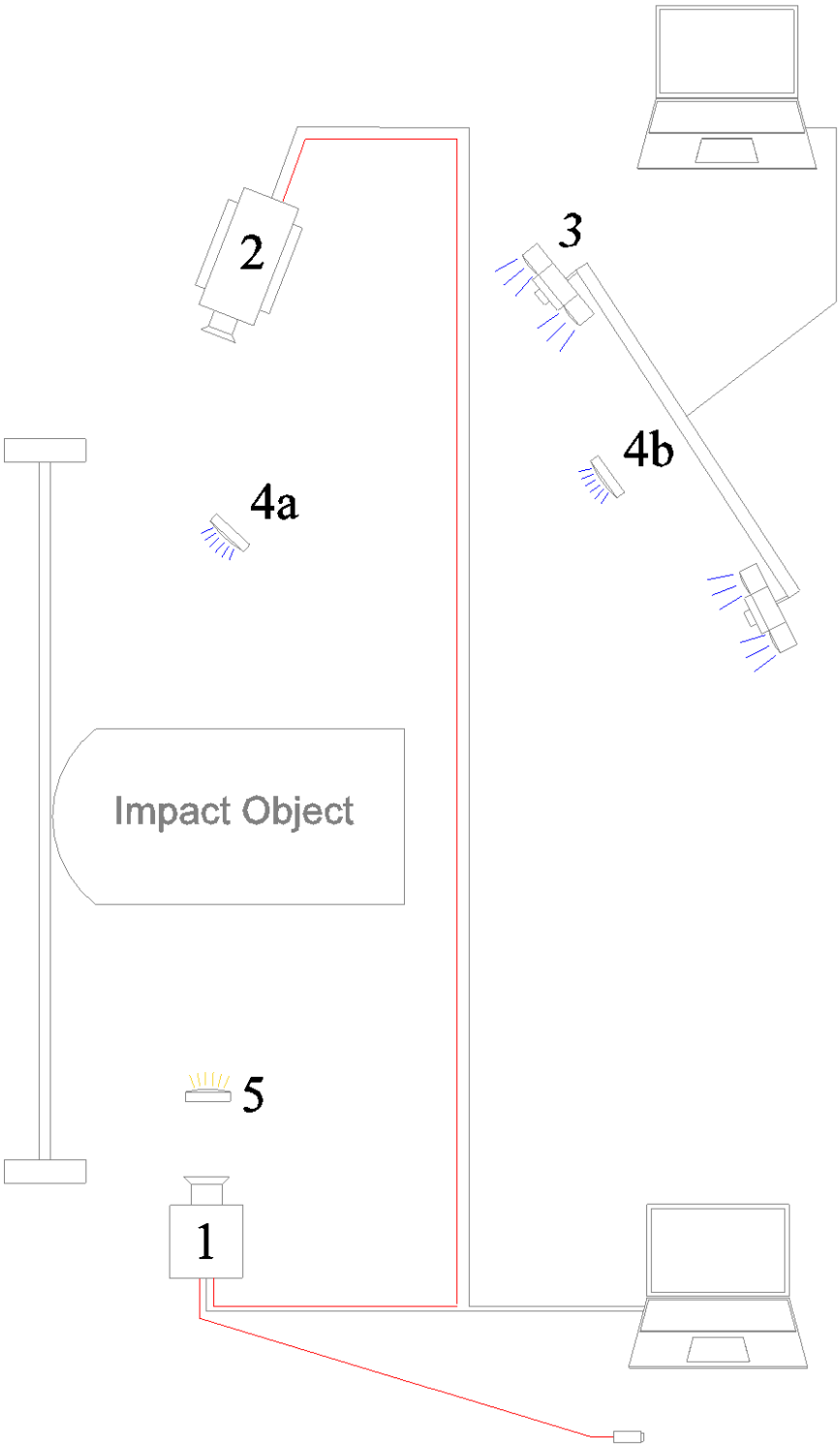


Figure 3.22: Schematic represenation of the setup.

Here is a list with a detailed description of each element.

- 1: Photron Fastcam Mini type 800K-M-32G
  Camera 1 is placed perpendicularly at a distance of 86.5 cm to the reference chess pattern, minimising its mm/pixel ratio and hence maximising the measurement precision. This is done using a lens with a focal length of 85 mm.
  The image resolution is 1280x1024 pixels and the used frame rate is 4000 fps.

- 2: Photron Fastcam SA3 Model 120K-M1
  Camera 2 is placed with a slight angle to the barrier at a distance of around 1.8 m (it is not important to have an exact distance, since no velocities are measured with this camera). The used lens has a focal length of 25 mm.
  The image resolution is 512x512 pixels and the used frame rate is 4000 fps. Camera 1 and 2 are connected to the same computer.

- 3: 25 Hz Aramis 3D DIC Camera
  Camera 3 is positioned in a larger angle to the barrier. The image resolution is fixed at 2752x2200 pixels and the used frame rate is 25 fps. It is connected to a computer different than the two other cameras.

- 4: Black Light Spots
  a) Positioned on the floor facing upwards towards the impact point.
  b) Positioned on a support above, facing down on the impact point.
  The positioning enables uniform illumination of the impact point from above and below.

- 5: Normal Spotlight
  This spot is used to increase the contrast in the chess pattern, which is attached to the impact object, in order to simplify the measurements. However, it must be positioned so that the light does not interfere with camera 3, which makes the effect less significant.

- In red: Manual Trigger
  This external manual trigger allows to start the recording of both cameras at the exact same instant.

In Figure 3.23 the final setup for the first measured test can be seen.

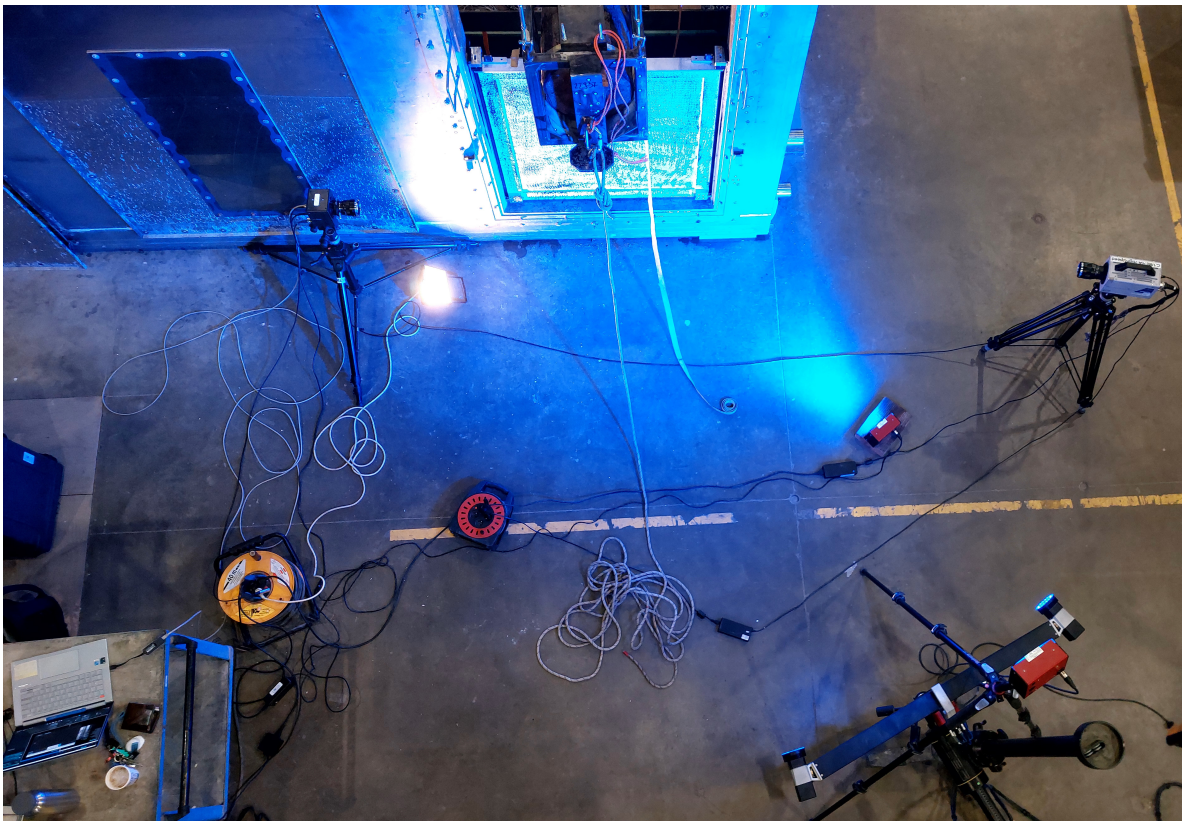


Figure 3.23: Final setup for the first test.

3.2.2 Test procedure

The complete test procedure can be divided into the preparation and the actual test for each of the three tests.

3.2.2.1 Hydrostatic test before impact

For the hydrostatic test, the metal structure with three openings, where ideally three different barriers are installed, is placed in a water tank and secured in such a way that everything is sealed and no water enters the structure itself. If fewer than three barriers are tested, the other openings are sealed tightly so that no leakage occurs that could influence the result of the tested barrier. The barriers will now remain in the steel frame until the end of all test series (see Fig. 3.24).

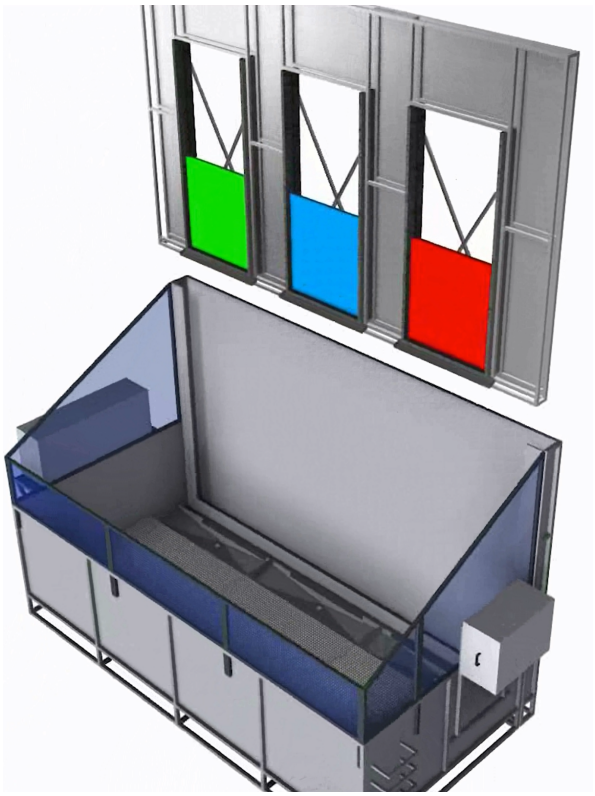


Figure 3.24: Structure with three openings placed in water tank.

Once everything is set up, the two tests can begin.

- Test 1: The water is brought to a height of 10 cm and the water leaks are measured at 15-minute intervals for two hours.

- Test 2: The water is brought to a height of 95 cm and the water leaks are measured at 15-minute intervals for 20 hours.

The second test therefore deviates from the American standard in that the water is not raised to 100% but to 95% of the maximum water design height of the barrier.

3.2.2.2 Impact test

For the impact test, the steel structure with the 3 openings is detached from the water tank and lifted out. It is then positioned so that it has steel pillars on both sides against which it can be leant and secured using tensioning straps (see Fig. 3.25).



(a) Structure lifted out of water tank. (b) Structure fixed on steel pillars.

Figure 3.25: Structure displacement.

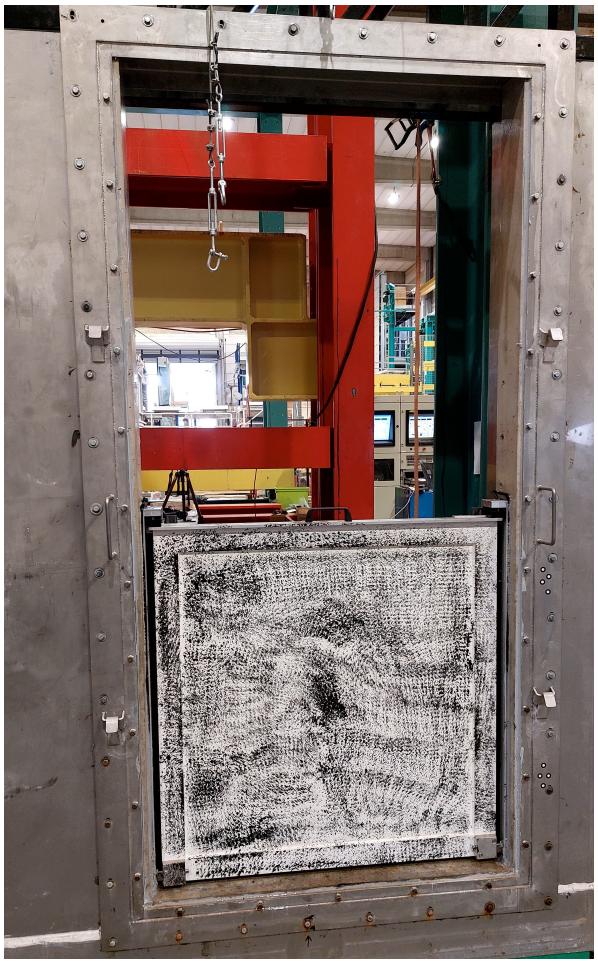


Figure 3.26: Painted barrier in one of the three openings.

Now black colour is applied to the barrier. It is dabbed onto the barrier to create lots of contrast points, which camera 3 can use to measure the 3D deformation. White dots with a black border must also be attached to the edge of the barrier so that the camera can better delimit the barrier and has reference points which it can be calibrated on (see Fig. 3.26).

Once this has been done, the impact object is weighed, and its centre of gravity is measured.

Then, the impact object can be aligned for the first impact test, which is an impact centred at 80% of the height of the barrier. The reference chess pattern can be attached to the steel frame of the impact object before or after the alignment. When setting up the cameras and spots, it is important to ensure that camera 1 is perfectly perpendicular to the reference object. It must also be aligned so that the reference pattern in the

camera image is perfectly parallel to the edges of the recording frame. This makes it possible to be more accurate when measuring the pixels.

Now, when the setup is ready, the height of the centre of gravity is measured from the ground and the measurements for positioning the impact object are obtained. The impact object can then be raised to the required height. With a weight of 50 kg, this would be a height of 1.22 m in order to achieve a potential energy of around 600 J.

The object is raised to the correct height using an electromagnet, which is released for the impact test. A countdown of 3 allows the recording for camera 1 and 2 to start shortly before impact, which is also necessary due to the short recording time.
For the second impact at the edge of the barrier the setup must be moved, readjusted and recalibrated.

3.2.2.3 Hydrostatic test after impact

After the impact tests there is a second series of hydrostatic tests, as described in the American standard. For the second hydrostatic test series, the metal structure is again placed in the water tank and secured so that everything is tight and no water leakages are in the structure itself.

Once everything is set up, the two tests can begin.

- Test 1: The water is brought to a height of 10 cm and the water leaks are measured at 15-minute intervals for one hour. If the results don't stabilise, the test is done over a length of 1.5 to 2 hours.
- Test 2: The water is brought to a height of 95 cm and the water leaks are measured at 15-minute intervals for one hour. If the results don't stabilise, the test is done over a length of 2 hours.

3.3 Analysis of the tests

In this section, the tests on two barriers are analysed. As the manufacturer may not be named for legal reasons, the barriers are simply labelled Barrier X and Barrier Y.

Note: During the 3D deformation measurements, it was observed that the steel frame with the three openings also experienced a slight shift. However, since this deformation was relatively minimal, it was neglected.

3.3.1 Barrier X

3.3.1.1 Description

Barrier X consists of two fixed guide profiles and a removable water barrier (Fig. 3.27). The tested barrier has a width (A) of 1 m and a height (B) of 1.2 m. The barrier itself consists of an aluminium shell with a foam-filled core. The barrier is sealed with an EPDM (ethylene propylene diene monomer rubber) seal. Another EPDM seal at the bottom ensures optimal tightness, even on rougher floors.

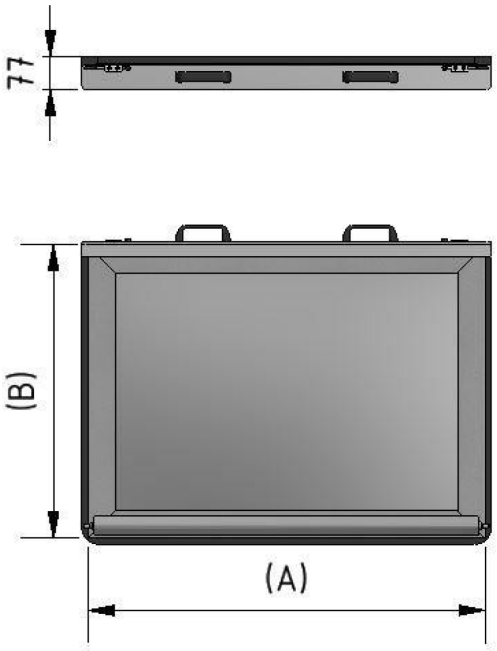


Figure 3.27: Dimensions barrier X. [5]

The guide profiles are attached to the wall with screws and must then be sealed with silicone. When waterlogging is imminent, the water barrier has to be inserted into the gap between the guide profiles and fixed in such a way that no leakages are possible. This is done using a pressure block, which pushes the barrier down when pushed in between the guide profiles. The installation of the barrier can be seen in Figure 3.28. [5]



(a) Fixation of the protruding pin in the provided opening.

(b) Placing the barrier in between the guide profiles.

(c) Pushing the barrier in against the guide profiles.

(d) Securing the barrier by sliding the bolt in place.

Figure 3.28: Barrier X installation. [5]

3.3.1.2 Hydrostatic test before impact

Test 1 - 10 cm		
Time step	Leakage [g]	Leakage < 1 L/h/m
8	0	OK
Test 2 - 95 cm		
Time step	Leakage [g]	Leakage < 1 L/h/m
2	0	OK
10	0	OK
80	0.7	OK

Table 3.9: Barrier X - Hydrostatic test results.

The system showed a significant leak at 10% before the water was increased to 95% and then back to 10%.
As a measure of leakage, the only information given from the system was that it was greater than 1 L/h/m. Given that the leakage rate was very significant, the water level was directly increased and it was observed that the leaks disappeared. When it went back to 10 cm, there were no more leaks. The installation of the product has to be discussed with the manufacturer.

For the first test of 2 hours at 10 cm water height, the results in Table 3.9 show a leakage measured in time step 8, within the last 15 minutes of the test. For the second test, with a water height of 95 cm for 20 hours, three measurements are shown, one at 30 minutes, one at 2.5 h and the last one at 20 h. It can be seen that there were nearly no leaks in both tests, after the leakage mentioned above disappeared by itself.

3.3.1.3 Impact Test

As described in the test procedure, two impact tests were carried out on Barrier X, one first test in the centre at 50% height of the barrier and a second test 18.5 cm from the edge, at 80% height of the barrier. For each time step used for measurement, i.e. 0.25, 0.5, 1, 2 and 4 ms, measurements were taken at three different points on the chess pattern instead of just one reference point in order to obtain even more accurate measurements and a more accurate mean value for the kinetic impact energy. The three points chosen can be seen in Figure 3.29. As the values for a time step of 4ms are the most accurate and are used for further analyses, they are the only ones listed here. The measurements for the other time steps can be found in Appendix C. For the return energy measurements, it is assumed that the impact object is rigid. It is therefore assumed that the object does not deform and that both, the speed and kinetic energy, are uniform across all parts of the object.

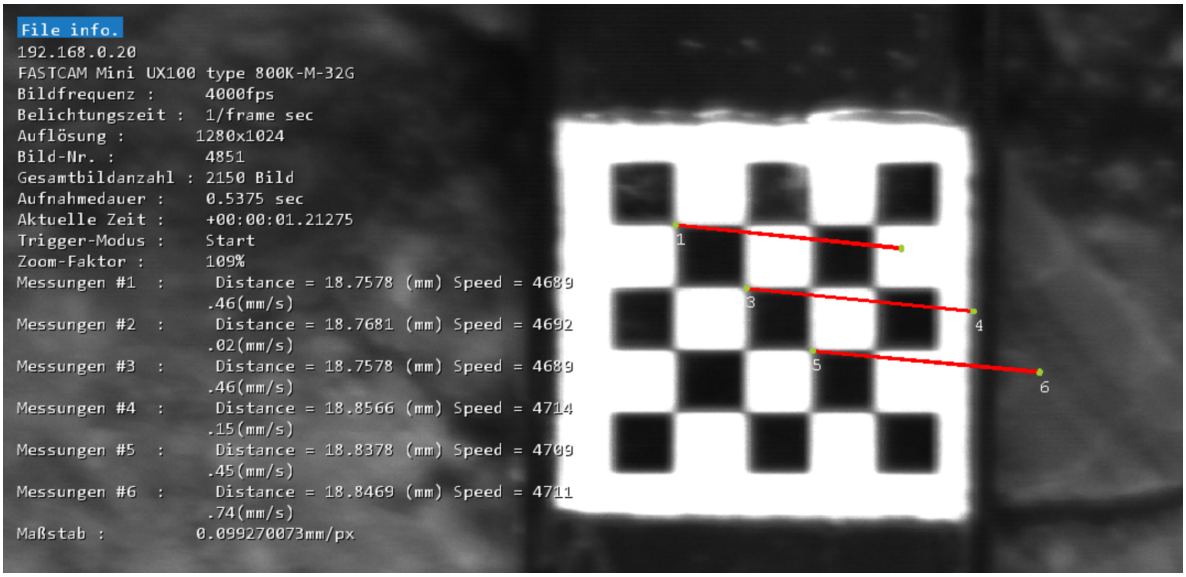


Figure 3.29: Measurements done on three reference points on the chess pattern.

The given values for both tests are shown in Table 3.10.

fps	4000
m [kg]	49.8
Δh_g [m]	1.22
$E_{pot,g}$ [J]	596.02

Table 3.10: Given values.

First test

The first impact was done in the centre at 50% height of the barrier and not at 80% as recommended. This is because it is the most defavorable positioning for deformation of the barrier itself. The scale in which the measurements were made was 97.84 µm/px. In a first part, the measurement of the impact energy was made.

Time step Δt [ms]	**4**					
Measurement	**1**		**2**		**3**	
v [m/s]	4.767	4.790	4.788	4.790	4.788	4.790
$E_{kin}[J]$	565.84	571.29	570.75	571.29	570.75	571.29
Ratio $\frac{E_{kin}}{E_{pot}}$ [%]	94.94	95.85	95.76	95.85	95.76	95.85
$\Delta\frac{E_{kin}}{E_{pot}}$ [%]	0.91		0.09		0.09	
Total Mean of E_{kin} [J]	**570.2**					
Total Mean of $\frac{E_{kin}}{E_{pot}}$ [%]	**95.67**					
Total Mean of $\Delta\frac{E_{kin}}{E_{pot}}$ [%]	**0.37**					

Table 3.11: Barrier X: First test - Measurements of the impact energy over a time step of 4 ms.

Looking at the results in Table 3.11, it can be observed that with a measuring error of only 0.37% of the ratio of the kinetic impact energy over the starting potential energy the kinetic energy of the pendulum right before the impact ranges from 569.11 to 571.31 J with a mean of 570.2 J. This means that only 4.33% of the initial potential energy was lost due to friction. For further analysis of the absorbed energy the mean kinetic energy of 570.2 J is taken as a reference impact energy $E_{kin,impact}$.
In a second part, the return energy $E_{kin,return}$ of the barrier was measured. The results are shown in Table 3.12. The same procedure was used.

Time step Δt [ms]	**4**					
Measurement	**1**		**2**		**3**	
v [m/s]	3.180	3.155	3.180	3.180	3.205	3.180
$E_{kin}[J]$	251.79	247.93	251.79	251.84	255.72	251.84
Ratio $\frac{E_{kin,return}}{E_{kin,impact}}$ [%]	94.94	95.85	95.76	95.85	95.76	95.85
$\Delta\frac{E_{kin,return}}{E_{kin,impact}}$ [%]	0.68		0.01		0.68	
Total Mean of E_{kin} [J]	**251.82**					
Total Mean of $\frac{E_{kin,return}}{E_{kin,impact}}$ [%]	**44.16**					
Total Mean of $\Delta\frac{E_{kin,return}}{E_{kin,impact}}$ [%]	**0.46**					

Table 3.12: Barrier X: First test - Measurements of the return energy over a time step of 4 ms.

Comparing the values in Table 3.13 of the return energy with the impact energy and looking at the results of camera 3 in Figure 3.30, some conclusions about the impact can be made.

Contact Time [ms]	69.75
$E_{kin,impact}$ [J]	570.2
$E_{kin,return}$ [J]	251.82
$E_{kin,absorbed}$ [%]	55.86
Maximum Deformation [mm]	3.343

Table 3.13: Results comparison.

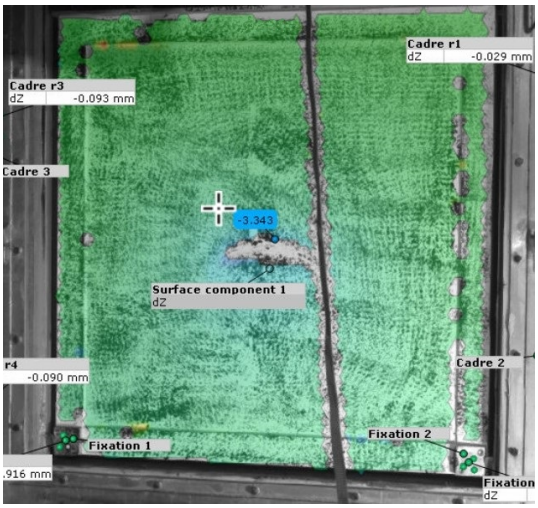


Figure 3.30: Barrier X after first impact.

First of all, a clear deformation can be seen in the centre of the barrier, at the impact point. However, the deformation is relatively small. With an absorbed energy $E_{kin,absorbed}$ of 55.86%, i.e. 55.86% of the kinetic energy lost at the impact, and a deformation of only 3.343 mm, it can be said that the barrier had mainly an elastic deformation and only a small part of the total deformation is plastic and therefore not

reversible. This reasoning can also be supported by the contact time of the impact, which at 69.75 ms is high compared to others. If the deformation is elastic, the contact time is higher, as the impact object touches the barrier not only in the outward but also in the return movement. The entire barrier remains fully functional at first glance due to the minimal plastic deformation.

Second test

A second test was done at 18.5 cm from the edge and 80% height of the barrier. This was mainly to test how the connection to the guide profiles would react to an impact near them. The scale in which the measurements were made was 95.105 µm/px.

Time step Δt [ms]	**4**					
Measurement	**1**		**2**		**3**	
v [m/s]	4.729	4.706	4.729	4.706	4.703	4.727
$E_{kin}[J]$	556.93	551.36	556.93	551.36	550.84	556.40
Ratio $\frac{E_{kin}}{E_{pot}}$ [%]	93.44	92.51	93.44	92.51	92.42	93.35
$\Delta\frac{E_{kin}}{E_{pot}}$ [%]	0.93		0.93		0.0.93	
Total Mean of E_{kin} [J]	**553.97**					
Total Mean of $\frac{E_{kin}}{E_{pot}}$ [%]	**92.95**					
Total Mean of $\Delta\frac{E_{kin}}{E_{pot}}$ [%]	**0.93**					

Table 3.14: Barrier X: Second test - Measurements of the impact energy over a time step of 4 ms.

Looking at the results in Table 3.14, it can be observed that with a measuring error of only 0.93% of the ratio of the kinetic impact energy over the starting potential energy the kinetic energy of the pendulum right before the impact ranges from 556.75 to 551.19 J with a mean of 553.97 J. This means that 7.05% of the initial potential energy was lost due to friction. For further analysis of the absorbed energy the mean kinetic energy of 553.97 J is taken as a reference impact energy $E_{kin,impact}$.
In a second part the return energy $E_{kin,return}$ of the barrier was measured. The results are shown in Table 3.15. The same procedure was used.

Time step Δt [ms]	**4**					
Measurement	**1**		**2**		**3**	
v [m/s]	2.76	2.74	2.74	2.71	2.71	2.74
$E_{kin,return}[J]$	189.62	186.36	186.27	183.14	183.14	186.36
Ratio $\frac{E_{kin,return}}{E_{kin,impact}}$ [%]	34.23	33.64	33.62	33.06	33.06	33.64
$\Delta\frac{E_{kin,return}}{E_{kin,impact}}$ [%]	0.55		0.52		0.54	
Total Mean of E_{kin} [J]	**185.82**					
Total Mean of $\frac{E_{kin,return}}{E_{kin,impact}}$ [%]	**33.54**					
Total Mean of $\Delta\frac{E_{kin,return}}{E_{kin,impact}}$ [%]	**0.54**					

Table 3.15: Barrier X: Second test - Measurements of the return energy over a time step of 4 ms.

Comparing the values in Table 3.16 of the return energy with the impact energy and looking at the results of camera 3 in Figure 3.31, some conclusions about the impact can be made.

Contact Time [ms]	56.75
$E_{kin,impact}$ [J]	553.97
$E_{kin,return}$ [J]	185.82
$E_{kin,absorbed}$ [%]	66.46
Maximum Deformation [mm]	4.58

Table 3.16: Results comparison.

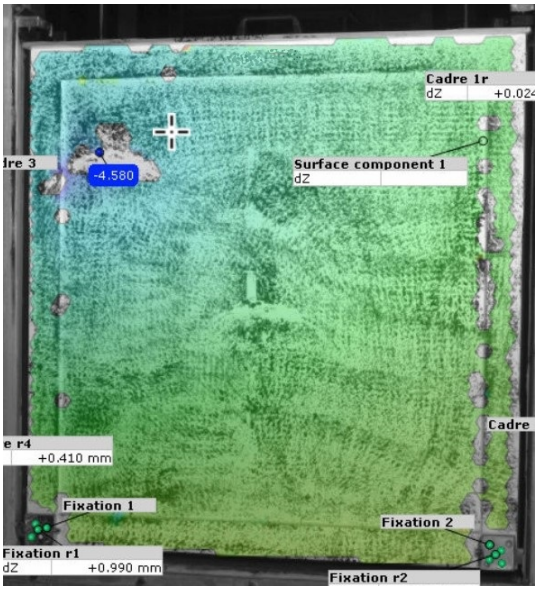


Figure 3.31: Barrier X after second impact.

As in the first test, a clear deformation can be seen at the impact point. Similar to the first impact, the final deformation is relatively small. With an absorbed energy $E_{kin,absorbed}$ of 66.46%, i.e. and a deformation of 4.58 mm, it can be said that the

barrier had a less elastic deformation than in the first test. This can be explained by the fact that the barrier near the edge cannot be elastically deformed as much as in the centre due to the guide profiles that hold the barrier in place. As a result, the contact time of the impact of 56.75 ms is also shorter than in the first test. Nevertheless, the deformation was largely elastic, which is why only a small plastic deformation remains visible at the end and the entire barrier remains fully functional.

3.3.1.4 Hydrostatic test after impact

The results for the hydrostatic tests after the impact test can be seen in Table 3.17. The leakage rate in [L/h/m] is calculated in the following way:

$$Leakagerate[L/h/m] = \frac{Leakage[g] \cdot 4}{1000 \cdot l} \tag{3.3}$$

where

- Leakage [g] is the water leakage measured over one time step of 15 minutes. So to receive the value in liters over one hour, the value has to be multiplied by 4 and divided by a thousand.
- l is the seal length. w being the width of the barrier and h_{water} the water height, it is calculated as follows:

  $$l = w + 2 \cdot h_{water} \tag{3.4}$$

  For Test 1, a seal length of 1.23 m and for Test 2, a seal length of 2.93 m can be found.

Test 1 - 10 cm			
Time step	Leakage [g]	Leakage [L/h/m]	$<$ 1 L/h/m
1	28	0.091	OK
2	60	0.195	OK
3	0	0	OK
4	0	0	OK
Test 2 - 95 cm			
Time step	Leakage [g]	Leakage [L/h/m]	$<$ 1 L/h/m
1	0	0	OK
2	0	0	OK
3	0	0	OK
4	0	0	OK
5	12	0.016	OK
6	51	0.070	OK
7	60	0.082	OK
8	62	0.085	OK

Table 3.17: Barrier X - Hydrostatic test after impact results.

Looking at the results in Table 3.17, the leakage stayed well under 1 $L/h/m$ at all times.

This means that Barrier X is still fully functional according to the norm even after 2 impacts of around 600 J. The only problem could be the reuse of the barrier. The guide profiles could be damaged after the impact tests, meaning that the barrier can no longer be reused. The barrier would therefore have to be completely replaced.

3.3.2 Barrier Y

3.3.2.1 Description

Barrier Y consists of two fixed profiles and a removable water barrier (Fig. 3.32) which in turn consists of two elements. As there was no access to a technical sheet of the barrier, no information can be provided on its exact dimensions or materials.

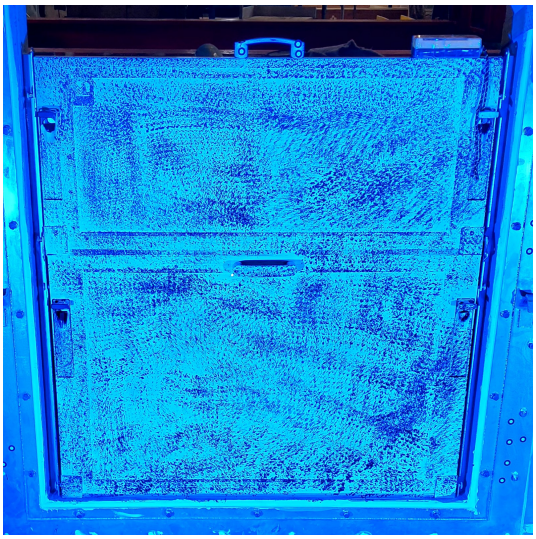


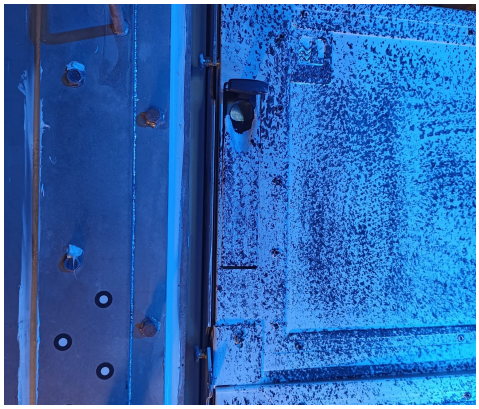
Figure 3.32: Barrier Y.

The guide profiles are attached to the wall with screws and must then be sealed with silicone.

The barrier must be installed in several steps. First, the element must be hooked in at the bottom and then rotated into a vertical position so that it fits into the track (Fig. 3.33a). The levers on the side must be pushed upwards. This secures the element at the top and presses it downwards, ensuring a watertight seal (Fig. 3.33b). The same procedure must then be repeated for the second element.



(a) The barrier is hooked onto the steel profile.



(b) Securing and sealing by operating the lever.

Figure 3.33: Barrier Y installation.

3.3.2.2 Hydrostatic test before impact

Test 1 - 10 cm			
Time step	Leakage [g]	Leakage [L/h/m]	Leakage $<$ 1 L/h/m
8	0	0	OK
Test 2 - 95 cm			
Time step	Leakage [g]	Leakage [L/h/m]	Leakage $<$ 1 L/h/m
2	328	0.448	OK
10	200	0.273	OK
80	13	0.018	OK

Table 3.18: Barrier Y - Hydrostatic test results.

For the first test of 2 hours at 10 cm water height, the results in Table 3.18 show the leakage measured in time step 8, the last 15 minutes of the test. There were no leakages for this test. For the second test, with a water height of 95 cm for 20 hours, three measurements are shown, one at 30 minutes, one at 2.5 h and the last one at 20 h. As can be seen, the values remained below 1 L/h/m in all measurements, as prescribed in the FM Approvals.

3.3.2.3 Impact test

As described in the test procedure, two impact tests were carried out on Barrier Y, one first test in the centre at 80% height of the barrier and a second test 14 cm from the left edge, also at 80% height of the barrier.

First test

The first impact was done in the centre at 80% height of the barrier as recommended. The scale in which the measurements were made was 97.84 µm/px. In a first part, the measurement of the impact energy was made.

Time step Δt [ms]	**4**					
Measurement	**1**		**2**		**3**	
v [m/s]	4.689	4.692	4.689	4.714	4.709	4.712
$E_{kin}[J]$	547.58	548.17	547.58	553.36	552.26	552.79
Ratio $\frac{E_{kin}}{E_{pot}}$ [%]	91.87	91.97	91.87	92.84	92.66	92.75
$\Delta\frac{E_{kin}}{E_{pot}}$ [%]	0.10		0.97		0.09	
Total Mean of E_{kin} [J]	**550.29**					
Total Mean of $\frac{E_{kin}}{E_{pot}}$ [%]	**92.33**					
Total Mean of $\Delta\frac{E_{kin}}{E_{pot}}$ [%]	**0.39**					

Table 3.19: Barrier Y: First test - Measurements of the impact energy over a time step of 4 ms.

Looking at the results in Table 3.19, it can be observed that, with a measuring error of only 0.39% of the ratio of the kinetic impact energy over the starting potential energy, the kinetic energy of the pendulum right before the impact ranges from 549.14 to 551.46 J with a mean of 550.29 J. This would mean that 7.67% of the initial potential energy was lost due to friction. For further analysis of the absorbed energy the mean kinetic energy of 550.29 J is taken as a reference impact energy $E_{kin,impact}$.
In a second part the return energy $E_{kin,return}$ of the barrier was measured. The results are shown in Table 3.20. The same procedure was used.

Time step Δt [ms]	**4**					
Measurement	**1**		**2**		**3**	
v [m/s]	2.387	2.411	2.411	2.436	2.411	2.408
$E_{kin}[J]$	141.86	144.79	144.79	147.75	144.79	144.34
Ratio $\frac{E_{kin,return}}{E_{kin,impact}}$ [%]	25.78	26.31	26.31	26.85	26.31	26.23
$\Delta\frac{E_{kin,return}}{E_{kin,impact}}$ [%]	0.49		0.50		0.07	
Total Mean of E_{kin} [J]	**144.72**					
Total Mean of $\frac{E_{kin,return}}{E_{kin,impact}}$ [%]	**26.30**					
Total Mean of $\Delta\frac{E_{kin,return}}{E_{kin,impact}}$ [%]	**0.35**					

Table 3.20: Barrier Y: First test - Measurements of the return energy over a time step of 4 ms.

Comparing the values in Table 3.21 of the return energy with the impact energy and looking at the results of camera 3 in Figure 3.34, some conclusions about the impact can be made.

Contact Time [ms]	43.25
$E_{kin,impact}$ [J]	550.29
$E_{kin,return}$ [J]	144.72
$E_{kin,absorbed}$ [%]	73.7
Maximum Deformation [mm]	16

Table 3.21: Results comparison.

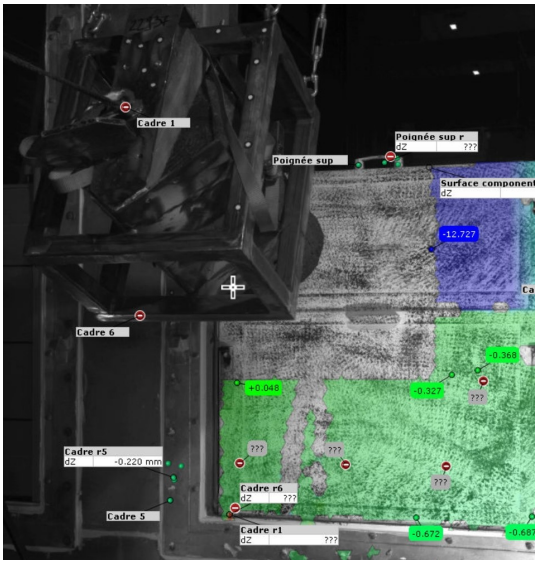


Figure 3.34: Barrier Y after first impact.

First of all, a clear deformation of the upper element of the barrier can be seen, where the impact object hit the barrier. The deformation is way higher than the ones on Barrier X. The lower element of the barrier did not deform at all.The deformation

was measured manually because the camera was unable to take measurements at the impact point, as shown in Figure 3.34. With an absorbed energy $E_{kin,absorbed}$ of 73.7%, i.e. 73.7% of the kinetic energy lost at the impact, and a deformation of 16 mm, it can be said that the deformation was largely plastic.
This reasoning can also be supported by the contact time, which at 43.25 ms, is low compared to the first impact on Barrier X at 69.75 ms. If the deformation is mostly plastic, the contact time is lower, as the impact object nearly only touches the barrier in the outward and not in the return movement.
At first inspection, no openings are visible, but it remains to be determined whether the tightness can be guaranteed due to the large deformation.

Second test

A second test was done at 14 cm from the edge, at 80% height of the barrier. This was mainly to test how the connection to the guide profiles would react to an impact near them. The scale in which the measurements were made was 96.11 µm/px.

Time step Δt [ms]	**4**					
Measurement	**1**		**2**		**3**	
v [m/s]	4.636	4.638	4.634	4.636	4.634	4.636
$E_{kin}[J]$	535.15	535.72	534.62	535.15	534.62	535.15
Ratio $\frac{E_{kin}}{E_{pot}}$ [%]	89.79	89.88	89.70	89.79	89.70	89.79
$\Delta\frac{E_{kin}}{E_{pot}}$ [%]	0.09		0.09		0.09	
Total Mean of E_{kin} [J]	**535.07**					
Total Mean of $\frac{E_{kin}}{E_{pot}}$ [%]	**89.77**					
Total Mean of $\Delta\frac{E_{kin}}{E_{pot}}$ [%]	**0.09**					

Table 3.22: Barrier Y: Second test - Measurements of the impact energy over a time step of 4 ms.

Looking at the results in Table 3.22, it can be observed that, with a measuring error of only 0.09% of the ratio of the kinetic impact energy over the starting potential energy, the kinetic energy of the pendulum right before the impact ranges from 534.98 to 535.16 J with a mean of 535.07 J. This means that 10.23% of the initial potential energy was lost due to friction. For further analysis of the absorbed energy the mean kinetic energy of 535.07 J is taken as a reference impact energy $E_{kin,impact}$.

In a second part the return energy $E_{kin,return}$ of the barrier was measured. The results are shown in Table 3.23. The same procedure was used.

Time step Δt [ms]	**4**					
Measurement	**1**		**2**		**3**	
v [m/s]	2.059	2.086	2.083	2.086	2.083	2.107
$E_{kin,return}[J]$	105.61	108.40	108.07	108.40	108.07	110.55
Ratio $\frac{E_{kin,return}}{E_{kin,impact}}$ [%]	19.19	19.70	19.64	19.70	19.64	20.09
$\Delta\frac{E_{kin,return}}{E_{kin,impact}}$ [%]	0.47		0.06		0.42	
Total Mean of E_{kin} [J]	**108.18**					
Total Mean of $\frac{E_{kin,return}}{E_{kin,impact}}$ [%]	**19.66**					
Total Mean of $\Delta\frac{E_{kin,return}}{E_{kin,impact}}$ [%]	**0.31**					

Table 3.23: Barrier Y: Second test - Measurements of the return energy over a time step of 4 ms.

Comparing the values in Table 3.24 of the return energy with the impact energy and looking at the results of camera 3 in Figure 3.35, some conclusions about the impact can be made.

Contact Time [ms]	35
$E_{kin,impact}$ [J]	535.07
$E_{kin,return}$ [J]	108.18
$E_{kin,absorbed}$ [%]	80.34
Maximum Deformation [mm]	5.454

Table 3.24: Results comparison.

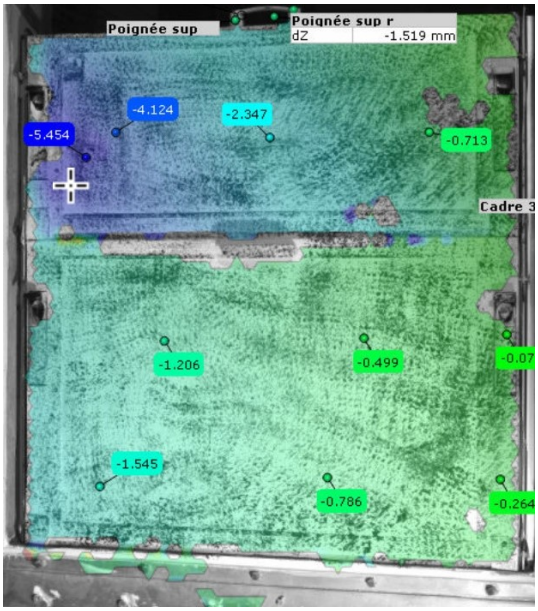


Figure 3.35: Barrier Y after second impact.

As in the first test, a deformation can be seen at the impact point. Contrary to the first impact, the final deformation is relatively small. With an absorbed energy $E_{kin,absorbed}$ of 80.34% and a deformation of 5.454 mm, it can be said that the impact was highly inelastic. Similar to the second test on Barrier X, the contact time is smaller than for the first test, here only 35 ms. This can be explained in the same way due to the impact position near the connection to the steel frame. In this case, the barrier appears to be much more resistant on the sides, which means that the structure absorbs most of the energy without a high deformation. So, this impact had no big influence on the overall structure of the barrier.

3.3.2.4 Hydrostatic test after impact

The results for the hydrostatic tests after the impact test can be seen in Table 3.25. The calculation of the leakage rate is explained in Section 3.3.1.2. The same seal lengths as for the Barrier X were used.

Test 1 - 10 cm			
Time step	Leakage [g]	Leakage [L/h/m]	< 1 L/h/m
1	0	0	OK
2	0	0	OK
3	0	0	OK
4	0	0	OK
Test 2 - 95 cm			
Time step	Leakage [g]	Leakage [L/h/m]	< 1 L/h/m
1	646	0.882	OK
2	529	0.722	OK
3	517	0.706	OK
4	479	0.654	OK
5	440	0.601	OK
6	397	0.542	OK
7	353	0.482	OK
8	334	0.456	OK

Table 3.25: Barrier Y - Hydrostatic test after impact results.

Looking at the results in Table 3.25, even though there were significantly higher water leakages than Barrier X had, the leakage stayed under the 1 L/h/m length of seal limit at all times.

This means that Barrier Y is still fully functional according to the norm even after 2 impacts of around 600 J, even though the leakage rate nearly doubled after those.
The advantage of Barrier Y is that only one of the two elements of the barrier is deformed by the impacts, thanks to the joint in the centre, which is why it would be possible to replace only one element, provided the guide profiles on the sides are not too badly damaged and the whole setup would need to be replaced.

3.4 Analysis of the results and improvements

3.4.1 Result comparison

In this section, the kinetic impact energies of the 4 tests are compared to see how accurate the measurement method using camera 1 is and what the possible errors are.

Test	Barrier X - 1	Barrier X - 2	Barrier Y - 1	Barrier Y - 2
E_{pot} [J]	**596.0164**			
$E_{kin,impact}$ [J]	570.2	553.97	550.29	535.07
Mean $E_{kin,impact}$ [J]	**552.38**			
$\frac{E_{kin,impact}}{E_{pot}}$ [%]	95.67	92.95	92.33	89.77
Mean $\frac{E_{kin,impact}}{E_{pot}}$ [%]	**92.68**			

Table 3.26: Comparison impact energies.

Looking at the values in Table 3.26, it can be seen that the average kinetic impact energy is around 552.4 J, i.e. 92.7% of the initial potential energy. This in turn means that around 7.3% of the initial energy is lost through friction. The problem with this is that the barrier is not tested to the planned 600 J, but less. Now, of course, the question is whether in the American norm, with their method of measuring the height of the impact object, the impact has this 7.3% more energy or, as in previous tests in the small model, goes significantly beyond this.
With a measured height of 1.22 m at the centre of gravity, the height measured from the tip of the object is 1.056 m, which would correspond to a difference of 16.4 cm. Due to the rotation of the pendulum, it can be assumed that this difference increases the higher the impact object is lifted. For the analysis, however, a difference of 16.4 cm is assumed.

$\Delta h, tip$ [m]	1.22
$\Delta h, g$ [m]	1.384
$E_{pot,g}$ [J]	676.14
$E_{kin,impact}$ [J]	626.64

Table 3.27: Impact energy with different height.

So, if a height of 1.22 m is assumed at the tip of the impact object the values in

Table 3.27 are obtained. Assuming that around 92.68% of the potential launch energy is converted into the kinetic impact energy, an impact energy of 626.64 J can be calculated, which is higher than 600 J. This is not acceptable, because it could be that a barrier breaks at 626.64 J, but would not do so at 600 J, which would be decisive for a possible certification.
This again confirms that it is important to measure the height at the centre of gravity and not at the tip of the impact object as described in the FM Approvals.

The correct approach would therefore be to increase the height at the centre of gravity as far as possible in order to achieve an impact energy of 600 J. However, the error in the measurement of the kinetic impact energy must be taken into account. By comparing the values in Table 3.26, it can be noticed that there is a difference of 35.13 J between the highest measured value of the kinetic impact energy and the lowest, or 5.9% as a percentage of the potential energy.

The safest method would therefore be to take the highest measured value as the reference value for the recalculation of the height, because if we take the average value, it is possible that the measurements result in values higher than 600 J, which is not acceptable for the reasons mentioned above.

$E_{kin,impact}$ [J]	600
$E_{pot,g}$ [J]	627.16
Δh_g [m]	1.284

Table 3.28: Height calculation.

Assuming that 95.68% of the potential energy is converted into impact energy, as can be seen in Table 3.28, a potential energy of 627.16 J is obtained for a kinetic energy of 600 J, which results in a height of 1.284 m. The problem is that if we now assume the other extreme, i.e. that only 89.77% is converted, this would mean that even with a potential energy of 627.16 J, only around 563 J remains as impact energy, which is still significantly less than the 600 J. To avoid this, it would therefore be worthwhile to reduce the percentage error as much as possible.

So what are the sources of error when measuring kinetic energy? The two extreme values are used to analyse various sources of error.

3.4.1.1 Height measurement

There can be several problems when measuring the height of the object. It is possible that the nail on which the measurement must be taken has moved. It may be that the correct measuring device, i.e. a laser, is not available and therefore a metre rule has to be used, which is less accurate. The biggest issue, however, is that the impact object swings up and down by around 2 cm, 1 cm up and 1 cm down. This makes it impossible to take an accurate measurement. Here is a comparison of what 2 cm make up for the two extreme measurements. In the first comparison, we assume an error of one cm, i.e. that the impact object was 1 cm higher than 1.22 m for the higher value and 1 cm lower for the lower value.

Test	Barrier X - 1	Barrier Y - 2
$E_{kin,impact}$ [J]	570.2	535.07
Δh [m]	1.23	1.21
E_{pot} [J]	600.9	591.1
$\frac{E_{kin,impact}}{E_{pot}}$ [%]	94.89	90.52
$\Delta\frac{E_{kin,impact}}{E_{pot}}$	**4.37%**	

Table 3.29: Comparison of a height difference of 1 cm.

Test	Barrier X - 1	Barrier Y - 2
$E_{kin,impact}$ [J]	570.2	535.07
Δh [m]	1.24	1.2
E_{pot} [J]	605.8	586.2
$\frac{E_{kin,impact}}{E_{pot}}$ [%]	93.87	91.45
$\Delta\frac{E_{kin,impact}}{E_{pot}}$	**2.43%**	

Table 3.30: Comparison of a height difference of 2 cm.

As can be seen in Table 3.29 the difference between the percentages is reduced from 5.9% to 4.37% with a height difference of 1 cm each, while for 2 cm each Table 3.30 shows that is reduced to 2.43%. It can be concluded that it is crucial to measure the height of the impact object precisely.

3.4.1.2 Camera calibration

The second reason why errors can occur in the measurements is due to the calibration of the camera. The measurement error due to inaccuracies in the pixels was reduced by increasing the number of frames used for the measurement. However, the problem is that if the camera calibration is incorrect from the outset, the measured values can also be higher or lower. This can happen if it is not possible to recognise an exact distinction between black and white in the chess pattern. This can be even worse if the image is overexposed and the correct black border disappears as a result.To put it simply, as soon as there is no clear contrast in the chess pattern, errors can occur.
In addition, the lens focus must be adjusted manually. It is therefore virtually impossible to find the exact focus at which the image is clearest. As in the previous section, the extreme values are used to test the extent of the error.

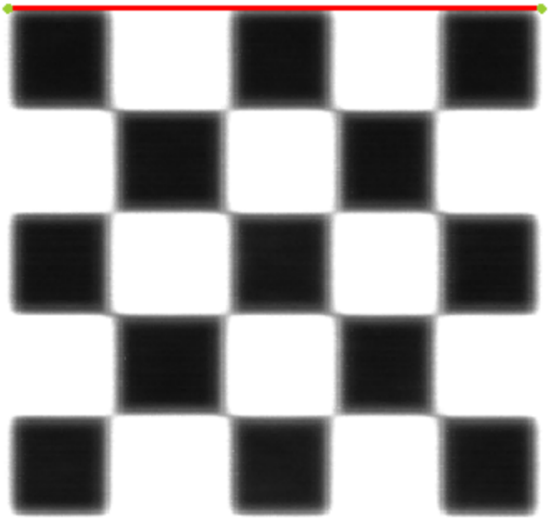


Figure 3.36: Calibration of the camera.

For the calibration, the length of the chess pattern is known, in this case 27.2 cm. Using the red line visible in Figure 3.36, the distance can be determined and thus set the calibration in mm/px. However, due to the problems mentioned above, it is possible that too many or too few pixels are taken into consideration. It is also not possible to use the same calibration for every test, because depending on how the impact object is released, the distance from the chess pattern to the camera is different. These differences could then result in errors. That is why two new calibrations were done. For Barrier

X - Test 1 Calibration 1 is the difference of one pixel on the left and one on the right respectively, so in total 2 pixels more. Calibration 2 is the difference of two pixels on the left and two on the right respectively, so in total 4 pixels more. For Barrier Y - Test 2 the new calibrations are the same only that the pixels were not added but subtracted. In Table 3.31 and 3.32 a comparison of the results with the different calibrations is shown for the tests of Barrier X - 1 and Barrier Y - 2 respectively.

Calibration	# Pixel	µm/pixel	Mean $E_{kin,impact}$ [J]	$\frac{E_{kin,impact}}{E_{pot}}$ [%]
Initial	280	97.84	566.2	94.99
1	282	97.14	558.1	93.64
2	284	96.45	550.2	92.32

Table 3.31: Barrier X - Test 1: Results for different calibrations.

Calibration	# Pixel	µm/pixel	Mean $E_{kin,impact}$ [J]	$\frac{E_{kin,impact}}{E_{pot}}$ [%]
Initial	283	96.11	535.1	89.77
1	281	96.8	542.7	91.06
2	279	97.49	550.5	92.37

Table 3.32: Barrier Y - Test 2: Results for different calibrations.

Based on this comparison, it can be observed that a difference of just 2 pixels in the calibration of the camera image results in a change of around 1.29-1.35% in the rate of kinetic impact energy over potential energy. With 4 pixels the change is around 2.6-2.67%. The latter is almost exactly the percentage by which the values of Test 1 on Barrier X and Test 2 on Barrier Y deviate from the average value of the kinetic impact energy being 92.68%. It therefore seems quite possible that the deviation is due to an error in the calibration.

3.4.2 Improvements

This section discusses ways to minimise the sources of error described above.

3.4.2.1 Height measurement solution

- In addition to using the right instruments, i.e. ideally a laser, to measure as accurately as possible, the nail should also be fixed well to minimise measurement errors due to displacement.

- The bigger problem was the oscillation of the impact object when it was lifted, which made it impossible to measure accurately.
  One recommendation is to lift the object to a provisional height and leave it there until the oscillations have stopped. Then, the height should be adjusted if necessary and it needs to be waited again until the oscillations have stopped. This process must be repeated until the exact height has been reached or at least to within a few millimetres to avoid errors of a higher percentage margin.
  However, as this procedure is very time-consuming, it was not possible to employ it in these test series.

3.4.2.2 Camera calibration solution

Since camera calibration is influenced by many factors, there are also several approaches to solving the problem. Here are some recommendations:

- The camera lens should ideally focus automatically rather than being adjusted manually. This helps to prevent additional blurring.

- The contrast between black and white in the camera image must be distinctly recognisable. This can be achieved by painting the pattern with a highly light-absorbing black paint. This ensures that the boundary between black and white doesn't fade away due to overexposure, especially under the high illumination needed for a clear image.

- If the exact border remains unclear, an alternative is to zoom further into the image. The higher the pixel count, the more precise the calibration. There are two possibilities:
  - Use a camera with a higher resolution.
  - Increase the lens's focal length to enable deeper zooming.

All of these options are highly dependent on the material. Ideally, one would combine all of them; however, it is likely that only a part of them is sufficient to avoid major errors in the measurements.

If the improvements have been implemented and the error has been significantly minimised, a new height can be determined, which is then adjusted to the obtained values, such that the kinetic impact energy ultimately reaches 600 J.
Ideally, a test series should be conducted specifically to determine what percentage of the potential energy is converted into kinetic energy before proceeding with the actual test series. However, it is crucial that all tests are conducted under the same conditions. Specifically, the impact object must remain identical across all trials, as even a slight change in weight or the centre of gravity can lead to a variation in the percentage of absorbed energy.
To calculate the height, we assume that the error has been reduced to zero, meaning that the average value represents exactly the percentage of potential energy that is converted into kinetic energy.
In this case, it is assumed that the mean kinetic energy calculated in Table 3.26 corresponds to the exact percentage of the potential energy which is transformed into kinetic energy. Based on this assumption, the difference in height can be calculated, which will be used for the actual test series. Assuming a percentage of 92.68%, as shown in Table 3.33, a final height of 1.325 m was found.

$E_{kin,impact}$ [J]	600
$\frac{E_{kin,impact}}{E_{pot,g}}$ [%]	92.68
$E_{pot,g}$ [J]	647.38
Δh_g [m]	1.325

Table 3.33: Final height calculation.

This height would then be used to start the actual test series on the various barriers to ensure that they are tested with an impact energy of 600 J, assuming that approximately the same percentage of energy is converted into kinetic energy at 1.325 m as at a height of 1.22 m.

3.5 Final methodology

This section presents a proposal for the final testing procedure and lists the steps to be followed.

3.5.1 Preparation

Since the test steel frame with the three door openings needs to be moved for each step, a general preparation is difficult. Therefore, the preparation only includes weighing the impact object, determining its centre of gravity, and attaching the chess pattern to the frame of the impact object.

3.5.2 Preliminary impact test series

The purpose of the preliminary test series is to determine what percentage of potential energy is converted into kinetic energy, specifically the actual impact energy for the given impact object. For this test series, it is sufficient to use Cameras 1 and 2, which are synchronised. These cameras must be installed at the optimal distance from the impact object, and Camera 1 must be calibrated to ensure perfect conditions and minimise errors for the measurements.

Following this, at least three tests should be conducted to get an idea of the measurement error's magnitude, but more are recommended. The tests can be conducted on previously tested barriers or simply on wooden boards, as the values to be determined depend solely on the impact object and not on the barrier.

For these tests, a height of 1.22 m, corresponding to a potential starting energy of 600 J, is recommended.
After completing the test series, the results must be analysed. This will allow the determination of the percentage of potential energy that has been converted. Ideally, the error will be very small; however, it is recommended to use the highest measured percentage as a reference to avoid generating impact energies greater than 600 J during the actual test series.

3.5.3 Hydrostatic load test

For the hydrostatic test, the three barriers to be tested can now be installed in the steel frame. Once this is done, the steel frame can be positioned and secured in the tank. The test series consisting of two tests can then be carried out.

- Test 1: Water at 10% barrier height for 2 hours
- Test 2: Water at 100% barrier height for 20 hours

Measurements are taken at 15-minute intervals. No measurement should exceed a leakage rate of 1 liter per hour per metre of joint.

Unlike the previous tests conducted on the two barriers, which were limited to 95% of the maximum water design water height, a test at 100% of the maximum water design height is proposed, similar to FM Approvals, to ensure the barriers are tested to their full capacity.

3.5.4 Impact test

If the hydrostatic test series is successfully completed, the impact test can proceed. To do this, the steel frame must be removed from the tank and secured against support columns or a wall to prevent it from moving due to the impact and affecting the barrier positively.
This time, all three cameras must be installed and calibrated. Cameras 1 and 2 are synchronised. The height to which the impact object is raised is the one determined during the preliminary test series.

While the hydrostatic test was conducted in parallel for all three barriers, each barrier must now be tested individually. This test series also consists of 2 tests.

- Test 1: The barrier is tested at the centre, at 80% of its height. The height can vary if a lower point is considered more critical and therefore of interest to test.
- Test 2: The barrier is tested at 80% of its height near the edge. This allows for assessing how the connection to the frame responds to an impact.

If it is of interest or requested by the manufacturer to test the barrier at other locations, this can be done. However, conducting too many tests risks compromising the

seal during the subsequent hydrostatic test.

With the measurements from this test series, the contact time with the impact object can be determined, as well as to what extent the barrier was elastically or plastically deformed and how much energy was absorbed by the barrier. This allows for the identification of direct weaknesses, which can help the manufacturer to improve the barrier if necessary.

3.5.5 Post hydrostatic load test

For the post hydrostatic impact test, the steel frame must be placed back into the tank and secured. This test series also consists of 2 tests.

- Test 1: Water at 10% barrier height for 1 hour
- Test 2: Water at 100% barrier height for 1 hour

Both test durations can be extended to 2 hours if stabilisation of the measurements is not observed. Similar to the first hydrostatic test series, measurements are taken at 15-minute intervals, and no measurement should exceed a leakage rate of 1 Liter per hour per metre of joint.

If the barrier does not exceed this threshold, it can be certified for this test series.

Chapter 4

Conclusion

As stated in the introduction, this master's thesis is part of the FLOOD project launched by Buildwise and collaborated by UCLouvain. The work falls into the area of creating the scientific basis for flood protection products. More specifically, flood barriers for opening barrier applications. The focus was on a better understanding of the impact test to simulate the impact of floating debris on such barriers and to lay the basis for further research and a future standard for flood barriers on the Belgian market. To achieve this, the work included a research part to establish a stronger link between the tests and real floods, and an experimental part in which two flood barriers for opening barrier applications were tested.

As was shown in the first part, floods cause several thousand deaths every year, affect several million people and cause damage running into billions. It was established that floods are increasing in frequency and severity, partly due to climate change. The flood of July 2021 in Belgium, which hit the country with unprecedented devastation, was a wake-up call that it is immensely important to take action to reduce the damage and protect against floods in the future. One form such action takes was described in the form of the FLOOD project, which was launched as a result of the floods in July 2021.

As one step in the process pursued by the FLOOD project, this work aimed to develop a good standard for a test procedure around a dynamic impact test for flood barriers. The criteria were mainly developed based on the guidelines of the American FM Approvals. The criterion for the impact test is that the barrier withstands two

impacts of 600 J and then remains functional in terms of the maximum leakage rate. A restriction on the maximum deformation, as exists in the British standard, could possibly be included in a Belgian standard if this would ensure the reusability of the flood barrier. However, this is a topic for further investigation.

Since the FM Approvals give no indication as to why 600 J was chosen as the minimum impact energy, it was important to make a connection between the 600 J impact test and real floods. As shown, an impact at 600 J equates to a log with a density of 700 kg/m^3, a length of 2 m and a diameter of 30 cm at a flow velocity of just under 3.5 m/s which impacts a barrier. Such an impact was established as a realistic, higher than average strain for flood barriers. It was shown that more than 50% of floating debris consists of wood logs of approximately this size or smaller, at least this was the case during the 2021 floods in Belgium. Furthermore, the majority of velocities outside the river bed were shown to be below 4.5 m/s, as well.

Based on the results of the velocities and the objects that can be expected as floating debris, it can be concluded that barriers certified for an impact of 600 J could have been used in the 2021 floods in Pepinster.
The results are quite satisfactory, but could still be improved. The results of the velocities can be improved by analysing and simulating further floods in other regions. The results could also be improved by following the development of the velocities over the entire simulation and not limiting it to a few points in time. More precise information on the sizes of the floating debris and the frequency of their occurrence in streets can refine the results.

It turned out that the impact energy on barriers during floods will usually be well below 600 J. Therefore, this minimum criterion covers pretty much everything except extreme cases that occur with a very low probability.

The experimental phase focused on developing a method for the test setup and procedure, which was then applied to two barriers. The test phase focused on developing a method for the test setup and procedure, which was then applied to two barriers. The final setup included three cameras:

Camera 1 measured the velocity of the impact object, enabling the calculation of

both impact energy and rebound energy. This helped determine how much of the 600 J potential energy was converted into kinetic energy and how much was absorbed by the barrier.

Camera 2, synchronised with Camera 1, determined the precise moment of impact and the contact time between the barrier and the impact object. This information was crucial for identifying when Camera 1's measurements should begin.

Camera 3 measured the 3D deformation of the barrier.
Key elements of the experimental setup included the positioning of the cameras, the placement of the spots, and determining the centre of gravity. During the tests on two barriers it was observed that a significant portion of energy, ranging from 4% to 10% of the potential energy, averaging around 45 Joules, was lost through the pendulum. Due to this energy loss, the barriers were not subjected to the full energy required by the standard. As a result, a barrier might receive certification according to the standard, even though it may not withstand the actual 600 J impact.

To address this issue, the results from the two barriers were compared to identify ways to minimise the interval of the energy loss. Two ways were identified: improving height measurement and enhancing camera calibration. However, these ways to minimise energy loss could not be implemented in this thesis. Once this is done in future research, it will be possible to determine the precise percentage of potential energy that is converted, allowing for the calculation of an accurate potential energy that ensures the kinetic impact energy is nearly 600 J. In this way, it can be ensured that barriers are tested with the correct energy value.

As our final result, we proposed a series of tests that could be used as a certification standard for flood barriers on the Belgien market in future assessments. This test series consists of a preparation phase, a preliminary impact test, a hydrostatic test, a 600 J impact test, and another hydrostatic test. The last three are identical to those in the FM Approvals and serve the same functions. The additional preparation is intended solely to determine the weight and the centre of gravity. The purpose of the preliminary impact test is to determine what percentage of the potential energy is converted into kinetic energy, so the main impact test can be adjusted to ensure that the kinetic energy at impact corresponds to 600 J and not less.

The next step in defining the impact test would be to implement this proposal, incorporate the suggested improvements, and evaluate whether these changes resolve the issues identified in this thesis. This approach would allow for further refinement of the tests, ensuring that the impact tests on barriers meet the energy values specified in the standard. This thesis therefore took a small but important step towards better protection against the increasing threat of floods in Belgium. Future research can build on these results to develop a full criteria catalogue for the consistent certification of flood barriers on the Belgian market.

Appendix

Appendix A

Flow velocity

Pour le graphique	
H (m)	∑Unorm/tranche de valeur de H
0	2,907226789
0,1	3,655458497
0,2	3,837755975
0,3	4,622327744
0,4	4,593822568
0,5	4,738182832
0,6	3,404353082
0,7	3,803919779
0,8	2,684313208
0,9	2,606307491
1	3,196769282
1,1	2,885876785
1,2	3,190169404
1,3	2,523849772
1,4	2,784186735
1,5	2,558758118
1,6	2,440699415
1,7	2,336200747
1,8	3,311255437
1,9	2,653429113
2	2,627538762
2,1	2,909543006
2,2	2,790822676
2,3	2,698759963
2,4	2,394328553
2,5	2,884047972
2,6	2,838068432
2,7	2,869415871
2,8	2,4803198
2,9	2,557192236
3	2,544750327
3,1	2,483025515
3,2	2,508279524
3,3	2,495086154
3,4	2,422397417

Figure A.1: Flow velocity for a 25 year return period. [10]

Appendix B

Energy variation for different wood densities

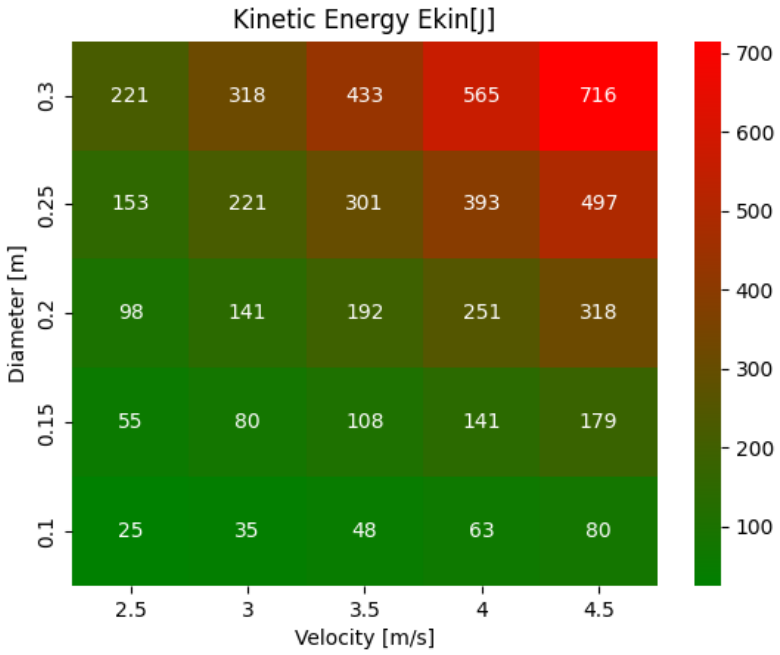


Figure B.1: Impact energy for common driftwood with a density of 500 kg/m^3.

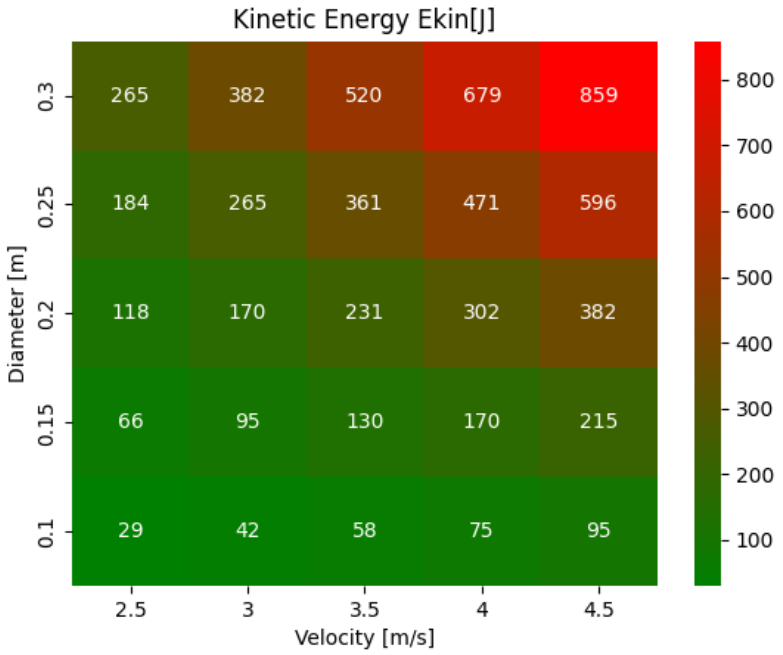


Figure B.2: Impact energy for common driftwood with a density of 600 kg/m^3.

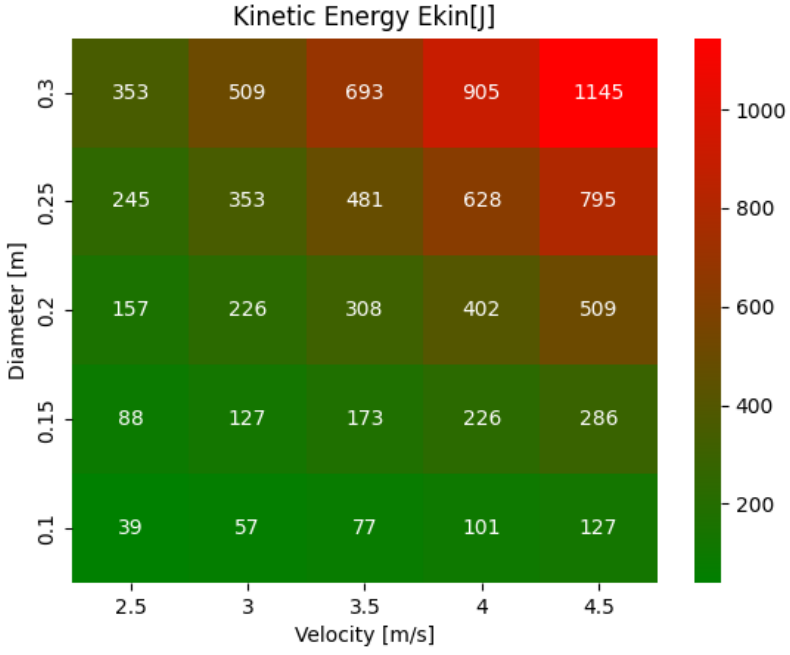


Figure B.3: Impact energy for common driftwood with a density of 800 kg/m^3.

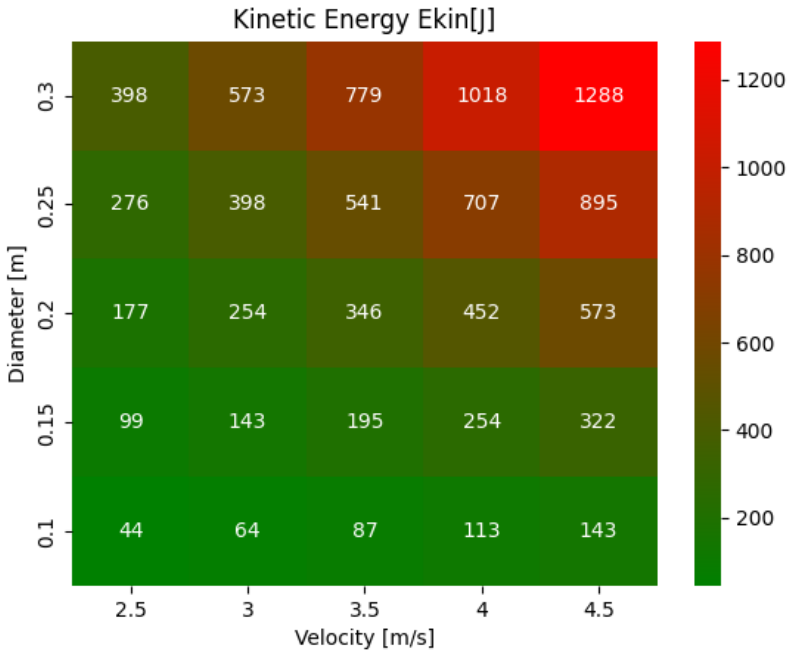


Figure B.4: Impact energy for common driftwood with a density of 900 kg/m^3.

Appendix C

Test results

C.1 Barrier X - Test results

C.1.1 First test

Time step Δt [ms]	**0.25**					
Measurement	**1**		**2**		**3**	
v [m/s]	5.103	4.713	5.103	4.713	5.103	4.713
$E_{kin}[J]$	648.36	553.01	648.36	553.01	648.36	553.01
Ratio $\frac{E_{kin}}{E_{pot}}$ [%]	108.78	92.78	108.78	92.78	108.78	92.78
$\Delta\frac{E_{kin}}{E_{pot}}$ [%]	16		16		16	
Total Mean of E_{kin} [J]	**600.69**					
Total Mean of $\frac{E_{kin}}{E_{pot}}$ [%]	**100.78**					
Total Mean of $\Delta\frac{E_{kin}}{E_{pot}}$ [%]	**16**					

Table C.1: Barrier X: First test results - Measurement over a time step of 0.25 ms.

Time step Δt [ms]	**0.5**					
Measurement	**1**		**2**		**3**	
v [m/s]	4.908	4.733	4.713	4.908	4.927	4.733
$E_{kin}[J]$	599.73	557.78	553.01	599.73	604.50	557.78
Ratio $\frac{E_{kin}}{E_{pot}}$ [%]	100.62	93.58	92.78	100.62	101.42	93.58
$\Delta\frac{E_{kin}}{E_{pot}}$ [%]	7.04		7.84		7.84	
Total Mean of E_{kin} [J]	**578.76**					
Total Mean of $\frac{E_{kin}}{E_{pot}}$ [%]	**97.10**					
Total Mean of $\Delta\frac{E_{kin}}{E_{pot}}$ [%]	**7.57**					

Table C.2: Barrier X: First test results - measurement over a time step of 0.5 ms.

Time step Δt [ms]	**1**					
Measurement	**1**		**2**		**3**	
v [m/s]	4.819	4.722	4.819	4.722	4.819	4.830
$E_{kin}[J]$	578.28	555.16	578.28	555.16	578.28	580.90
Ratio $\frac{E_{kin}}{E_{pot}}$ [%]	97.02	93.14	97.02	93.14	97.02	97.46
$\Delta\frac{E_{kin}}{E_{pot}}$ [%]	3.88		3.88		0.44	
Total Mean of E_{kin} [J]	**571.01**					
Total Mean of $\frac{E_{kin}}{E_{pot}}$ [%]	**95.80**					
Total Mean of $\Delta\frac{E_{kin}}{E_{pot}}$ [%]	**2.73**					

Table C.3: Barrier X: First test results - Measurement over a time step of 1 ms.

Time step Δt [ms]	**2**					
Measurement	**1**		**2**		**3**	
v [m/s]	4.819	4.770	4.819	4.770	4.819	4.770
$E_{kin}[J]$	578.28	566.66	578.28	566.66	578.28	566.66
Ratio $\frac{E_{kin}}{E_{pot}}$ [%]	97.02	95.07	97.02	95.07	97.02	95.07
$\Delta\frac{E_{kin}}{E_{pot}}$ [%]	1.95		1.95		1.95	
Total Mean of E_{kin} [J]	**572.47**					
Total Mean of $\frac{E_{kin}}{E_{pot}}$ [%]	**96.05**					
Total Mean of $\Delta\frac{E_{kin}}{E_{pot}}$ [%]	**1.95**					

Table C.4: Barrier X: First test results - Measurement over a time step of 2 ms.

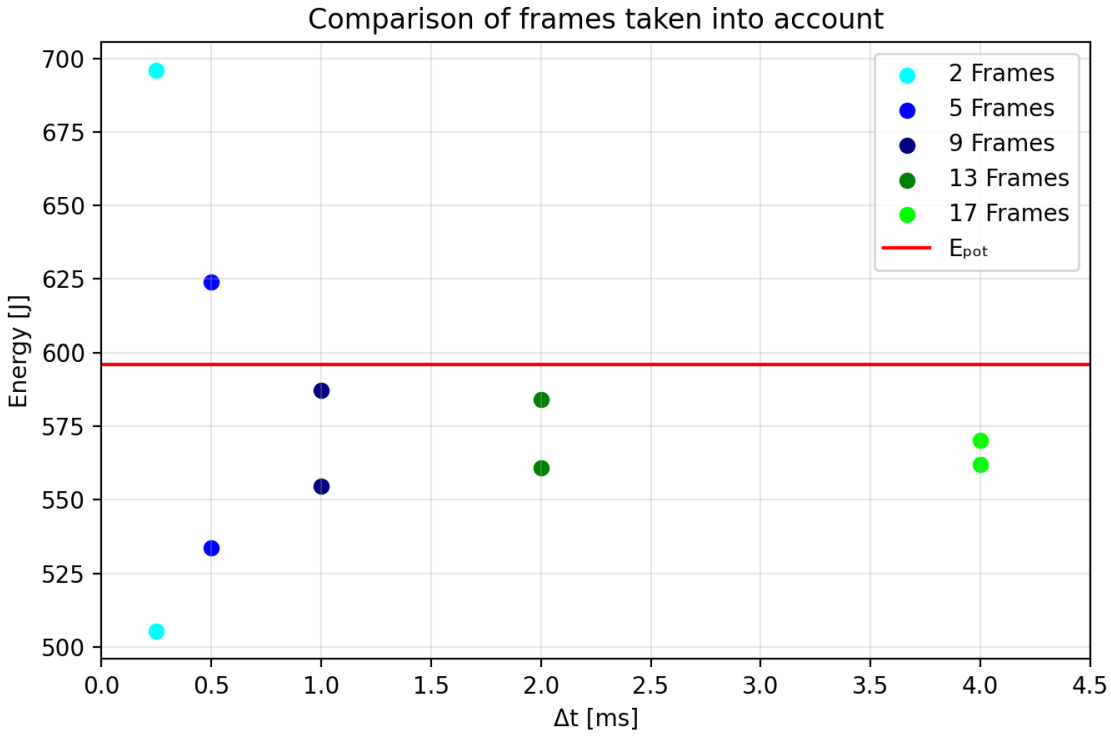


Figure C.1: Barrier X - Test 1: Graphical representation of the measurements with different time steps.

C.1.2 Second test

Time step Δt [ms]	**0.25**					
Measurement	**1**		**2**		**3**	
v [m/s]	4.581	4.960	4.581	4.960	4.581	4.638
$E_{kin}[J]$	522.51	612.59	522.51	612.59	522.51	533.32
Ratio $\frac{E_{kin}}{E_{pot}}$ [%]	87.67	102.78	87.67	102.78	87.67	89.48
$\Delta\frac{E_{kin}}{E_{pot}}$ [%]	15.11		15.11		1.81	
Total Mean of E_{kin} [J]	**554.34**					
Total Mean of $\frac{E_{kin}}{E_{pot}}$ [%]	**93.01**					
Total Mean of $\Delta\frac{E_{kin}}{E_{pot}}$ [%]	**10.68**					

Table C.5: Barrier X: Second test results - Measurement over a time step of 0.25 ms.

Time step Δt [ms]	**0.5**					
Measurement	**1**		**2**		**3**	
v [m/s]	4.960	4.770	4.581	4.770	4.770	4.789
$E_{kin}[J]$	612.59	566.65	522.51	566.65	566.65	571.16
Ratio $\frac{E_{kin}}{E_{pot}}$ [%]	102.78	95.07	87.67	95.07	95.07	95.83
$\Delta\frac{E_{kin}}{E_{pot}}$ [%]	7.71		7.71		0.76	
Total Mean of E_{kin} [J]	**567.70**					
Total Mean of $\frac{E_{kin}}{E_{pot}}$ [%]	**95.25**					
Total Mean of $\Delta\frac{E_{kin}}{E_{pot}}$ [%]	**5.29**					

Table C.6: Barrier X: Second test results - Measurement over a time step of 0.5 ms.

Time step Δt [ms]	**1**					
Measurement	**1**		**2**		**3**	
v [m/s]	4.676	4.779	4.684	4.779	4.684	4.779
$E_{kin}[J]$	544.36	568.68	546.38	568.68	546.38	568.68
Ratio $\frac{E_{kin}}{E_{pot}}$ [%]	91.33	95.41	91.67	95.41	91.67	95.41
$\Delta\frac{E_{kin}}{E_{pot}}$ [%]	4.08		3.74		3.74	
Total Mean of E_{kin} [J]	**557.19**					
Total Mean of $\frac{E_{kin}}{E_{pot}}$ [%]	**93.49**					
Total Mean of $\Delta\frac{E_{kin}}{E_{pot}}$ [%]	**3.85**					

Table C.7: Barrier X: Second test results - Measurement over a time step of 1 ms.

Time step Δt [ms]	**0.25**					
Measurement	**1**		**2**		**3**	
v [m/s]	4.727	4.732	4.727	4.732	4.727	4.732
$E_{kin}[J]$	556.40	557.47	556.40	557.47	556.40	557.47
Ratio $\frac{E_{kin}}{E_{pot}}$ [%]	93.35	93.53	93.35	93.53	93.35	93.53
$\Delta\frac{E_{kin}}{E_{pot}}$ [%]	0.18		0.18		0.18	
Total Mean of E_{kin} [J]	**556.94**					
Total Mean of $\frac{E_{kin}}{E_{pot}}$ [%]	**93.44**					
Total Mean of $\Delta\frac{E_{kin}}{E_{pot}}$ [%]	**0.18**					

Table C.8: Barrier X: Second test results - Measurement over a time step of 2 ms.

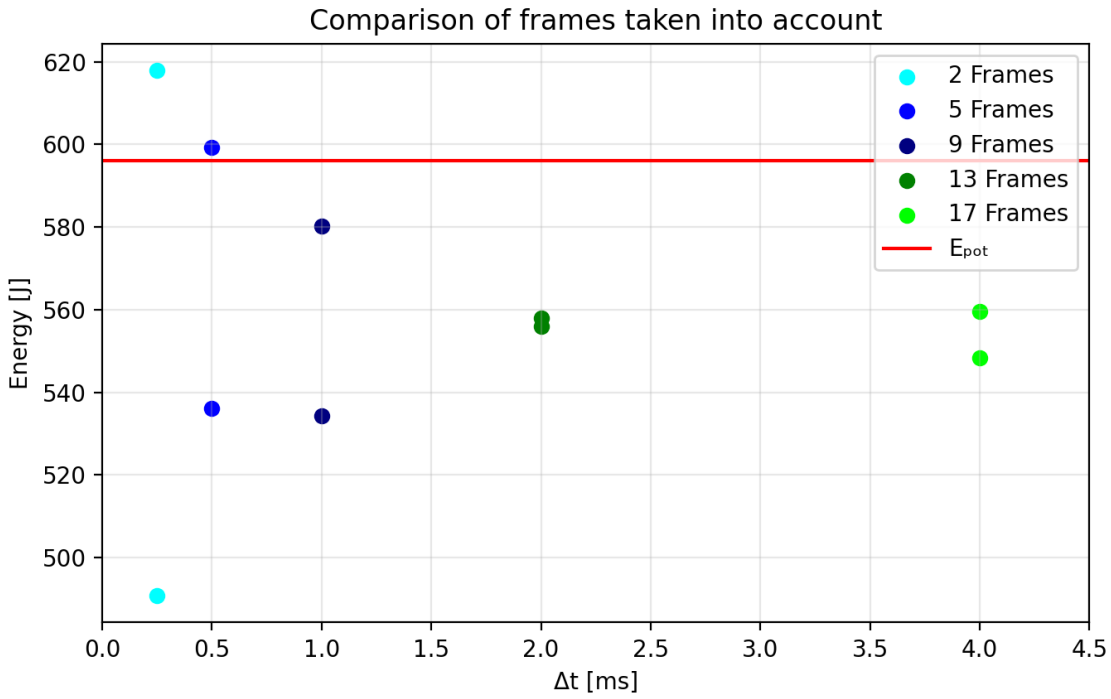


Figure C.2: Barrier X - Test 2: Graphical representation of the measurements with different time steps.

C.2 Barrier Y - Test results

C.2.1 First test

Time step Δt [ms]	**0.25**					
Measurement	**1**		**2**		**3**	
v [m/s]	4.790	4.402	4.790	4.782	4.790	4.848
$E_{kin}[J]$	571.31	482.49	571.31	569.50	571.31	585.32
Ratio $\frac{E_{kin}}{E_{pot}}$ [%]	95.85	80.95	95.85	95.55	95.85	98.21
$\Delta\frac{E_{kin}}{E_{pot}}$ [%]	14.9		0.3		2.35	
Total Mean of E_{kin} [J]	**558.54**					
Total Mean of $\frac{E_{kin}}{E_{pot}}$ [%]	**93.71**					
Total Mean of $\Delta\frac{E_{kin}}{E_{pot}}$ [%]	**5.85**					

Table C.9: Barrier Y: First test results - Measurement over a time step of 0.25 ms.

Time step Δt [ms]	**0.5**					
Measurement	**1**		**2**		**3**	
v [m/s]	4.781	4.584	4.802	4.781	4.802	4.781
$E_{kin}[J]$	569.28	523.15	574.19	569.28	574.19	569.28
Ratio $\frac{E_{kin}}{E_{pot}}$ [%]	95.51	87.77	96.34	95.51	96.34	95.51
$\Delta\frac{E_{kin}}{E_{pot}}$ [%]	7.74		0.82		0.82	
Total Mean of E_{kin} [J]	**563.23**					
Total Mean of $\frac{E_{kin}}{E_{pot}}$ [%]	**94.5**					
Total Mean of $\Delta\frac{E_{kin}}{E_{pot}}$ [%]	**3.13**					

Table C.10: Barrier Y: First test results - Measurement over a time step of 0.5 ms.

Time step Δt [ms]	**1**					
Measurement	**1**		**2**		**3**	
v [m/s]	4.683	4.593	4.791	4.683	4.791	4.802
$E_{kin}[J]$	545.97	525.35	571.49	545.97	571.49	574.19
Ratio $\frac{E_{kin}}{E_{pot}}$ [%]	91.60	88.14	95.88	91.60	95.88	96.34
$\Delta\frac{E_{kin}}{E_{pot}}$ [%]	3.46		4.28		0.45	
Total Mean of E_{kin} [J]	**555.74**					
Total Mean of $\frac{E_{kin}}{E_{pot}}$ [%]	**93.24**					
Total Mean of $\Delta\frac{E_{kin}}{E_{pot}}$ [%]	**2.73**					

Table C.11: Barrier Y: First test results - Measurement over a time step of 1 ms.

Time step Δt [ms]	**2**					
Measurement	**1**		**2**		**3**	
v [m/s]	4.687	4.643	4.687	4.692	4.736	4.687
$E_{kin}[J]$	547.01	536.70	547.01	548.17	558.60	547.01
Ratio $\frac{E_{kin}}{E_{pot}}$ [%]	91.78	90.05	91.78	91.97	93.72	91.78
$\Delta\frac{E_{kin}}{E_{pot}}$ [%]	1.73		0.2		1.95	
Total Mean of E_{kin} [J]	**547.42**					
Total Mean of $\frac{E_{kin}}{E_{pot}}$ [%]	**91.85**					
Total Mean of $\Delta\frac{E_{kin}}{E_{pot}}$ [%]	**1.29**					

Table C.12: Barrier Y: First test results - Measurement over a time step of 2 ms.

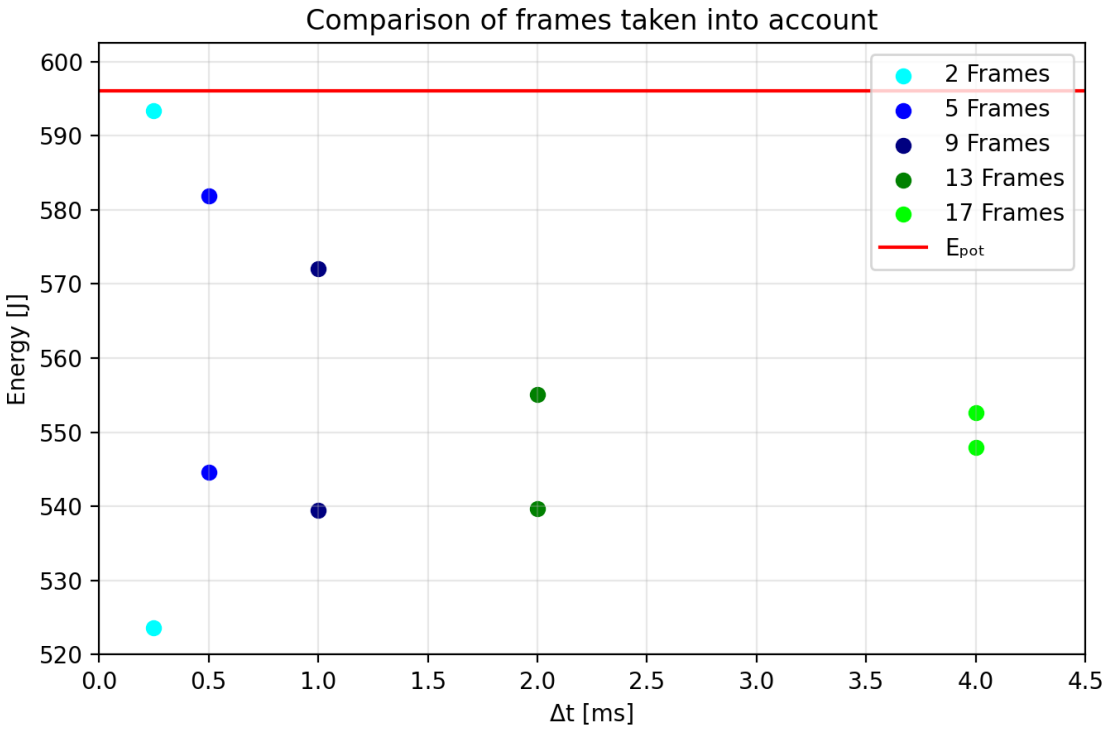


Figure C.3: Barrier Y - Test 1: Graphical representation of the measurements with different time steps.

C.2.2 Second test

Time step Δt [ms]	**0.25**					
Measurement	**1**		**2**		**3**	
v [m/s]	4.629	5.057	4.629	4.246	4.629	5.013
$E_{kin}[J]$	533.65	636.69	533.65	449.00	533.65	625.65
Ratio $\frac{E_{kin}}{E_{pot}}$ [%]	89.54	106.82	89.54	75.33	89.54	104.97
$\Delta\frac{E_{kin}}{E_{pot}}$ [%]	17.29		14.20		15.44	
Total Mean of E_{kin} [J]	**552.05**					
Total Mean of $\frac{E_{kin}}{E_{pot}}$ [%]	**92.62**					
Total Mean of $\Delta\frac{E_{kin}}{E_{pot}}$ [%]	**15.64**					

Table C.13: Barrier Y: Second test results - Measurement over a time step of 0.25 ms.

Time step Δt [ms]	**0.5**					
Measurement	**1**		**2**		**3**	
v [m/s]	4.649	4.629	4.821	4.629	4.649	4.629
$E_{kin}[J]$	538.25	533.65	578.73	533.65	538.25	533.65
Ratio $\frac{E_{kin}}{E_{pot}}$ [%]	90.31	89.54	97.10	89.54	90.31	89.54
$\Delta\frac{E_{kin}}{E_{pot}}$ [%]	0.77		7.56		0.77	
Total Mean of E_{kin} [J]	**542.69**					
Total Mean of $\frac{E_{kin}}{E_{pot}}$ [%]	**91.05**					
Total Mean of $\Delta\frac{E_{kin}}{E_{pot}}$ [%]	**3.04**					

Table C.14: Barrier Y: Second test results - Measurement over a time step of 0.5ms.

Time step Δt [ms]	**1**					
Measurement	**1**		**2**		**3**	
v [m/s]	4.638	4.629	4.638	4.629	4.638	4.629
$E_{kin}[J]$	535.72	533.65	535.72	533.65	535.72	533.65
Ratio $\frac{E_{kin}}{E_{pot}}$ [%]	89.88	89.54	89.88	89.54	89.88	89.54
$\Delta\frac{E_{kin}}{E_{pot}}$ [%]	0.35		0.35		0.35	
Total Mean of E_{kin} [J]	**534.68**					
Total Mean of $\frac{E_{kin}}{E_{pot}}$ [%]	**89.71**					
Total Mean of $\Delta\frac{E_{kin}}{E_{pot}}$ [%]	**0.35**					

Table C.15: Barrier Y: Second test results - Measurement over a time step of 1 ms.

Time step Δt [ms]	**2**					
Measurement	**1**		**2**		**3**	
v [m/s]	4.638	4.686	4.634	4.638	4.586	4.634
$E_{kin}[J]$	535.72	546.81	534.62	535.72	523.64	534.62
Ratio $\frac{E_{kin}}{E_{pot}}$ [%]	89.88	91.74	89.70	89.88	87.86	89.70
$\Delta\frac{E_{kin}}{E_{pot}}$ [%]	1.86		0.18		1.84	
Total Mean of E_{kin} [J]	**535.19**					
Total Mean of $\frac{E_{kin}}{E_{pot}}$ [%]	**89.79**					
Total Mean of $\Delta\frac{E_{kin}}{E_{pot}}$ [%]	**1.3**					

Table C.16: Barrier Y: Second test results - Measurement over a time step of 2 ms.

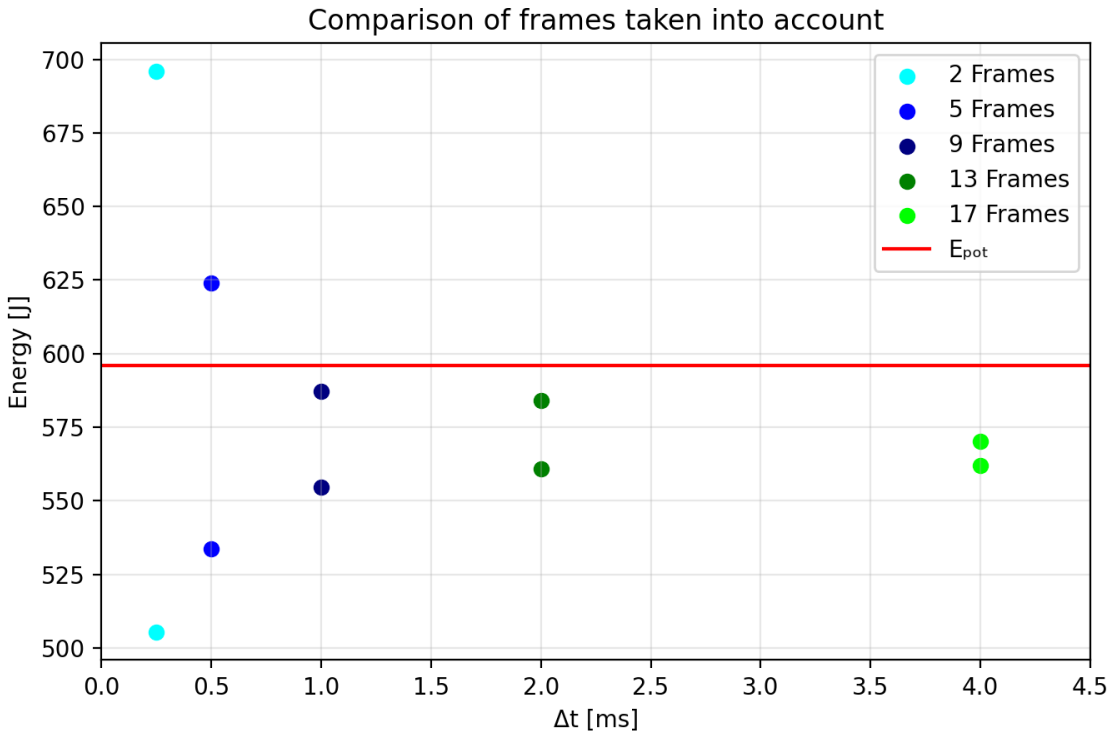


Figure C.4: Barrier Y - Test 2: Graphical representation of the measurements with different time steps.

List of Figures

1.1 Number of natural disasters worldwide. [19] 2
1.2 Deaths from floods. [19] 3
1.3 Number of people affected by floods worldwide. [19] 4
1.4 Economic damages due to floods. [19] 5
1.5 Deaths from floods in Europe. [19] 6
1.6 People affected by floods in Europe. [19] 7
1.7 Average number of people affected by floods in Europe. [19] 8
1.8 Pepinster 2021. [22] 9
1.9 Remaining mud in a house after the 2021 floods in Pepinster. [22] . . . 9
1.10 3-task scheme. [7] 11

2.1 Impact test scheme. [4] 22
2.2 Wave and current testing depths. [11] 25
2.3 Dynamic impact test of the British standard. [11] 27
2.4 Catchment area of the Vesdre river. [10] 31
2.5 Water velocity as a function of the water depth for different return periods. [10] 32
2.6 Debris accumulation, Germany 2021 (photo by D. Poppema). 34
2.7 Debris accumulation, Belgium 2021 (photo by D. Poppema). 35
2.8 Debris accumulation, Belgium 2021 (photo by D. Poppema). 35
2.9 Debris accumulation, Belgium 2021 (photo by D. Poppema). 36
2.10 Impact energy in function of the velocity. 37
2.11 Impact energy for large objects. 38
2.12 Distribution according to length. [8] 39
2.13 Distribution according to diameter. [8] 39
2.14 Impact energy for common driftwood with a density of 700 kg/m^3. . . . 40

2.15 Impact energy for common driftwood with varying density. 41
2.16 Course of the Vesdre and Hoëgne river. [1] 42
2.17 Pepinster flood. [2] 43
2.18 Pepinster flood. [13] 43
2.19 Damage due to scour. [6] 44
2.20 Broken windows. [20] 44
2.21 Damage due to impact. [20] 44
2.22 Water traces up to the middle of the door opening. [20] 44
2.23 Flooded area and domain outline. [1] 45
2.24 Discharge of the Vesdre river after confluence. [1] 46
2.25 Velocity at 18:00 on 15 July 2021 (graphic by C.Noiset). 47
2.26 Velocity at 15:00 on 15 July 2021 (graphic by C.Noiset). 48
2.27 Velocity at 21:00 on 15 July 2021 (graphic by C.Noiset). 48

3.1 Setup low-velocity out-of-plane impact tests on double wythe unreinforced brick masonry walls instrumented with optical fibre measurements. [16] 53
3.2 First setup with dart barrel as impact object. 55
3.3 Camera images dart setup. 56
3.4 Setup first tests at Buildwise. 1: Photron Fastcam Mini type 800K-M-32G 2: Photron Fastcam SA3 Model 120K-M1 3: 25 Hz Aramis 3D DIC Camera 4: Black light spots 58
3.5 Calibration pictures with chess pattern on barrier and impact object. . 59
3.6 Method to measure height h. 61
3.7 Pictures of the first test at Buildwise. 62
3.8 Setup small scale model. 1: Photron Fastcam Mini type 800K-M-32G 2: Photron Fastcam SA3 Model 120K-M1 3: Spotlights 65
3.9 Setup first test small scale model. 66
3.10 Calibration methods. 67
3.11 Camera positionings. 69
3.12 Picture quality differences. 70
3.13 Setup small scale model - Second test series. 1: Photron Fastcam Mini type 800K-M-32G 2: Spotlights 71
3.14 Drop height measurement (in red: centre of gravity). 72
3.15 Measurements for a 0.25 ms time step. 74

3.16 Graphical representation of the measurements with different time steps. 76
3.17 Camera calibrated on reference chess pattern. 78
3.18 Chess pattern fixed on steel frame. 78
3.19 Setup small scale model - Third test series. 79
3.20 Setup small scale model. 1: Photron Fastcam Mini type 800K-M-32G 2: Photron Fastcam SA3 Model 120K-M1 3: Spotlights In red: Manual Trigger 81
3.21 Determination centre of gravity. 83
3.22 Schematic represenation of the setup. 84
3.23 Final setup for the first test. 86
3.24 Structure with three openings placed in water tank. 87
3.25 Structure displacement. 88
3.26 Painted barrier in one of the three openings. 89
3.27 Dimensions barrier X. [5] 91
3.28 Barrier X installation. [5] 92
3.29 Measurements done on three reference points on the chess pattern. . . . 94
3.30 Barrier X after first impact. 96
3.31 Barrier X after second impact. 98
3.32 Barrier Y. 101
3.33 Barrier Y installation. 101
3.34 Barrier Y after first impact. 104
3.35 Barrier Y after second impact. 106
3.36 Calibration of the camera. 112

A.1 Flow velocity for a 25 year return period. [10] 124

B.1 Impact energy for common driftwood with a density of 500 kg/m^3. . . . 125
B.2 Impact energy for common driftwood with a density of 600 kg/m^3. . . . 126
B.3 Impact energy for common driftwood with a density of 800 kg/m^3. . . . 126
B.4 Impact energy for common driftwood with a density of 900 kg/m^3. . . . 127

C.1 Barrier X - Test 1: Graphical representation of the measurements with different time steps. 130
C.2 Barrier X - Test 2: Graphical representation of the measurements with different time steps. 133

C.3 Barrier Y - Test 1: Graphical representation of the measurements with different time steps. 135
C.4 Barrier Y - Test 2: Graphical representation of the measurements with different time steps. 138

List of Tables

2.1 Performance Test Series - Flood barriers for opening barrier applications. 18
2.2 Percentage distribution of velocities at 18:00 on 15 July 2021. 50
2.3 Percentage distribution of velocities at 15:00 on 15 July 2021. 50
2.4 Percentage distribution of velocities at 21:00 on 15 July 2021. 50

3.1 Given values and results. 56
3.2 Values and results. 60
3.3 Given values. 68
3.4 First test results. 68
3.5 Given values. 73
3.6 Results: Second test series - Time steps 0.25, 1 and 2 ms. 75
3.7 Results: Second test series - Time steps 3 and 4 ms. 75
3.8 Results: Contact time and absorbed energy. 77
3.9 Barrier X - Hydrostatic test results. 93
3.10 Given values. 95
3.11 Barrier X: First test - Measurements of the impact energy over a time step of 4 ms. 95
3.12 Barrier X: First test - Measurements of the return energy over a time step of 4 ms. 96
3.13 Results comparison. 96
3.14 Barrier X: Second test - Measurements of the impact energy over a time step of 4 ms. 97
3.15 Barrier X: Second test - Measurements of the return energy over a time step of 4 ms. 98
3.16 Results comparison. 98
3.17 Barrier X - Hydrostatic test after impact results. 100

3.18 Barrier Y - Hydrostatic test results. 102
3.19 Barrier Y: First test - Measurements of the impact energy over a time step of 4 ms. 103
3.20 Barrier Y: First test - Measurements of the return energy over a time step of 4 ms. 104
3.21 Results comparison. 104
3.22 Barrier Y: Second test - Measurements of the impact energy over a time step of 4 ms. 105
3.23 Barrier Y: Second test - Measurements of the return energy over a time step of 4 ms. 106
3.24 Results comparison. 106
3.25 Barrier Y - Hydrostatic test after impact results. 108
3.26 Comparison impact energies. 109
3.27 Impact energy with different height. 109
3.28 Height calculation. 110
3.29 Comparison of a height difference of 1 cm. 111
3.30 Comparison of a height difference of 2 cm. 111
3.31 Barrier X - Test 1: Results for different calibrations. 113
3.32 Barrier Y - Test 2: Results for different calibrations. 113
3.33 Final height calculation. 115

C.1 Barrier X: First test results - Measurement over a time step of 0.25 ms. 128
C.2 Barrier X: First test results - measurement over a time step of 0.5 ms. . 129
C.3 Barrier X: First test results - Measurement over a time step of 1 ms. . . 129
C.4 Barrier X: First test results - Measurement over a time step of 2 ms. . . 130
C.5 Barrier X: Second test results - Measurement over a time step of 0.25 ms. 131
C.6 Barrier X: Second test results - Measurement over a time step of 0.5 ms. 131
C.7 Barrier X: Second test results - Measurement over a time step of 1 ms. 132
C.8 Barrier X: Second test results - Measurement over a time step of 2 ms. 132
C.9 Barrier Y: First test results - Measurement over a time step of 0.25 ms. 133
C.10 Barrier Y: First test results - Measurement over a time step of 0.5 ms. . 134
C.11 Barrier Y: First test results - Measurement over a time step of 1 ms. . . 134
C.12 Barrier Y: First test results - Measurement over a time step of 2 ms. . . 135
C.13 Barrier Y: Second test results - Measurement over a time step of 0.25 ms. 136
C.14 Barrier Y: Second test results - Measurement over a time step of 0.5ms. 136

C.15 Barrier Y: Second test results - Measurement over a time step of 1 ms. 137
C.16 Barrier Y: Second test results - Measurement over a time step of 2 ms. 137

Bibliography

[1] Lisa Adyns and Delphine Adriaens. "Etude expérimentale de la résistance des bâtiments en cas de crue". In: UCLouvain, 2022-2023.

[2] AFP News Agency. *Flooding in the Belgian city of Pepinster | AFP*. URL: https://www.youtube.com/watch?app=desktop&v=pvP_78_oNkY (visited on 08/12/2024).

[3] FM Approvals. URL: https://www.fmapprovals.com/ (visited on 07/24/2024).

[4] FM Approvals. "Approval Standard for Flood Mitigation Equipment". In: (2019).

[5] *Barrier X User Manual*.

[6] belga. In: *Grenzecho* (May 15, 2024). URL: [Video]%20%E2%80%9EApr%C3%A8s%20la%20pluie%E2%80%9C%20l%C3%A4sst%20die%20Flut%20Revue%20passieren%20und%20stellt%20die%20Frage%20%E2%80%9Enach%20dem%20Danach%E2%80%9C (visited on 08/12/2024).

[7] Buildwise. *Recherche FLOOD*. URL: https://www.buildwise.be/fr/recherche-innovation/showroom-des-projets/construire-et-renover-en-zones-inondables-flood/recherche/recherche-flood/ (visited on 07/26/2024).

[8] Josef Hess Christian Rickli. "Aspects de la formation des bois flottants". In: (2009).

[9] *Hochwasserbeständige Fenster und Türen*. ift Rosenheim GmbH, 2005. ISBN: 978-3-86791-000-2.

[10] Lilas Hougardy. "Constructions sur pilotis : Étude de prédimensionnement pour des bâtiments résidentiels situés en zone d'alé". In: Université de Liège, 2022-2023.

[11] The British Standards Institution. *Flood resistance products Part 1: Building products – Specification*. BSI Standards Limited, 2019. ISBN: 978 0 580 99726 6.

[12] Alan James. "How long does it take to dry out water damage?" In: Dantherm Group, June 13, 2024. URL: https://www.danthermgroup.com/uk/insights/how-long-does-it-take-to-dry-out-water-damage (visited on 08/14/2024).

[13] eda Labeye. "PHOTOS| Inondations: La situation est toujours critique à Pepinster". In: *l'avenir* (July 15, 2021). URL: https://www.lavenir.net/regions/verviers/pepinster/2021/07/15/photos-inondations-la-situation-est-toujours-critique-a-pepinster-46KDU5VVYVB7HD73CJNFKDEBUM/ (visited on 08/12/2024).

[14] LIGNORAMA. *Holz als Roh- und Werkstoff Leitz-Anwenderlexikon*. URL: https://www.lignorama.com/holz-als-roh-und-werkstoff/ (visited on 08/17/2024).

[15] Jonas Maeder. "Objektschutz gegen Hochwasser Hochwasserschutz durch ins Gebäude integrierte Abschlüsse". In: (2017).

[16] Natalie Williams Portal Michele Godio Mathias Flansbjer. "Low-velocity out-of-plane impact tests on double-wythe unreinforced brick masonry walls instrumented with optical measurements". In: *International Journal of Impact Engineering* (2023).

[17] *Minimum Design Loads and Associated Criteria for Buildings and Other Structures*. American Society of Civil Engineers, 2017. ISBN: 978 0 7844 7996 4.

[18] Eve Powell. "Going home after a flood". In: GO.COMPARE, June 18, 2024. URL: https://www.gocompare.com/household-tips/returning-after-a-flood/ (visited on 08/14/2024).

[19] Hannah Ritchie and Pablo Rosado. "Natural Disasters". In: *Our World in Data* (2022). https://ourworldindata.org/natural-disasters.

[20] Charles Ryckmans. *Présentation de la visite de pepinster*. 2022.

[21] LGCIV2055 students. "Nature Based Solutions". In: (2023-2024).

[22] Michaël Torfs. "90 percent of Walloon municipalities hit by the floods, death toll is still rising". In: *vrt news* (July 18, 2021). URL: https://www.vrt.be/vrtnws/en/2021/07/18/from-railroads-to-tap-water-the-impact-of-the-floods-is-huge/ (visited on 08/14/2024).

UNIVERSITÉ CATHOLIQUE DE LOUVAIN
École polytechnique de Louvain
Rue Archimède, 1 bte L6.11.01, 1348 Louvain-la-Neuve, Belgique | **www.uclouvain.be/epl**